An investigation into the performance of a *power-of-two* coefficient transversal equalizer in a 34Mbit/s QPSK digital radio during frequency-selective fading conditions.

by

Brindsley Broughton Archer

31 January 1997

Submitted to the University of Cape Town in partial fulfilment of the requirements for the degree of Master of Science in Engineering.

Declaration

I declare that this thesis is my own unaided work and is being submitted to the University of Cape Town in partial fulfilment of the requirements for the degree of Master of Science in Engineering. It has not been submitted before to any other university for any degree or examination.

_____ 31 January 1997

B.B. Archer.

Acknowledgements

Many people have contributed to make this dissertation possible. The first person I would like to mention is Dave Crouch, who encouraged me to pursue my field of interest and the subject of equalizers, in particular. Having expressed this desire to my superior at Plessey S.A., Johan Gericke, I received much support from him. Not only did he provide an undistracted environment, but his practical insight into complex issues and his enthusiasm for engineering, have also been an inspiration to me. I would also like to thank my other colleagues at Plessey for the many interesting discussions and pleasant camaraderie; namely: Dave Upton, Donald Gammon, Derek Richardson, Duncan Bender, Ian Koetzen and Paul Bremer.

Then I would like to express my thanks to my supervisor at the University of Cape Town, Dr. Robin Braun, for his input and guidance. I did not realise the vastness and maturity of the subject of equalization at the outset, and as I discovered more about the field, so my field of investigation kept expanding! Dr. Braun was instrumental in keeping me on the *straight and narrow*, which resulted in this dissertation actually being written (albeit one percent of the original proposal!). I would also like to thank two other lectures at U.C.T., namely, Prof. John Green and Dr. Norman Morisson. Prof. Green's inspiring course on *Adaptive and Evolving Systems* resulted in me considering a power-of-two adaption algorithm and hence provided the motivation for the investigation contained in this dissertation. Dr. Morisson's thoroughness, enthusiasm for engineering and the Fourier Transform in particular, and his commitment to lecturing, are an inspiration to me.

It goes without saying that one's parents play a fundamental role in the educational process, but I am specifically grateful to my parents for buying me a PC and EPROM programmer when I was fourteen years old. These items brought me much joy in my youth and resulted in me pursuing a degree in Electronic Engineering.

Last, and most importantly, I would like to thank Sarah, who became my wife during this period, for tolerating my melancholic nature as I went through the painful learning process, and for her patience when my thesis took preference to *more important things*.

Abstract

Under certain atmospheric conditions, multipath propagation can occur. The interaction of radio waves arriving at a receiver, having travelled via paths of differing length, results in the phenomenon of frequency-selective fading. This phenomenon manifests as a notch in the received spectrum and causes a severe degradation in the performance of a digital radio system. As the total power in the received bandwidth may be unaffected, the Automatic Gain Control is not able to correct for this distortion, and so other methods are required. The dissertation commences with a summary of the phenomenon of multipath as this provides the context for the investigations which follow.

The adaptive equalizer was developed to combat the distortion introduced by frequency-selective fading. It achieves this by applying an estimate of the inverse of the distorting channel's transfer function. The theory on adaptive equalizers has been well established, and a summary of this theory is presented in the form of Wiener Filter theory and the Wiener-Hopf equations.

An adaptive equalizer located in a 34MBit/s QPSK digital radio is required to operate at very high speed, and its digital hardware implementation is not a trivial task. In order to reduce the cost and complexity, a compromise was proposed. If the tap weights of the equalizer could be represented by *power-of-two* binary numbers, the equalizer circuitry can be dramatically simplified. The aim of the dissertation was to investigate the performance of this simplified equalizer structure and to determine whether a *power-of-two* equalizer was a viable consideration.

In order to perform the investigation, a computer simulation model was developed and the simulation was conducted at baseband to shorten the computer run-time. The underlying theory to create a baseband equivalent system is presented in the dissertation. Having performed the simulations, it was concluded that a *power-of-two* equalizer can be employed to significantly improve the performance of a digital radio system.

Table of Contents

List of illustrations

Figures:

Tables:

Nomenclature

Acronyms:

AGC	:	Automatic Gain Control
ASIC	:	Application Specific Integrated Circuit
AWGN	:	Additive White Gaussian Noise
BER	:	Bit Error Rate
BPSK	:	Binary Phase Shift Keying
DSP	:	Digital Signal Processing
EA	:	Eye Aperture
E_b/N_0	:	Bit energy to noise ratio
FDE	:	Frequency Domain Equalizer/Equalization
FIR	:	Finite Impulse Response
FPGA	:	Field Programmable Gate Array
I	:	In-phase channel
IEA	:	Inverse Eye Aperture
IF	:	Intermediate Frequency
ISI	:	Inter-symbol interference
LMS	:	Least Mean Square
LOS	:	Line-of-sight
$N_0/2$	:	Double-sided noise power spectral density
MBaud	:	2 million bits of information per second for QPSK
MBit/s	:	1 million bits of information per second
pdf	:	Probability density function
PO2	:	power-of-two, that is: 0, 1, 2, 4, 8, 16, 32, 64, etc
Q	:	Quadrature channel
QAM	:	Quadrature Amplitude Modulation
QPSK	:	Quadrature Phase Shift Keying
RF	:	Radio Frequency
Rx	:	Receiver
S/N	:	Signal to noise ratio
TDE	:	Time Domain Equalizer/Equalization
TDL	:	Tapped-delay line
Tx	:	Transmitter
VLSI	:	Very Large Scale Integration
2PM	:	Two-path model
3PM	:	Three-path model

Mathematical:

α	:	Raised-cosine roll-off factor
A	:	Fade level for 3PM in dB
$A(t)$, $B(t)$	:	Temporary simplification terms
a	:	Overall attenuation parameter for 3PM
B	:	Notch depth in dB
B, W	:	Bandwidth
b	:	Shape parameter for 3PM
d	:	Distance
$E[\,]$	:	Expectation operator
f, w	:	Frequency
$sgn(\,)$	:	Signum function
T	:	Symbol period
$\boldsymbol{w}_0$	:	Vector of optimal equalizer coefficients
w_0	:	Notch position for 3PM
t	:	Time
τ	:	Delay parameter for 3PM

CHAPTER 1

Introduction

The enormous amount of information which modern man generates, and his desire to communicate this to his fellow man, has placed tremendous pressure on the existing communications structures. One element in this vast structure is the digital microwave radio link. As more information needs to be transmitted in the available spectral bandwidth, so the modulation schemes become more complex. Although the more complex schemes carry more information, they are also more susceptible to disturbances. One such disturbance is caused by the phenomenon of multipath, which occurs when there exists more than one route by which a transmitted signal can reach the receiver.

One method of counteracting the harmful effects of multipath propagation is to incorporate an adaptive equalizer into the receiver. The equalizer's function is to undistort the received data waveform by applying an estimate of the inverse transfer function of the propagation channel. The equalizer is said to be adaptive because it tracks the changing channel conditions. The fundamental theory relating to adaptive equalization is well established, however difficulties arise when one attempts to design a physical system and to specify the parameters of the equalizer. The biggest complicating factor is the limited performance of the hardware, which necessitates that certain compromises be made.

1.1. Dissertation overview

This dissertation investigates the effect of one of these compromises, that of reduced precision of the equalizer's coefficients. The equalizer is situated in the receiver of a 34Mbit/s digital radio employing Quadrature Phase Shift Keying (QPSK) as the modulation scheme. At this high data rate, conventional baseband equalizer implementation becomes very difficult. The main problem lies with the Very Large Scale Integration (VLSI) implementation of the multiplication circuitry, which is complex and requires much of the VLSI resources. If it were possible to constrain the equalizer coefficients to powers of two, the multiplication operation could be replaced by a shift

register. Shift registers are easy to implement at high speed and are hardware efficient. The use of non-optimal coefficients will, however result in inferior equalizer performance, but given the robustness of QPSK to multipath fading, this inferior performance may be acceptable.

A novel technique to adapt such a *power-of-two* equalizer has recently been considered by the author, but before its usefulness can be established, it is necessary to investigate what performance can be expected from an equalizer having *power-of-two* (PO2) coefficients.

With the above as an introduction, the objectives of this dissertation can be stated as follows:

1) Establish a theoretical basis for the investigation.

2) Implement a suitable computer simulation model from which performance comparisons can be made between different sets of equalizer coefficients.

3)Determine the performance of a 34Mbit/s QPSK modem during multipath conditions given the following:

a) There is no equalizer in the system.

b) There is a 7-tap equalizer with infinite precision coefficients.

c) There is a 7-tap equalizer with PO2 coefficients.

4) Draw conclusions as to whether the *power-of-two* equalizer is a practical consideration.

The investigation proceeded in the following manner. Firstly a literature search was conducted to establish the necessary background theory and to see what had been achieved in the field of adaptive equalization. A summary of the more relevant articles can be found in chapter three. Articles which are not of direct relevance to the topic of this dissertation, but which are of interest in a broader context, can be found in the bibliography.

The next task was to identify a suitable simulation program. It was decided to use SystemView from Elanix, as this is a powerful simulation tool for DSP and communications work, and it is extremely user friendly. A model for QPSK and a fading channel model were then implemented on SystemView. As the work in this dissertation is to form the basis of future baseband adaptive equalizer development, it was expedient to do the simulations at baseband in order to save on computer run-time. Therefore, the RF and IF stages, including the channel model, were transformed to their baseband equivalent. A fixed equalizer was used in a further attempt to keep the simulations simple. This is acceptable as it is the static, not the dynamic, behaviour of the equalizer which is under investigation in this dissertation. Details of the SystemView model can be found in chapter five.

In order to determine the performance of the fixed equalizer, it was necessary to be able to calculate the values of the coefficients to which the equalizer would have converged if it had been adaptive. Wiener filter theory, as presented in chapter four, was used to accomplish this.

In chapter six, the simulation results for the various coefficient sets are presented and discussed. Chapter seven draws conclusions as to the usefulness of a PO2 equalizer and makes recommendations for further study.

It is thought that an introduction to the multipath phenomenon is a good starting point. The next chapter looks at the physical mechanisms producing multipath, the probability of occurrence, multipath models and the means by which to assess multipath degradation on a radio link, that is the dispersion signature or M-curve.

1.2. Background information

At the start of this project an extensive hardware search was conducted to establish what hardware was available and at what cost. Custom made VLSI circuits performing adaptive equalization are available from Stanford Telecoms but are prohibitively expensive (approximately R4000) and are possibly an over-kill for the relatively simple QPSK modulation scheme. A chip set is also available from Broadcom for a very reasonable price, but it is subject

to a 10MBaud operating limit.

Various FIR filter structures of varying price, performance and length are available from GEC Plessey, Harris, Motorola, Atmel and Raytheon. A scheme was looked at in which the transversal filter was implemented using one of the above devices. Two methods were considered for the coefficient adaption. In the first method, a "snapshot" of data samples is taken. The adaption algorithm is calculated off-line in a fast digital signal processor and the updated coefficients then written back to the FIR filter. Such a scheme was prototyped but did not exhibit stable convergence behaviour. It was finally concluded that the Least Mean Squares (LMS) algorithm needs to operate on continuous adjacent samples and the coefficients need to be updated on every data sample, in order to converge. The implementation idea was inspired by reference [1] which demonstrated a working system. However, on closer reading it was noted that the authors had lowered the data rate such that all the coefficients were updated on every sample.

The second proposed method was to implement the coefficient adaption on a Field Programmable Gate Array (FPGA) where the coefficients would be updated on every sample, but there would be a slight delay in this process. The effect of this delay in coefficient adaption has been investigated in [2] and [3]. The algorithm is known as the Delayed LMS and has the disadvantage of slower convergence and hence inferior tracking ability. The circuitry to implement this scheme would be physically large and would cost about R1000 to implement.

Having considered the above options, it was proposed that the equalizer should be implemented on an Application Specific Integrated Circuit (ASIC), as is done by other digital radio manufacturers. However, due to the lack of expertise and the high cost involved, this was considered to be impractical. An FPGA can be programmed to perform the same function as an ASIC, but is cheaper and more flexible. The downside of the FPGA is that the capacity is smaller and the performance not as good as an ASIC so if this device were to be used to implement a complete adaptive equalizer, some simplifications and compromises would need to be made. Since the FPGA implementation is desirable, in spite of its inherent limitations, this investigation into the *power-of-two* compromise was undertaken.

1.3. Chapter references

1. Young, M.C.S. and P.M. Grant, **Reduction of multipath propagation effects in microwave digital radio communication systems.** Electronics and Communication Engineering Journal, February 1990, p.4-10.

2. Long, G., F. Ling and J.G. Proakis, **The LMS algorithm with delayed coefficient adaption.** IEEE transactions on acoustics, speech and signal processing, Vol. 37, No. 9, September 1989, p.1397-1405.

3. Long, G., F. Ling and J.G. Proakis, **Corrections to "The LMS algorithm with delayed coefficient adaption".** IEEE transactions on signal processing, Vol. 40, No. 1, January 1992, p.230-232.

CHAPTER 2

The phenomenon of multipath fading

Digital radio performance on line-of-sight (LOS) paths is degraded by two main effects, namely multipath distortion and rain attenuation. Below 10GHz multipath distortion is predominant whilst above 17GHz, rain attenuation is the predominant degrading factor [1]. As this dissertation is concerned with 8GHz carrier frequencies, performance degradation due to multipath distortions alone, will be considered.

2.1. Fundamental physics of multipath fading events

There are three situations which can result in fading of a received signal due to multiple propagation paths arriving at a receiver, namely, obstructions (diffraction), reflections and refraction. Figure 2.1 is a graphical presentation of the various forms of fading and demonstrates a typical AGC output of a receiver during multipath fading [2]. As the effects of obstructions and reflections can be minimised by the microwave link engineer using well established theory and methods [2], these effects will not be considered further. However, fading due to refraction is a function of the atmosphere and is not easily minimised by the link engineer. It is to this type of fading that the term *multipath fading* strictly applies. The mechanisms involved in producing multipath fading will now be discussed.

2.1.1. Atmospheric propagation

The index of refraction for the atmosphere is defined as the ratio of the velocity of light in a vacuum to the local velocity in the atmosphere. The spatial variations in the index of refraction are dependent upon meteorological conditions, that is, temperature, pressure and humidity. See the ITU-R recommendations [3] for the formulae to calculate the refractive index from meteorological data. The recommendation also has maps displaying the global seasonal values for the refractive index. It is the vertical variation of the index which significantly affects LOS links. For convenience the refractivity, N, is used and is defined as the number of parts per million that the index of refraction exceeds unity, that is:

$$N(h) = [n(h)-1]*10^6 \tag{2.1}$$

where *n(h)* is the index of refraction at an altitude of *h* kilometres.

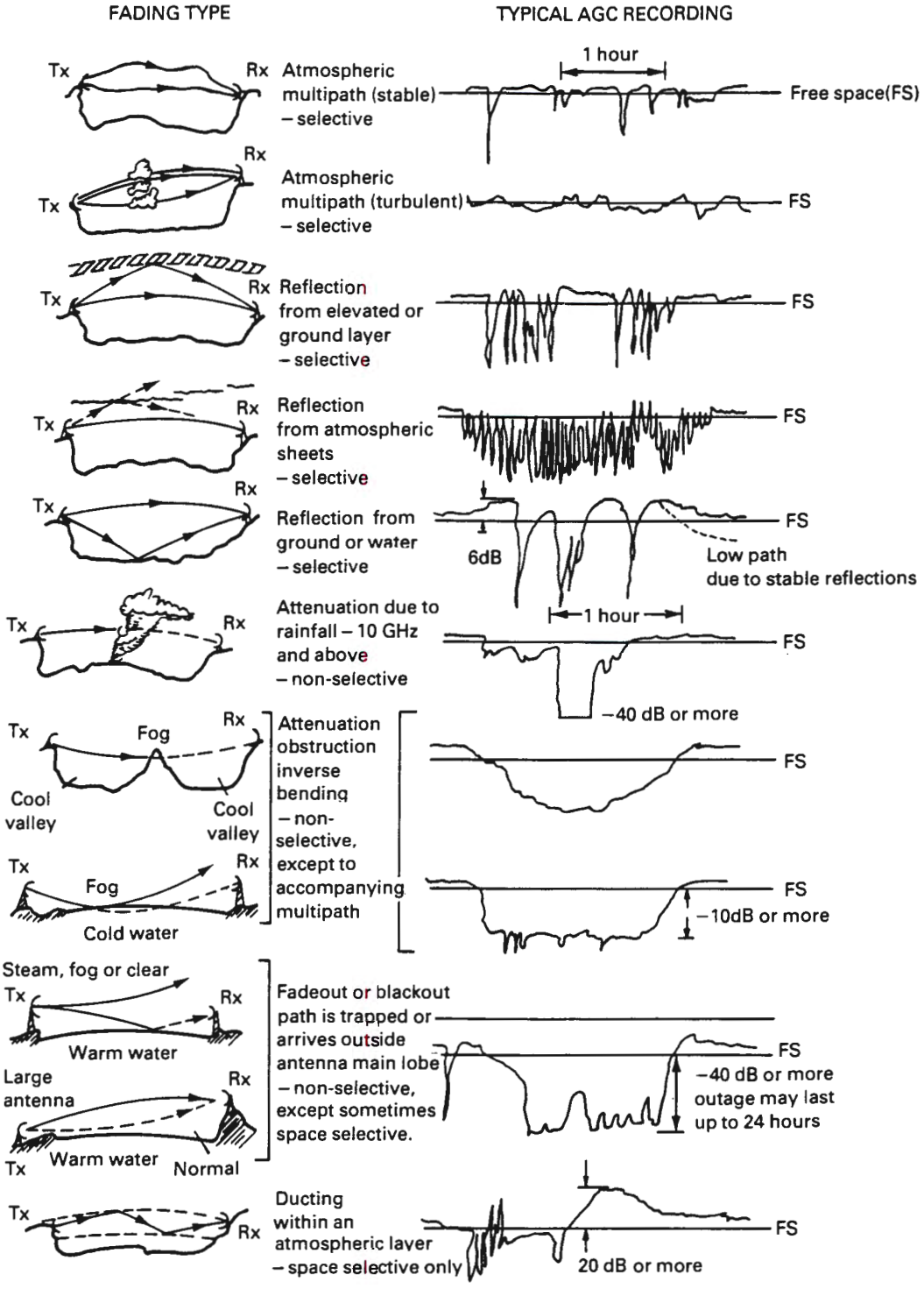

Figure 2.1: Fading types and receiver AGC recordings [2, p.249]

Using Snell's law it can be shown that a ray path of a wave travelling nearly horizontally through the atmosphere has a curvature given by:

$$\frac{1}{\epsilon} = -\frac{dn}{dh} \tag{2.2}$$

where ϵ is the radius of curvature.

The reference value for *dN/dh* is -40 N units/km, yielding a radius of curvature of about 4*a*, where *a* is the radius of the earth ($6.37*10^6$m). Figure 2.2a shows such a path with a curvature $1/\epsilon$ above the earth, which has a curvature of $1/a$. Figure 2.2b shows a transformation of the co-ordinates to make the ray path straight. This transformation results in an effective radius for the earth as follows:

$$a_{effective} = k.a \tag{2.3}$$

where *k*, known as the k-factor, is given by:

$$k = \frac{1}{1 + a\frac{dn}{dh}} \tag{2.4}$$

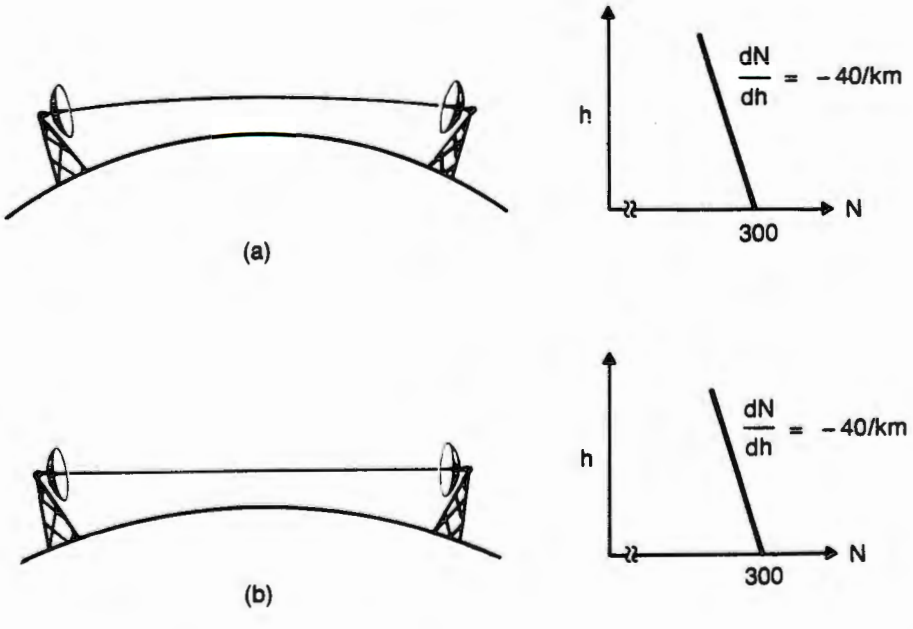

Figure 2.2: Ray propagation over true earth (a) and transformed earth (b) [4, p.131]

For a standard atmosphere with $dn/dh = -1/4a$, k has the value of 4/3. As has already been noted, k depends on meterological data, which translates to the effective radius of the earth changing as the atmospheric conditions change. Figure 2.3 shows the situation with $k = 2/3$, in which the *earth bulge* interferes with the desired signal causing obstruction fading. This occurs in sub-refractive atmospheres, that is when $dN/dh > -40$ N units/Km. When $dN/dh < -40$ N units/Km the atmosphere is described as being super-refractive, but does not result in fading.

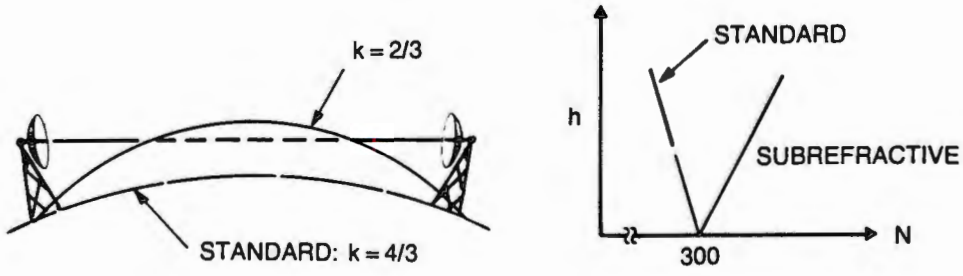

Figure 2.3: Propagation in a sub-refractive atmosphere [4, p.132]

2.1.2. Ducting conditions

When the atmosphere is extremely super-refractive ($dN/dh < -100$ N/Km) over a limited altitude range as shown in figure 2.4, ducting can occur. This would typically occur on a hot, humid, cloudless and wind-still summer evening. In figure 2.4 the transmitter and receiver are located at an altitude of 100m and the duct at 150m. A vectorial combination of these rays produce a fade that varies with frequency within the radio channel. This effect is known as *frequency-selective fading.*

From the above discussion, it can be seen that the refractivity gradient statistics for the 100m of atmosphere directly above the surface of the earth, are useful for estimating the probability of the occurrence of ducting and hence multipath conditions. When more reliable data is not available, charts [3] can be used which show the percentage of time that $dN/dh <= -100$ N/Km for different seasons.

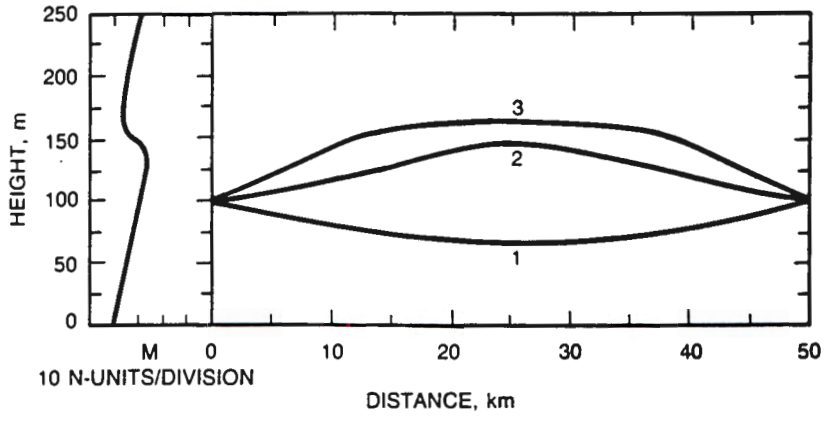

Figure 2.4: A ducting situation [4, p.133]

2.2. Probability of occurrence and rates of change

2.2.1. Narrow-band measurements

Owing to the fact that accurate measurements of the refractive index over a LOS path is extremely difficult, multipath fading can not be related directly to parameters describing the atmosphere, but must be characterised by making propagation measurements on actual paths. One of the most extensively measured quantities is the single-frequency (narrow-band) received power. Figure 2.5 shows a trace of the received signal power at 6GHz on a 42.5 km path during a period of multipath fading [4]. The rapid changes in signal strength are apparent, as is the randomness of the discrete fading events.

For narrow-band or low capacity digital systems (<= 10 Mbits/s [5]), the statistics of single frequency fading at the carrier frequency, determine the statistics of system performance. These statistics are described by the time-faded-below (TFB) distribution of the fade level. For fade levels deeper than 20dB, the fade time is proportional to the square of the relative received signal voltage. Using this as a basis, researchers developed the results presented in the next section.

2.2.2. Narrow-band fading distributions

In the ITU-R recommendations [6], a method is presented for predicting narrow-band fading distribution for any part of the world. The path profile can be included in these calculations, but

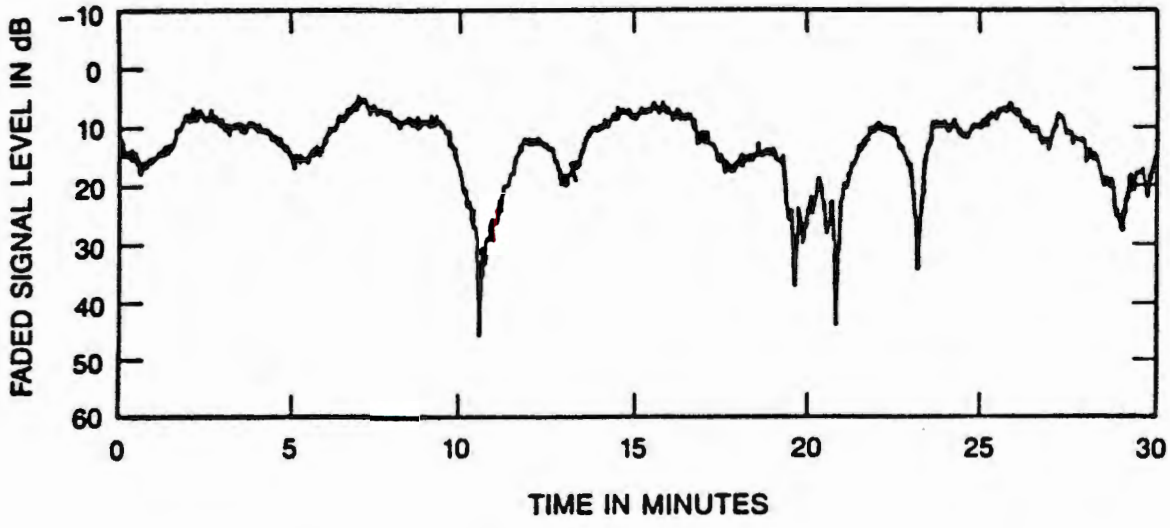

Figure 2.5: Received signal strength during multipath fading [4, p.161]

will not be considered here. The percentage time that a narrow-band fade depth A (dB) is exceeded in the average worst month is given by:

$$p_w = K \cdot d^{3.6} \cdot f^{0.89} \cdot 10^{-\frac{A}{10}} \quad \% \tag{2.5}$$

for fade depths greater than 15dB or for $p_w < 0.1\%$, whichever is greater. K is the geoclimatic factor pertaining to a certain region of the globe and will be discussed below, d is the distance in km and f is the frequency in GHz. From **(2.5)** it can be seen that the probability of fading increases dramatically with increasing path length.

To establish K within Africa, the following formulae are applied depending on the terrain:

$K = 10^{-6.2} p_L^{1.5}$ - for overland links for which the lower of the transmitting and receiving antennas is less than 700m above mean sea-level.

$K = 10^{-6.8} p_L^{1.5}$ - for overland links for which the lower of the transmitting and receiving antennas is higher than 700m above mean sea-level.

$K = 10^{-5.6} p_L^{1.5}$ - for links over medium sized bodies of water, coastal areas beside such

bodies of water, or regions of many lakes.

$K = 10^{-5.2} p_L^{1.5}$ - for links over large bodies of water or coastal areas beside such bodies.

The value for p_L, the percentage of time that the average refractive gradient in the lowest 100m of the atmosphere is less than -100 N/km, can be estimated from the charts mentioned in section 2.1.2.

2.2.3. Fading occurrence as a function of path length

For fade depths less than 15dB, a more complicated calculation needs to be followed as given in [6]. This procedure was used to obtain figure 2.6. This graph shows the percentage time a certain fade depth is exceeded for a given distance. The geoclimatic factor was calculated assuming an overland path within South Africa, at sea-level during November. The graph was produced using a Mathcad sheet, a copy of which is included in appendix I.

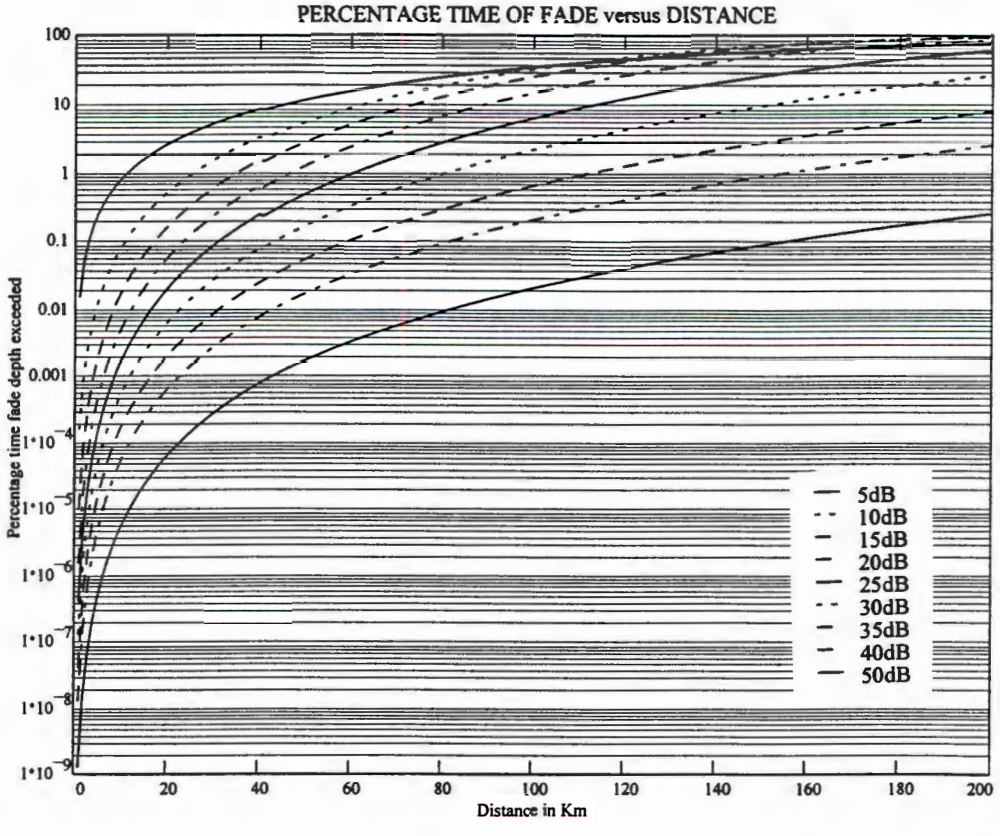

Figure 2.6: Graph of percentage time that fade-depth(A) is exceeded versus distance

2.2.4. Rates of change associated with fading events

From reference [7], it appears that a fade rate of 100dB/s is considered an upper bound to the rate at which a notch can form within the channel bandwidth. For highly dispersive paths, the power of the received signal fades at a lower rate because the signal covers a wide bandwidth.

Typical measurements of notch speed as the notch moves through the channel, are from 10-30MHz/s, with some measurements indicating notch speeds ranging up to 100MHz/s.

2.3. Multipath fading models

In order to estimate the performance of a digital radio during periods of frequency selective fading, it is necessary to have a statistical model of the fading channel. The most widely used is the *simplified three-path model* (3PM) developed by Rummler [8] in 1978. The simpler *two-path model* (2PM) is more intuitive and is often used in theoretical investigations. The 2PM's transfer function is a special case of the 3PM, but the statistics describing the model parameters are completely different. Other models, such as the polynomial model [9], do exist but these will not be considered.

Assuming the multipath fading channel to be linear, the fading can be characterised by a transfer function of the channel $H(f,t)$, which is a two dimensional random process in frequency f and time t. For any continuous random process, the minimum separation required to guarantee decorrelation with respect to each argument can be determined [10].

For the time varying transfer function $H(f,t)$, let t_d and f_d be the decorrelation separations in the time and frequency variables, respectively. If t_d is a measure of the time correlation in seconds, then:

$$\sigma_t = \frac{1}{2\pi t_d} \quad Hz \tag{2.6}$$

is a measure of the fading rate or bandwidth of the random channel. The quantity σ_t is often referred to as the *Doppler spread* because it is a measure of the width of the received spectrum when a single sine wave is transmitted through the channel.

The dual relationship for the frequency decorrelation f_d in hertz suggests that a delay variable:

$$\sigma_f = \frac{1}{2\pi f_d} \quad seconds \tag{2.7}$$

defines the extent of the multipath delay. The quantity σ_f is often referred to as the *multipath delay spread* as it is a measure of the width of the received process in the time domain when a single impulse function is transmitted through the channel.

A typical value for the fade rate or Doppler spread over 30 to 70km microwave radio transmission paths is 0.01Hz and the multipath delay spread is typically less than 10ns with 6.3ns being widely used [11].

If it is assumed that the time variation of the channel response is much slower than the dynamic response of the radio equipment and that the performance of the radio at any time is uniquely related to the current state of the channel (i.e. there is no hysteresis in the system behaviour), then the dependence on time can be ignored for modelling purposes [7].

2.4. Simplified three-path model (Rummler's model)

A three-path model can be written as [12]:

$$S_r(t) = S(t) + \alpha S(t-\tau_1) + \beta S(t-\tau_0) \tag{2.8}$$

which in the frequency domain is equivalent to:

$$G_r(w) = G(w).(1 + \alpha e^{-jw\tau_1} + \beta e^{-jw\tau_0}) \tag{2.9}$$

The transfer function of the channel is:

$$H(w) = 1 + \alpha e^{-jw\tau_1} + \beta e^{-jw\tau_0} \tag{2.10}$$

Since we are dealing with bandpass channels it is convenient to regard w as $(w\text{-}w_c)$, where w_c is a reference frequency, conveniently set to the channel centre. Then $|w| \leq B/2$ where B is the bandwidth of the RF channel. The first premise of the Rummler model is that $B\tau_1 \ll 1$ which implies that $e^{jw\tau_1} \approx 1$. Then by setting $\tau_0 = \tau$, **(2.10)** can be written as:

$$H(w) = 1 + \alpha + \beta e^{-jw\tau} \qquad \textbf{(2.11)}$$

The next step in the model is to identify a *notch* frequency w_0 (with respect to the reference) for which $H(w)$ is a minimum. Hence the final form of the model is:

$$H(w) = a[1 - be^{-j(w-w_0)\tau}] \qquad \textbf{(2.12)}$$

where $a = 1 + \alpha$ is the overall attenuation parameter and $b = -\beta/(1+\alpha)$ is called a shape parameter. Notice that, because of the assumptions made, the three-path model is effectively the same as a two-path model.

Equation **(2.12)** has too many variables to be useful, and so Rummler showed that the delay was the only parameter that could be fixed to produce a reasonable model. Originally, τ was chosen to be the reciprocal of six times the measurement bandwidth, which happened to be 6.3ns. This value has become the standard, although any value may be used which permits **(2.12)** to be fitted to almost all fading events for some choice of a, b and w_0. Therefore, no physical significance should be placed on the delay, τ. It must also be noted that the joint statistics of these fitted parameters will depend on the choice of τ.

The squared-amplitude response of this channel is:

$$|H(w)|^2 = a^2[1 + b^2 - 2b.\cos(w - w_0)\tau] \qquad \textbf{(2.13)}$$

and the group delay is given by the negative derivative of the phase characteristic:

$$D(w) = -\frac{d\phi(w)}{dw}$$

$$= \tau \frac{b(b - \cos(w - w_0)\tau}{1 + b^2 - 2b.\cos(w - w_0)\tau} \qquad \textbf{(2.14)}$$

If $b<1$ the transfer function is *minimum-phase* since it only has zeros in the left-half of the s plane. For $b>=1$, the transfer function is nonminimum-phase because its zeros are in the right-half of the s plane. Typical amplitude and delay responses based on **(2.13)** and **(2.14)** are shown in figure 2.7.

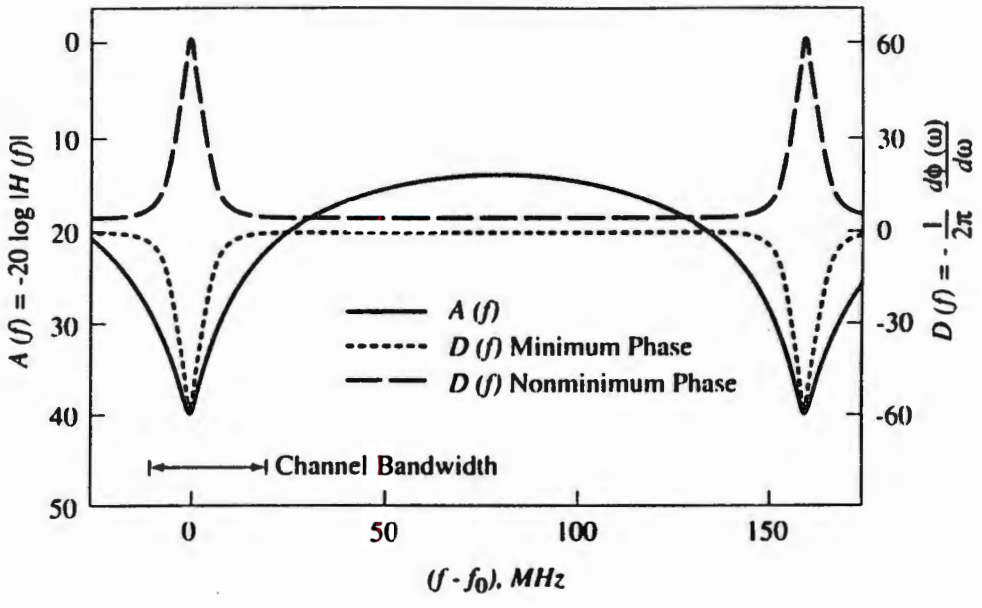

Figure 2.7: The transfer function of Rummler's fading channel model [12, p.380]

For minimum-phase fades, the fade level is measured in decibels as:

$$A = -20 \log (a) \qquad \textbf{(2.15)}$$

and the relative notch depth is:

$$B = -20 \log (1 - b) \qquad \textbf{(2.16)}$$

For nonminimum-phase fades, the range of b is unbounded and it is convenient to rephrase **(2.12)** as:

$$H'(w) = ab\left[e^{-j(w-w_0)\tau} - \frac{1}{b}\right] \qquad \textbf{(2.17)}$$

and we can now define:

$$A = -20 \log (ab) \qquad \textbf{(2.18)}$$

$$B = -20 \log (1 - 1/b) \qquad \textbf{(2.19)}$$

The minimum and nonminimum-phase fades are equally likely to occur.

The validity of the model was confirmed by fitting measured propagation data to the model derived from 25000 swept-frequency scans, representing 8400s of fading activity. By analysing the errors in fitting the observed characteristics to the model, Rummler was able to show that the simple three-path model is indistinguishable from a perfect model of a LOS microwave radio channel.

Concerning the statistics of the model, Rummler showed that the distribution of the notch frequency is independent of the other parameters and is uniform over all frequencies of interest. The relative notch depth, B, and the fade level, A, are partially correlated. The B distribution is a one-sided exponential and the A distribution is Gaussian.

2.5. Multipath dispersion signatures

A dispersion signature, or M-curve, is an effective means of characterising the performance of a digital radio system during multipath fading conditions. The concept of an M-curve, so named from its distinctive M shape, was introduced by Emshwiller [13] in 1978.

An M-curve is measured by introducing a 3PM notch at a specific frequency. The notch depth is then increased until a certain BER is obtained. This point is plotted and the procedure repeated for the next frequency. Eventually an M-shaped contour of equal BER's is obtained, and the area

below the curve indicates the outage region. Figure 2.8 shows a typical curve. Note that the value of τ must be displayed as different values will result in different curves.

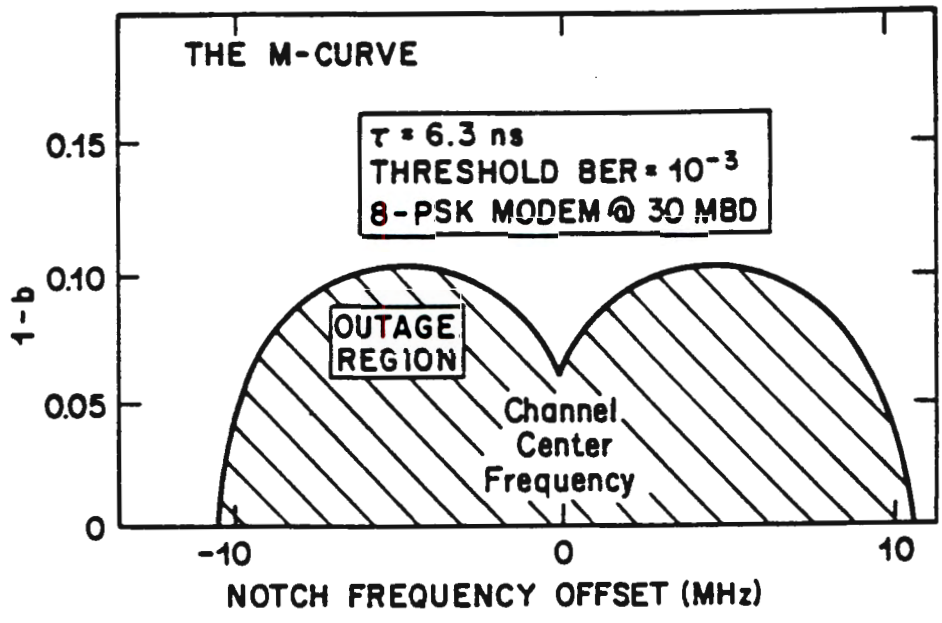

Figure 2.8: Typical dispersion signature or M-curve [18, p.183]

The width of the signature curve is not usually much larger than the channel bandwidth, reflecting the fact that the most damaging notches are the ones that occur in-band. The dip at the centre signifies that slightly off-centre notches can be worse than centered ones because they introduce more cross-channel interference. Emshwiller was able to show, using a 2PM, that the conditional outage probability due to multipath distortion is proportional to the mean-squared value of the τ - distribution.

This important scaling relationship for distortion-dominated receivers was separately derived by Campbell and Coutts [14], who showed additionally that the outage time scales with the square of the symbol rate, $1/T$. This knowledge permits the radio system investigator to measure a single signature curve, integrate the appropriate pdf over the interior of that curve, and scale the result by a simple rule to obtain outage for any $\overline{\tau}^2$ and $1/T$.

The utility of a single signature curve in assessing outage applies equally well to the simplified three-path model. In this case, τ in **(2.12)** is fixed at 6.3ns. Having obtained a single curve of critical B versus w_0, conditional outage probability is found by just integrating the joint pdf of B and w_0 over the outage region defined by this curve.

The influence of equipment characteristics is directly expressed by the area of the measured signature. A normalized system parameter K_n can be used for this purpose [15]. Conceptually, one can consider the normalised system parameter as being evaluated from a *normalized system signature* . If one scales system signatures to a specific baud period (1ns) and relative echo delay (1ns), then such scaled system signatures, known as *normalized signatures*, are a characteristic of the system parameters such as modulation method, roll-off factor and type of equalizer. Using a rectangular approximation for the signature, K_n is given by:

$$K_n = \frac{T^2.W.\lambda_a}{\tau_r} \qquad \textbf{(2.20)}$$

where: T : system baud period (ns)

W : signature width (Ghz)

λ_a : average of (linear) signature, $\lambda_c(w) = 1 - b_c(w)$

τ_r : reference delay for λ_a (ns)

Table 2.9 shows values of K_n for receivers without adaptive equalization. The use of adaptive baseband transversal equalizers improves system performance so that the figures in table 2.9 are reduced by approximately one tenth.

Modulation method	K_n
64-QAM	15.4
16-QAM	5.5
8-PSK	7.0
QPSK	1.0

Table 2.9: Values for K_n for various modulation methods

2.6. Multipath fading counter-measures

There are a number of countermeasures to compensate for the damaging effects of the channel transfer function described by Rummler's model, namely: space diversity combining; multi carrier operation (frequency diversity); forward error correcting (FEC) codes; cross-polarisation interference cancellation; and adaptive equalization.

2.6.1. Space and frequency Diversity

The effect of fading on the availability of a digital radio link can be minimized by space or frequency diversity techniques, as illustrated in figure 2.10 [16]. Both of these techniques are based on the hypothesis that simultaneous fading on both radio transmission paths is unlikely.

In a frequency diversity configuration the same digital information is fed into two transmitters, Tx 1 and Tx 2. A wide radio-frequency separation of these transmitters ensures less correlation between the fades of the individual radio waves. This results in better system performance.

In the space diversity system the same radio frequency band is used for the transmission of the digital information. Diversity results from separating the two receiver antennas in a vertical plane. This ensures that the radio waves travel through different transmission paths. This reduces the chance of both receivers being simultaneously affected by fading.

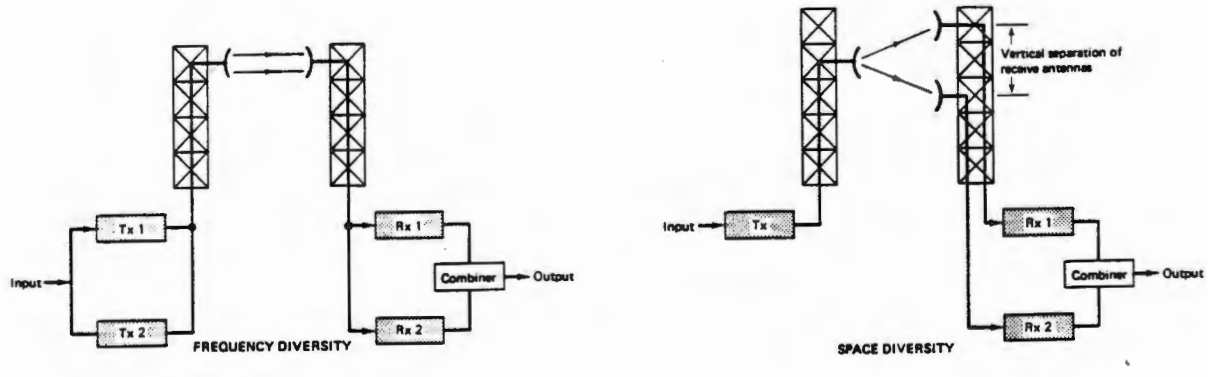

Figure 2.10: Illustration of frequency and space diversity [16, p.217]

2.6.2. Equalization

Adaptive equalizers, in conjunction with space diversity, are the most widely used form of fading counter-measures in digital radio systems due to their ability to compensate for the time varying nature of the transmission channel. There are two main types of equalizers, the frequency domain equalizer and the time domain equalizer.

2.6.2.a. Frequency domain equalization (FDE).

FDEs operate at the IF and correct for amplitude distortions in the receiver's passband. The most simple form is the *slope equalizer* which restores the spectrum by introducing an amplitude tilt. They can only compensate for fades which produce nulls out of the band. To overcome this, more complex notch equalizers have been used but their performance under nonminimum-phase fading is limited.

Adaptive transversal equalizers can be implemented at IF but the delayed samples must feed complex weighting networks. The IF equalizer has lower complexity but is difficult to implement digitally, which is the preferred solution for accuracy. For more information on analog IF equalizers, consult the book by Baccetti and Tartara [17].

2.6.2.b. Time domain equalization (TDE).

TDE is the popular implementation due to the advances in VLSI technology. In addition to compensating for the distortions in amplitude response, it is able to compensate for group delay distortions as well. Implementation of the TDE requires a tapped delay line. Each tap is fed to a multiplier, the other input to the multiplier is fed with a value determined by the adaption algorithm. The multiplier outputs are then all summed together. This structure is known as a *transversal filter*.

From an examination of the various pulse shapes during fading, it has been concluded that most of the inter-symbol interference comes from immediately neighbouring symbols to the symbol under decision. For this reason, the number of taps for digital radio systems is typically 5 or 7. Usually the centre tap is considered as reference, and taps on the right of the centre compensate

for postcursor ISI, whereas taps on the left compensate for precursor ISI.

Nonlinear or decision feedback (DFE) equalizers very effectively cancel postcursor ISI by using the knowledge of previous symbols stored in feedback tapped delay lines. Their main advantage is that the cancellation of the ISI is virtually noise-free, and effective equalization for deep notches is possible. The main drawback of this equalizer is the limited improvement during nonminimum-phase fading where most of the ISI comes from precursors. They also suffer from error propagation. This occurs when an incorrect decision is fed back causing the equalizer to reflect this error for the duration of several symbols.

Initially, equalizers with tap spacing equal to the symbol period were developed, but the use of fractionally spaced taps, that is less than the symbol period, increases the tolerance of the receiver to inaccuracies in the recovered clock. An additional advantage of a fractionally spaced equalizer is that the equalizer will adapt in such a way as to implement a matched filter at the receiver.

2.7. Chapter references

1. Recommendation ITU-R F.1101, 1994, **Characteristics of digital radio-relay systems below about 17GHz.** p.231-249.

2. Townsend, A.A.R., **Analog line-of-sight radio links.** Prentice-Hall, UK, 1987.

3. Recommendation ITU-R PN.453-4, 1994, **The radio refractive index: its formula and refractivity data.** p.206-213.

4. Ivanek, F., **Terrestrial Digital Microwave Communications.** Artech House, 1989, CH4.

5. Recommendation ITU-R F.1101, 1994, **Characteristics of digital radio-relay systems below about 17GHz.** p.231-249.

6. Recommendation ITU-R PN.530-5, 1994, **Propagation data and prediction methods required for the design of terrestrial line-of-sight systems.** p.297-318.

7. Rummler, W.D., R.P. Coutts and M. Liniger, **Multipath fading channel models for microwave digital radio.** IEEE Communications Magazine, Nov 1986, Vol. 24, No. 11, p.30-42.

8. Rummler, W.D., **A new selective fading model: application to propagation data.** Bell Systems Technical Journal, 1979, 58, p.1037-1071.

9. Wong, W.C. and L.J. Greenstein., **Multipath fading models and adaptive equalizers in microwave digital radio.** IEEE Transactions on Communications, Aug 1984, Vol. COM-32 No.8, p.928-934.

10. Monsen, P., **Fading channel communications.**, IEEE Communications Magazine, Vol 18, Jan 1980, p.27-36.

11. Young, M.C.S. and P.M. Grant., **Reduction of multipath propagation effects in microwave digital radio communication systems.** Electronics and Communication Engineering Journal, Feb 1990, p.4-10.

12. Jeruchim, M.C., P. Balaban and K.S. Shanmugan, **Simulation of communication systems.** Plenum Publishing Corporation, New York, 1994, p.379.

13. Emshwiller, M., **Characterization of the performance of PSK digital radio transmission in the presence of multipath fading.** Microwave digital radio, IEEE press, 1988, p.209-214.

14. Campbell, J.C., and R.P. Coutts, **Outage prediction of digital radio systems.** Microwave digital radio, IEEE press, 1988, p.78-79.

15. Recommendation ITU-R F.1093, 1994, **Effects of multipath propagation on the design and operation of line-of-sight digital radio-relay systems.** p.50-61.

16. Feher, K., **Digital Communications - Microwave applications.** Prentice-Hall, Englewood Cliffs, New Jersey, 1981, p. 216.

17. Baccetti, B., and G. Tartara, **Equalization and quality predictions in digital radio systems.** GTE Telecomunicazioni S.p.A, 1983.

18. Greenstein, L.J. and M. Shafi, **Outage calculation methods for microwave digital radio.** Microwave digital radio, IEEE press, 1988, p.179-187.

CHAPTER 3

Literature overview

For a good introduction to the subject of adaptive equalization, read the paper by Qureshi [1] or chapter 12 of reference [2]. References [3], [4], [5], [6], [7], and [8] can also be consulted for introductory information on adaptive equalization. The book by Ivanek [9] is a useful general introduction. For an overview of the historical development of this subject, read chapter 1 of Haykin's book [10]. This book is also an excellent source of information on various structures and algorithms which can be applied to the equalization problem. For the remainder of this chapter, a more detailed look will be taken at some specific papers which are relevant to the subject matter of this dissertation.

3.1. Performance of QPSK during frequency-selective fading.

Jakes [11] in 1979, was the first researcher to do a theoretical analysis of the effects of multipath on a digital transmission system. His method was to assume that excessively high BER ($>10^{-2}$) would occur if the total peak-to-peak envelope delay distortion contained within the channel bandwidth is some fraction k of the symbol length of the digital signal being passed through this bandwidth. Correlating his theoretical calculations with observations from laboratory experiments in which a simulated two path propagation situation was present, he was able to establish that k was equal to 0.7 for QPSK. This result agrees with that obtained by Ott et al [12]. (In [12], the authors performed measurements on a physical QPSK system to establish the BER performance as a function of two path delay, normalized to a symbol period.) Jakes then used this value of k to obtain the following formula which estimates the critical value of delay, τ_c, which, if exceeded can cause a QPSK system to "break":

$$\tau_c \approx 0.75\ (1-r)\ T \qquad \textbf{(3.1)}$$

where: r is the relative amplitude of the secondary ray ($r < 1$)

T is the symbol length in nanoseconds

For example, a 34MBit/s QPSK system has a symbol length T = 59ns. If a maximum fade of 20dB (r=0.9) occurred at the band edge, the system would "break" if the delay exceeded 4.43ns. Ruthroff's paper [13] gives an expression for the maximum value of delay difference τ_m for paths propagating through an atmospheric model containing a layer of air having an anomalous refractive index, as:

$$\tau_m = 1.11 * 10^{-4} \, d^3 \qquad \textbf{(3.2)}$$

where: d is the pathlength in kilometers

τ_m is maximum delay difference in nanoseconds

Applying this result yields a path length of 34Km. Thus for paths less than 34Km and fades less than 20dB, a 34MBit/s QPSK system should be functional (BER < 10^{-2}) without an adaptive equalizer. Although this result is not particularly useful, it gives one a feel for the order of magnitude involved.

Reference [14] compares the performance of different digital radio techniques in the presence of multipath fading. The performance measure used is the expected fraction of time, conditioned on the occurrence of a fading event, that the eye pattern at the receiver is closed. This measure is plotted against spectral efficiency (bit rate divided by channel bandwidth) for various modulation schemes, including QPSK, and for various forms of carrier recovery, timing recovery, Tx/Rx filtering and equalization. The fading model used is that of a first order complex polynomial. As the study is of a comparative nature, quoting isolated results is meaningless, but the major principles identified by their study are as follows:

- The specific types of spectral shaping (raised-cosine versus bandpass filtering), carrier recovery, and timing recovery used in a digital radio design do not have major impact on the performance during multipath fading events.

- Higher-level modulation schemes perform better during multipath fading, *for a given bit rate and bandwidth.* The reason being that their lower symbol rates permit less severe

spectral shaping. When the spectral shape is narrowed, the side lobes of the pulse shape increase and result in increased potential for interference.

- Offset modulation schemes, while offering a more constant RF envelope than non-offset schemes, display inferior performance during multipath fading events.

A more recent paper written by Metzer and Valentine [15], investigates the sensitivity of different modulation techniques to frequency-selective fading. The performance of these techniques during multipath fading are compared on the basis of signatures calculated for idealized systems. To compute the signatures, it is necessary to know how the two-path fading conditions affect the carrier phase and timing offset. The same methods are used as in [14], but it is shown that fourth powers of the signal produced by the non-linear timing recovery circuit need to be included for more accurate results. This is especially true for QPSK.

Figure 3.1 shows the result of calculations (solid line) and measurements (dashed) for an offset QPSK 34MBit/s system with a roll-off factor of 0.8. Note that the width of the signature is almost independent of the delay time τ.

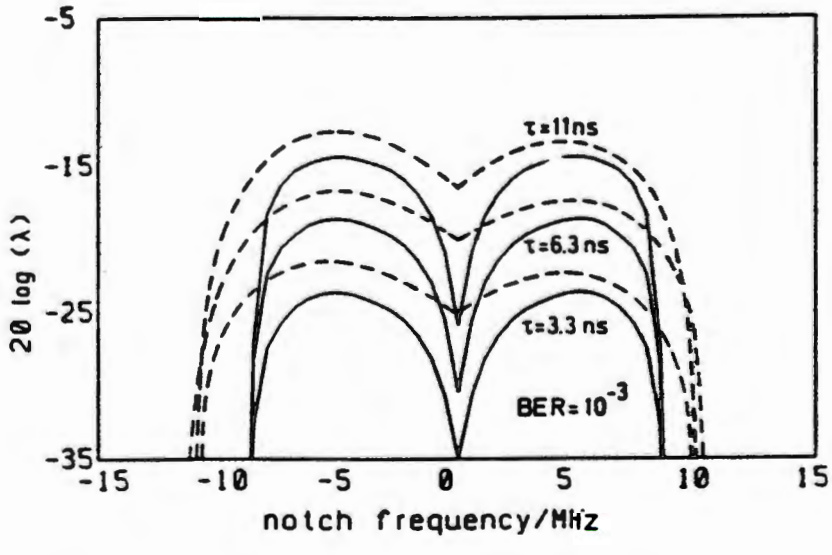

Figure 3.1: Measured and calculated signatures for different delay times [15, p.990]

To compare different modulation techniques, the difference in spectral efficiency needs to be taken into account. Comparisons can only be made on the basis of equal bit rates R or equal overall IF bandwidths W. For the investigated modulation schemes and a rolloff factor of 0.5, the spectral efficiency in bits/s/Hz is equal to R/W = 2.66 for 16 QAM, 2 for QPRS, and 1.33 for QPSK. In the results shown in Figure 3.2 for equal bit rates, the occupied overall bandwidth is therefore 52.5, 70, and 105 MHz, respectively. In Figure 3.3 for the same modulation schemes, the bandwidth is fixed at 52.5 MHz, resulting in a bit rate of 140, 105, and 70 Mbit/s, respectively. All cases show that QPSK is more robust than the higher level modulation schemes, with the disadvantage, however, of a lower spectral efficiency.

The paper ends with an example of how outage probability can be calculated and this result is used in predicting the probability of outage versus path length in a Rician fading channel over north west Europe. Figure 3.4 shows the results for different modulation schemes operating at 140MBit/s.

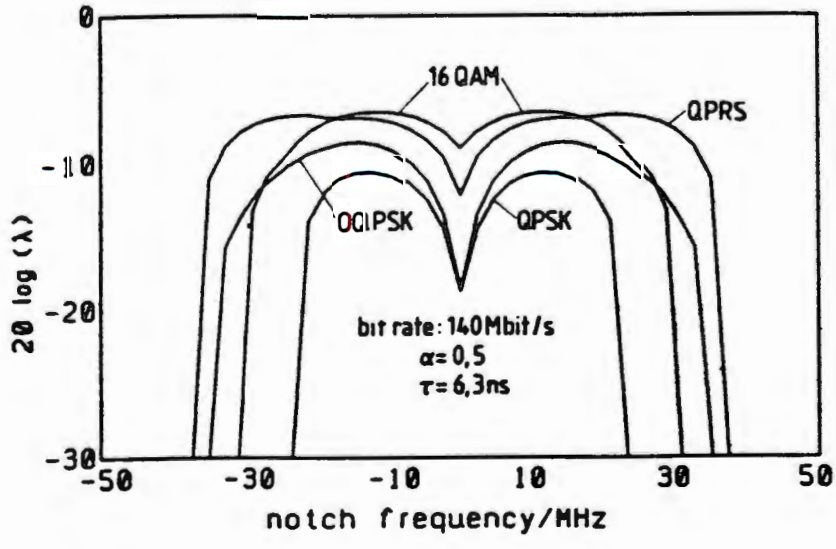

Figure 3.2: Calculated signatures for equal bit rates [15, p.990]

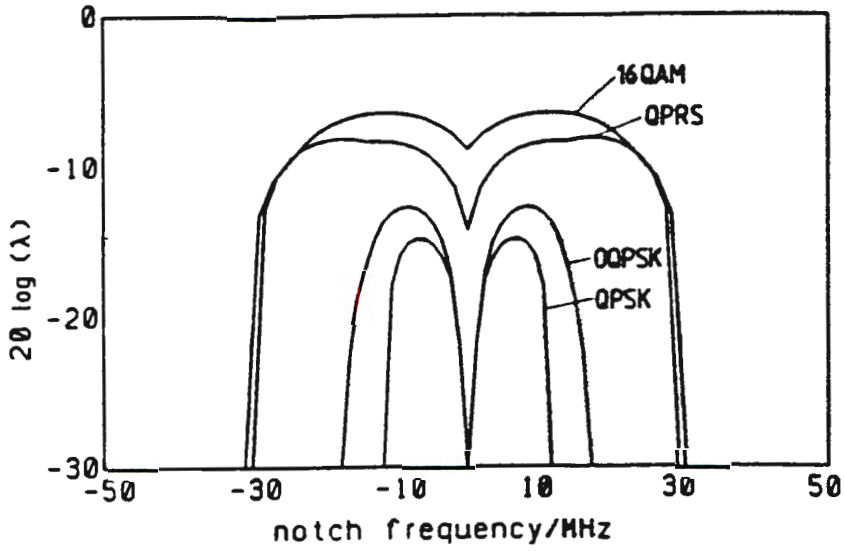

Figure 3.3: Calculated signatures for equal overall bandwidth [15, p.991]

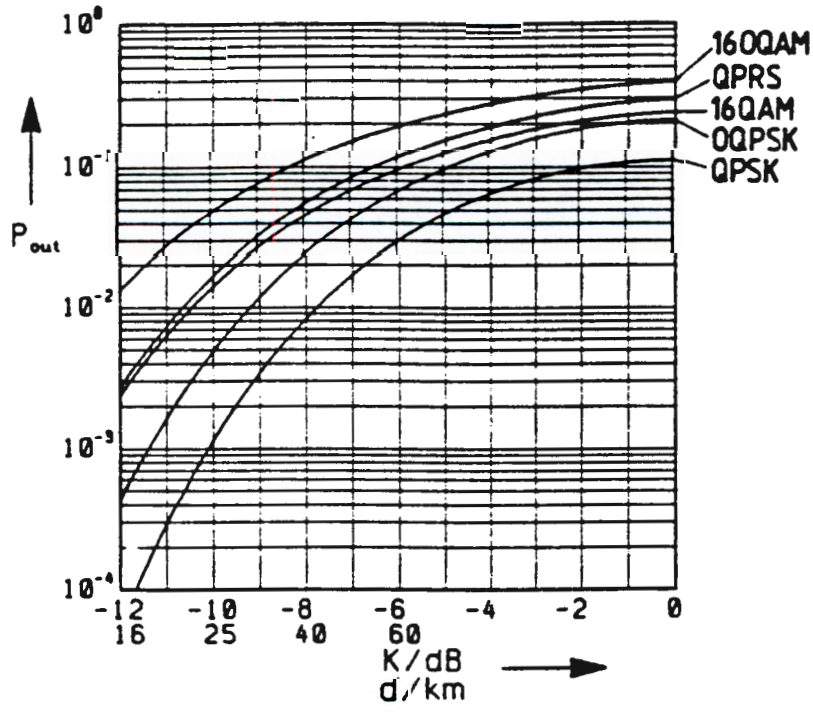

Figure 3.4: Calculated probability of outage versus path length [15, p.992]

In reference [16], Marias et al, studied the effects of the amplitude and delay slope components of frequency-selective fading on QPSK having a bit rate of 44.7MBit/s. As an example of the results obtained, an amplitude slope of 0.3dB/MHz in the passband will result in a 1.2dB degradation in the S/N ratio for a probability of error P_e of 10^{-4}. In a perfect QPSK system, an E_b/N_0 ratio of approximately 8.3dB results in a P_e of 10^{-4}. However, the presence of the 0.3dB/MHz slope implies that an E_b/N_0 of 9.5dB is needed to achieve the same performance. A delay slope of 0.3ns/MHz results in approximately 0.2dB S/N degradation.

3.2. Performance improvement via equalization

The earliest paper presenting the performance results for transversal-filter equalization of QPSK signals with two-component multipath and demodulator phase error, was written by Ziemer and Ryan in 1973 [17]. A summary of the same paper can also be found in [5]. This text provides a good insight by developing an analytical expression for optimum minimum mean-square-error tap weights, in terms of the multipath and signal parameters. Probability of error results for no equalization and for equalization with optimal tap weights (2 and 4 complex taps) are compared. The improvement gained through equalization is greatest for high crosstalk situations. Demodulator phase error is a cause of crosstalk, and it is demonstrated that a 4 tap equalizer is capable of fully compensating for demodulator phase errors of 10°. This ability permits less stringent specifications to be placed on the carrier acquisition loops in the receiver.

Reference [18] is a very informative paper on the performance of digital radio systems which incorporate finite-tap adaptive equalizers. Unfortunately, results are only presented for 16, 64 and 256 QAM systems. The major finding of the study is that very few taps (of the order of 5) are needed to approximate the performance of an ideal infinite tap equalizer. It was found that a simple, sub-optimal form of timing recovery is generally adequate, and that fractionally spaced equalizers are more advantageous than symbol spaced equalizers having the same number of taps. *However, this advantage is minor for systems having a raised-cosine roll-off factor of 0.5 or larger, but increases dramatically as the roll-off factor approaches zero.*

3.3. Multiplication-free transversal equalizers.

The papers of most relevance to this thesis are [19] and [20]. Having checked the citation indexes, these papers do not appear to have been cited again in connection with equalizer work. A possible reason for this apparent lack of interest is that digital radio manufacturers are implementing their adaptive equalizers on ASIC's, which have vast logic resources and very high performance. However, if one does not want to invest the large sums of money required for ASIC development, the next best solution is to consider an FPGA implementation. As an FPGA has lower performance and is more limited in its resources, the hardware implementation has to be simplified. Using PO2 coefficients is a good means of achieving this simplification, but leads to new questions as to what performance can be expected and what algorithm would be used to adapt this simplified structure.

These issues were first addressed in 1980 by Yan and Yao [19]. Their paper starts by presenting the standard theory on Wiener filters (see next chapter) as applied to a simple Tapped Delay Line (TDL) structure. The optimal taps can be calculated using Wiener theory, but an optimization procedure is needed to find the optimal PO2 coefficients. The Branch-and-Bound search procedure was chosen for this, and an algorithm based on this technique is then developed. As this algorithm appears to be too complex to implement in VLSI, it will not be discussed here. The paper ends by presenting results for an 11-tap (real coefficients) TDL structure operating an a dispersive channel with impulse response as shown in figure 3.5.

In figure 3.5, the mean square equalization error of the above channel is given for a 6-bit Max quantizer [21]. (A Max quantizer is optimal in the sense of introducing a minimum mean square error for Gaussian inputs.) The top solid curve represents the classical minimum mean square error solution while the middle dashed line represents the optimal multiplier-free solution. The open circle points are the rounded PO2 classical solution results.

In figure 3.6, the error probabilities are given. It can be seen that the rounded PO2 solution performs significantly worse than the classical solution for this specific channel model. Note the good performance of the optimal PO2 coefficients.

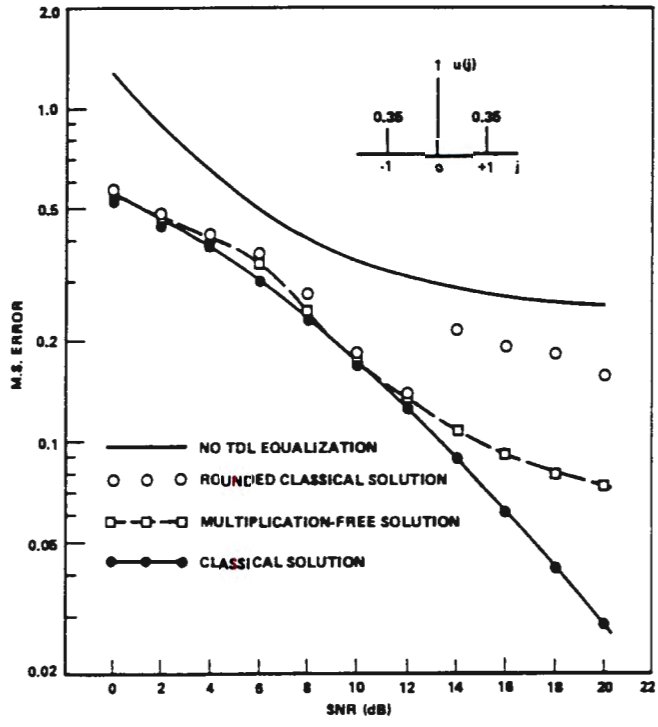

Figure 3.5: Mean-square error equalization of an ISI channel for binary data [19, p.324]

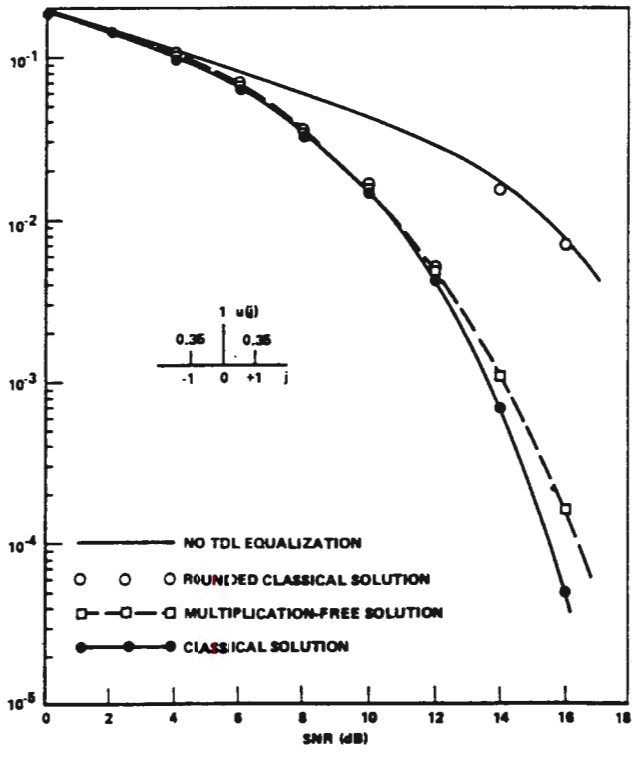

Figure 3.6: Error probabilities for an ISI channel for binary data [19, p.324]

Although this paper presents a good starting point, its results are not that useful for a QPSK microwave radio channel, which necessitates a complex TDL structure. Additionally, the channel model used is too simplistic and performance comparisons can not be made on only one set of model parameters. The difference in performance will change for different channel model values.

In 1984, Pirani and Zingarelli [20] authored a paper extending the results of Yan and Yao's paper to a BPSK microwave channel. The main focus of their paper, however, was to produce an algorithm to adapt the PO2 equalizer in time-varying channels. Two adaption strategies were developed and compared in terms of complexity, accuracy and convergence speed. As a background to their work, Pirani and Zingarelli describe the multiplier-free solution and present some results related to a fixed equalizer operating in a BPSK system having a 3-path model dispersion characteristic. The system performance was evaluated by calculating the eye aperture and the average bit error probability. The modulation format was 35Mbit/s BPSK with a raised-cosine factor of 0.7.

Figure 3.7 shows the eye apertures pertaining to the system without equalization (I), the infinite precision (IPCE), the optimal PO2 (OPCE) and the rounded PO2 (RPCE) verses the number N of equalizer coefficients. The multipath conditions modelled were τ=6.31ns and the notch depth was 19dB at the carrier frequency. The number of bits per sample of the analogue to digital converter was 10, while the number of bits for the coefficients was 12.

The aim of this dissertation is to extend the above investigations to the QPSK modulation scheme. Although the above papers investigate optimal PO2 coefficients, it is hypothesized that rounded PO2 coefficients will perform satisfactorily in equalizing a QPSK link, given that an adequate coefficient quantization is used.

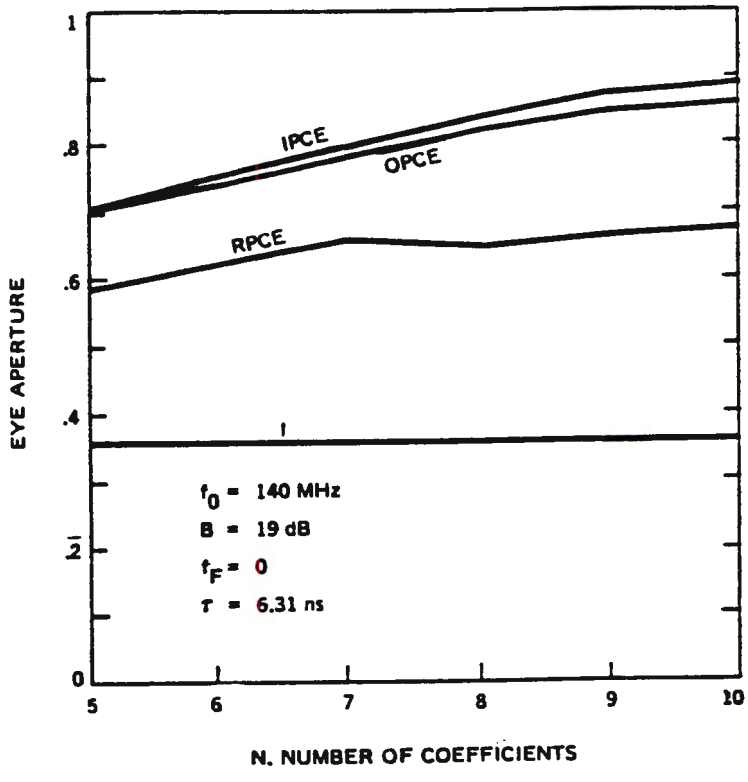

Figure 3.7: Eye aperture verses number of coefficients [20, p. 1027]

3.4. Chapter references

1. Qureshi, S., **Adaptive equalization.** IEEE communications magazine, March 1982, p.9-16.

2. Feher, K., **Advanced digital communications**, Prentice-Hall Books, CH 12.

3. Ziemer, R.E., and R.L. Peterson, **Introduction to digital communications.** Macmillan Publishing Company, 1992, p.202-225.

4. Ziemer and Tranter, **Principles of communications**, 3e, p.499-516.

5. Ziemer, R.E., and R.L. Peterson, **Digital communications and spread spectrum systems**, p.146-183.

6. Chamberlain, J.K., F.M. Clayton, H. Sari and P. Vandamme, **Receiver techniques for microwave digital radio.** Microwave digital radio, IEEE press, 1988, p.131-141.

7. Gitlin, R.D., J.F. Hayes and S.B. Weinstein, **Data Communications Principles.** Plenum Press, New York, 1992.

8. Lee, E.A. and D.G. Messerschmitt, **Digital Communication.** Kluwer Academic Publishers, CH 9.

9. Ivanek, F., **Terrestrial Digital Microwave Communications.** Artech House, 1989, CH4.

10. Haykin, S., **Adaptive Filter Theory**, Second Edition, Prentice Hall, Englewood cliffs, NJ, 1991.

11. Jakes, W.C., **An approximate method to estimate an upper bound on the effect of multipath delay distortion on digital transmission.** IEEE transaction on communications, Vol. COM-27 No. 1, January 1979, p.76-81.

12. Ott, R.H., M.C. Thompson, E.J. Violette and K.C. Allen, **Experimental and theoretical assessment of multipath effects on QPSK.** IEEE transactions on communications, Vol. COM-26 No. 10, October 1978, p.1475-1477.

13. Ruthroff, C.L., **Multiple-path fading on line-of-sight microwave radio systems as a function of path length and frequency.** Bell System Technical Journal, Vol. 50, No. 7, September 1971, p.2375-2398.

14. Greenstein, L.J., and B.A. Czekaj-Augun, **Performance comparisons among digital radio techniques subjected to multipath fading.** IEEE transactions on communications, vol. COM-30, No. 5, May 1982, p.1184-1197.

15. Metzger, K., and R. Valentin, **An analysis of the sensitivity of digital modulation techniques to frequency-selective fading.** IEEE transactions on communications, Vol. COM-33, No. 9, September 1985, p.986-992.

16. Morais, D.H., and A. Sewerinson and K. Feher. **The effects of the amplitude and delay slope components of frequency selective fading on QPSK, Offset QPSK and 8 PSK systems.** IEEE transactions on communications, Vol. COM-27 No. 12, December 1979, p.1849-1853.

17. Ziemer, R.E. and C.R. Ryan, **Equalization of QPSK data transmission in specular multipath.** IEEE transactions on aerospace and electronic systems, Vol. AES-10, No. 5, September 1974, p.588-594.

18. Amitay, N., and L.J.Greenstein, **Multipath outage performance of radio receivers using finite-tap adaptive equalizers.** IEEE Transactions on communications, Vol. COM-32 No. 5, May 1984, p.597-608.

19. Yan, T.-Y. and K. Yao, **A multiplication-free solution for the linear minimum mean-square estimation and equalization using the branch-and-bound principle.** IEEE transactions on information theory, Vol. IT-26, No. 3, May 1980, p.316-326.

20. Pirani, G., and V. Zingarelli, **Adaptive multiplication-free transversal equalizers with application to digital radio systems.** IEEE Trans. Comm, Vol. COM-32 no. 9, September 1984, p.1025-1033.

21. Max, J., **Quantization for minimum distortion.** IRE Transactions on Information Theory, Vol. IT-6, 1960, p.7-12.

CHAPTER 4

Essential mathematical background

A good theoretical background in communications processes is needed in order to facilitate the development of a simulation model. This chapter presents theory which is directly relevant to the subject matter of this thesis. Two main areas are considered. Firstly, the theory relating to an equivalent baseband description of a transmission system, is presented. Secondly, the theory relating to the calculation of the optimal equalizer coefficients, is presented and then applied to the SystemView simulation environment.

4.1. Equivalent baseband transmission system description

The material for this section has largely been summarized from [1], which is an excellent source of information pertaining to equalizers.

4.1.1. Analytic signals and the Hilbert Transform

By way of introduction, we start with a verbal definition of an analytic signal [2]. "An analytic signal is a complex-valued signal where spectral density is one-sided and whose real part is the original real-valued signal. Not all complex-valued signals are analytic signals but all analytic signals must be complex-valued."

Consider a given real-valued signal *s(t)* ; let its analytic signal representation be $\tilde{s}(t)$, where ~ indicates a complex function. Maintaining *s(t)* as the real part of $\tilde{s}(t)$, we can write:

$$\tilde{s}(t) = s(t) + j\hat{s}(t) \qquad \textbf{(4.1)}$$

where $\hat{s}(t)$ is yet to be determined.

The Fourier Transform of **(2.1)** is:

$$\tilde{S}(w) = S(w) + j\hat{S}(w) \tag{4.2}$$

To be an analytic signal, $\tilde{S}(w)$ must be one-sided. Now making $\tilde{S}(w) = 0$ for $w < 0$, we must have:

$$\hat{S}(w) = jS(w) \qquad w < 0 \tag{4.3}$$

To maintain a phase characteristic which is an odd function of frequency then requires that:

$$\hat{S}(w) = -jS(w) \qquad w > 0 \tag{4.4}$$

Combining **(4.3)** and **(4.4)**, we get:

$$\begin{aligned} \hat{S}(w) &= \begin{cases} -jS(w) & w > 0 \\ jS(w) & w < 0 \end{cases} \\ &= -jS(w).sgn(w) \end{aligned} \tag{4.5}$$

Using **(4.5)** in **(4.2)** it can now be verified that the spectral density of $\tilde{s}(t)$ is one-sided:

$$\tilde{S}(w) = \begin{cases} 2S(w) & w > 0 \\ 0 & w < 0 \end{cases} \tag{4.6}$$

The conditions described by **(4.5)** define the Hilbert Transform. If the inverse Fourier Transform is taken of **(4.5)**, we obtain $\hat{s}(t)$ which is called the quadrature function of *s(t)*.

A Hilbert filter acts in such a way as to retard the phase of each spectral component by 90 degrees. Thus it turns a cosine function into a sine and a sine function into a negative cosine.

4.1.2. Baseband data as a complex number sequence

The general form of a passband signal is:

$$s(t) = A(t)\cos[w_c t + \theta(t)] \tag{4.7}$$

where $A(t)$ is the amplitude of $s(t)$ and $\theta(t)$ the phase. Varying either or both can be used to convey information. Equation **(4.7)** can be expanded into:

$$s(t) = m_i(t)\cos(w_c t) - m_q(t)\sin(w_c t) \tag{4.8}$$

where:

$$\begin{aligned} m_i(t) &= A(t)\cos[\theta(t)] \\ m_q(t) &= A(t)\sin[\theta(t)] \end{aligned} \tag{4.9}$$

are the in-phase and quadrature modulations, respectively.

Now if we define the complex baseband signal to be:

$$\tilde{m}(t) = m_i(t) + jm_q(t) \tag{4.10}$$

then the complex passband signal is defined to be:

$$\tilde{s}(t) = \tilde{m}(t)\, e^{jw_c t} \tag{4.11}$$

Expanding **(4.11)**, we get:

$$\begin{aligned} \tilde{s}(t) &= m_i(t)\cos w_c t - m_q(t)\sin w_c t + j\{m_q(t)\cos w_c t + m_i(t)\sin w_c t\} \\ &= s(t) + j\hat{s}(t) \end{aligned} \tag{4.12}$$

This is a significant observation as it enables us to treat the baseband data as a complex number sequence. Furthermore, the modulator can be replaced by a multiplication with the desirable $e^{jw_c t}$ function. If one needs to know what the actual transmitted signal looks like, one takes the

real part of the complex passband signal. It can also be seen that $\tilde{s}(t)$ is an analytic signal, and hence has a one-sided spectrum.

As an example of the application of the above theory, we will develop a description of Rummler's model, as described in chapter 2, in terms of real time domain functions alone. The complex impulse response of the 3PM is:

$$\begin{aligned}\tilde{h}(t) &= a\delta(t) - ab.\cos(w_0 t)\delta(t-\tau) - jab.\sin(w_0 t)\delta(t-\tau) \\ &= A(t) + jB(t)\end{aligned} \tag{4.13}$$

Convolving the complex passband signal given in **(4.12)** with the above equation, we get:

$$\tilde{s}(t)*\tilde{h}(t) = A(t)*s(t) - B(t)*\hat{s}(t) + j\{A(t)*\hat{s}(t) + B(t)*s(t)\} \tag{4.14}$$

Taking the real part, and describing the real distorted signal as *y(t)*, we get:

$$\begin{aligned}y(t) &= \{\tilde{s}(t) * \tilde{h}(t)\} \\ &= A*s(t) - B*\hat{s}(t) \\ &= a\delta(t) - ab.\cos(w_0\tau)s(t-\tau) + ab.\sin(w_0\tau)\hat{s}(t-\tau)\end{aligned} \tag{4.15}$$

The above equation operates on a real passband signal *s(t)* to produce a real distorted transmission signal. This result is very useful for computer simulation purposes, especially if one needs to have access to the real distorted signal.

4.1.3. The complex baseband version of Rummler's model

In this subsection it is proved that the complex impulse response of the 3PM as given by **(4.13)**, is in fact the complex baseband equivalent to the passband version of the 3PM.

Let's define **(4.13)** as the complex baseband signal:

$$\tilde{h}_B(t) = A(t) + jB(t) \tag{4.16}$$

Now the complex passband model is defined as:

$$\begin{aligned} \tilde{h}(t) &= \tilde{h}_B \, e^{jw_c t} \\ &= h(t) + j\hat{h}(t) \end{aligned} \tag{4.17}$$

Now the top expression in **(4.17)** is expanded and multiplied out. The Dirac functions are simplified and a trig identity applied. Finally, the real and imaginary parts are equated to the lower expression to yield the following:

$$\begin{aligned} h(t) &= a.\delta(t) - ab.\delta(t-\tau).\cos(w_c+w_0)\tau \\ \hat{h}(t) &= - ab.\delta(t-\tau).\sin(w_c+w_0)\tau \end{aligned} \tag{4.18}$$

Therefore the complex passband channel model is:

$$\tilde{h}(t) = a\delta(t) - ab.\delta(t-\tau).\cos(w_c+w_0)\tau - jab.\delta(t-\tau).\sin(w_c+w_0)\tau \tag{4.19}$$

It can be seen from this equation that the notch position has shifted in accordance with the carrier frequency. Thus the model has been translated up in frequency, thereby proving the initial assumption.

4.1.4. Equivalent baseband noise

In a typical system, the received signal (real) is the transmitted signal convolved with the channel impulse response. This received signal has noise added to it, which is considered to be white and Gaussian in nature. Thus:

$$r(t) = s(t) * h(t) + n(t) \tag{4.20}$$

To derive the equivalent baseband noise component, we presume a bandpass noise process *n(t)* with a spectrum limited to $|w| < 2W_c$. We represent the noise as:

$$\begin{aligned} n(t) &= Re\{\ \tilde{n}_B(t)\ e^{jw_c t}\ \} \\ &= n_i(t)\ \cos\ w_c t\ -\ n_q(t)\ \sin\ w_c t \end{aligned} \tag{4.21}$$

where $\tilde{n}_B(t) = n_i(t) + jn_q(t)$ is the equivalent complex baseband noise.

In order to derive the statistics of $n_i(t)$, $n_q(t)$ and $\tilde{n}_B(t)$ from those of $n(t)$, we start by stating the autocorrelation $\phi_{nn}(\tau)$ of $n(t)$ as:

$$\phi_{nn}(\tau) = \phi_{ii}(\tau).\cos(w_c\tau) - \phi_{qq}(\tau).\sin(w_c\tau) \tag{4.22}$$

If more information is required, the reader is requested to consult p.314 of [1] for a more complete derivation.

We now need to find the autocorrelation function $\phi_{BB}(\tau)$ of the equivalent complex baseband noise function:

$$\begin{aligned} \phi_{BB}(\tau) &= E\{\ \tilde{n}(t+\tau).n_B^*(t)\ \} \\ &= 2\phi_{ii}(\tau) + 2j\phi_{qi}(\tau) \end{aligned} \tag{4.23}$$

The power density function $S_{BB}(w)$ is defined as the Fourier Transform of $\phi_{BB}(\tau)$. From **(4.21)** and **(4.22)** we get:

$$\phi_{nn}(\tau) = 1/2\ Re\{\ \phi_{BB}(\tau)\ e^{w_c t}\ \} \tag{4.24}$$

But from [1]:

$$F\{\ 2Re[\phi_{BB}(\tau)e^{jw_c t}]\ \} = S_{BB}(w - w_c) + S_{BB}(-w - w_c) \tag{4.25}$$

Thus the power density spectrum of $n(t)$ is:

$$S_n(w) = F\{ \phi_{nn}(\tau) \}$$
$$= 1/4 \ [S_{BB}(w - w_c) + S_{BB}(-w - w_c)] \qquad \textbf{(4.26)}$$

For white noise with two-sided spectral power density $N_0/2$, we presume that a perfect bandpass filter has limited the noise spectrum to a bandwidth $2W$ rad/s about w_c. Then from **(4.25)**:

$$S_{BB}(w) = \begin{cases} 2N_0 & |w| \leq W \\ 0 & |w| > W \end{cases} \qquad \textbf{(4.27)}$$

with corresponding autocorrelation function:

$$\phi_{BB}(\tau) = 2N_0 \frac{\sin(W\tau)}{\pi\tau} \qquad \textbf{(4.28)}$$

As $S_{BB}(w)$ is symmetric about w=0, we know from the properties of the Fourier Transform that $\phi_{BB}(\tau)$ is real and $\phi_{qi}(\tau) = 0$. Thus $n_i(t)$ and $n_q(t)$ are uncorrelated for all time shifts and hence for Gaussian noise, they are independent. This means that the power spectral density $S_{BB}(w)$ is the sum of the power spectral densities $S_i(w)$ and $S_q(w)$. Thus $S_i(w)$ and $S_q(w)$ are each equal to N_0 for $|w| \leq W$. This is an important result for the implementation of the computer simulation model.

4.1.5. The complex analytic transmission system

Just as we defined a complex analytic transmitted signal $\tilde{s}(t)$ in **(4.1)**, we can define a complex analytic received signal $\tilde{r}(t)$, as shown in figure 4.1. The expression for $\tilde{r}(t)$ as a function of the carrier frequency and an equivalent baseband received signal, is defined as the complex analytic function whose real part is the actual real received signal $r(t)$. We further define $\tilde{r}_B(t)$ as the equivalent baseband received signal for which:

$$\tilde{r}(t) = \tilde{r}_B(t) \ e^{jw_c t} \qquad \textbf{(4.29)}$$

We will derive an expression for $\tilde{r}_B(t)$.

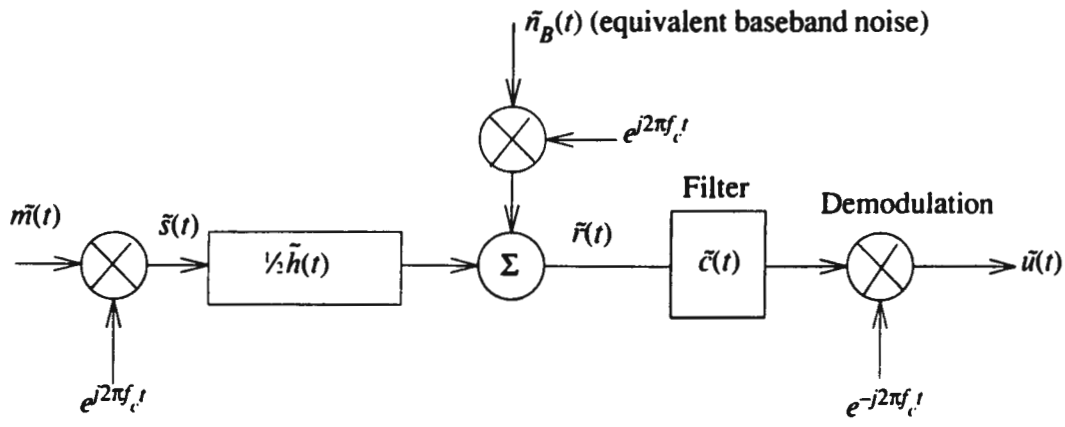

Figure 4.1: Complex analytic representation of a linear transmission system [1, p.312]

Considering **(4.20)**, lets derive an expression for $s(t)*h(t)$. Notice that:

$$\begin{aligned} Re\ \{\ \tilde{s}(t)*\tilde{h}(t)\ \} &= s(t)*h(t) - \hat{s}(t)*\hat{h}(t) \\ &= 2\ s(t)*h(t) \end{aligned} \tag{4.30}$$

Thus:

$$s(t)*h(t) = Re\ \{\ 1/2\ \tilde{s}(t)*\tilde{h}(t)\ \} \tag{4.31}$$

Now using **(4.11)** and **(4.17)**:

$$\begin{aligned} \tilde{s}(t)*\tilde{h}(t) &= \int \tilde{s}(\tau).\tilde{h}(t-\tau)\ d\tau \\ &= \left[\tilde{m}(t)*\tilde{h}_B(t)\right] e^{jw_c t} \end{aligned} \tag{4.32}$$

Therefore **(4.20)** becomes:

$$r(t) = Re\{ [1/2\ \tilde{m}(t)*\tilde{h}_B(t)]\ e^{jw_c t} \} + n(t) \tag{4.33}$$

Substitute the expression for *n(t)*, as given in **(4.21)**, in the above equation and comparing to **(4.29)**, we obtain:

$$\tilde{r}_B(t) = \frac{1}{2}\ \tilde{m}(t)*\tilde{h}_B(t) + \tilde{n}_B(t) \tag{4.34}$$

Returning to figure 4.1 which shows the complex analytic representation of a linear system, it should be noted that the factor of ½ has been coupled to the channel impulse response. The figure also includes a complex filter which could be implemented as an equalizer. The same relationship exists for this filter, namely:

$$\tilde{c}(t) = \tilde{c}_B(t)\ e^{jw_c t} \tag{4.35}$$

Figure 4.2 shows the equivalent baseband complex transmission system, which is the representation of interest to us.

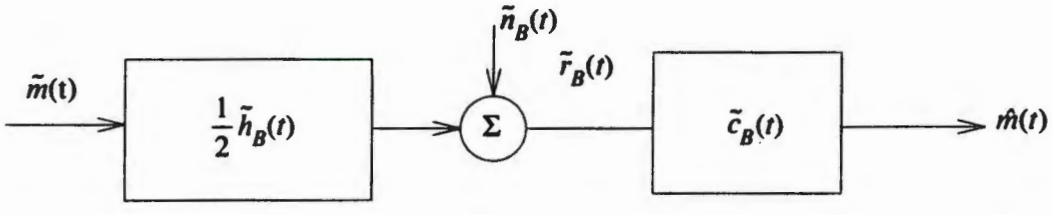

Figure 4.2: Equivalent baseband complex transmission system [1, p.313]

Although figure 4.1 shows the equalizer before the demodulator, this could equally be placed after the demodulator. Consider:

$$\begin{aligned} \tilde{r}(t)\ e^{-jw_c t} * \tilde{c}_B(t) &= \int_{-\infty}^{\infty} \tilde{c}_B(\tau)\ \tilde{r}(t-\tau)\ e^{-jw_c(t-\tau)}\ d\tau \\ &= e^{-jw_c t}\left[\ \tilde{r}(t) * \tilde{c}_B(t) e^{jw_c t}\ \right] \\ &= \left[\ \tilde{r}(t) * \tilde{c}(t)\ \right] e^{-jw_c t} \end{aligned} \qquad \textbf{(4.36)}$$

where the first expression describes demodulation followed by baseband equalization, and the last describes passband equalization followed by demodulation.

A receiver with equalization preceding demodulation is desirable, since this avoids inserting the delay of the equalizer into the control loop generating the demodulation phase. The inclusion of this delay impairs the loop's ability to correct for channel phase jitter. Further practical implementation issues such as carrier and timing recovery, will not be considered here but will be addressed, where neccessary, in the simulation implementation as discussed in the next chapter. This concludes the necessary background theory for an equivalent baseband transmission system. In the next subsection, the above theory is applied to simplify the implementation of the simulation model.

4.1.6. Baseband transmission simulation model

Consider **(4.34)** with $\tilde{n}_B(t)$ set to zero. Define:

$$\begin{aligned} \tilde{m}(t) &= I(t) + jQ(t) \\ \tilde{h}_B(t) &= A(t) + jB(t) \end{aligned} \qquad \textbf{(4.37)}$$

where $I(t)$ and $Q(t)$ are the shaped baseband data streams, and $A(t)$ and $B(t)$ are as defined in **(4.13)**.

We now define:

$$R_I(t) = Re\{\ \tilde{r}_B(t)\ \}$$
$$R_Q(t) = Im\{\ \tilde{r}_B(t)\ \} \qquad \textbf{(4.38)}$$

Applying the convolution integral and the sampling (sifting) property of the Dirac delta, these equations become:

$$R_I(t) = \frac{1}{2}\left\{aI(t) - ab.\cos(w_0\tau).I(t-\tau) + ab.\sin(w_0\tau).Q(t-\tau)\right\}$$
$$R_Q(t) = \frac{1}{2}\left\{aQ(t) - ab.\cos(w_0\tau).Q(t-\tau) - ab.\sin(w_0\tau).I(t-\tau)\right\} \qquad \textbf{(4.39)}$$

The above equations are used to directly generate the distorted received signal in the simulation model presented in the next chapter. For more insight into this important simplification, consult Appendix II.

4.2. Calculating the optimal equalizer coefficients

This section presents a summary of Wiener Filter theory as applied to a base-band transversal equalizer. It is based on chapter 5 of Haykin's book, Adaptive Filter Theory [3].

4.2.1. Wiener Filter theory

Consider figure 4.3, in which all values are complex. The filter input consists of a time series $u(0)$, $u(1)$, ..., and the filter is characterised by its impulse response w_0, w_1, ... At some discrete time n, the filter produces an output denoted by $y(n)$. This output is used to provide an estimate of a desired response denoted by $d(n)$. With the filter input and the desired response representing single realizations of the respective stochastic processes, the estimation is accompanied by an error with statistical characteristics of its own. In particular, the estimation error, denoted by $e(n)$, is defined as the difference between the desired response $d(n)$ and the filter output $y(n)$. The requirement is to minimise the estimation error $e(n)$ in the mean squared sense.

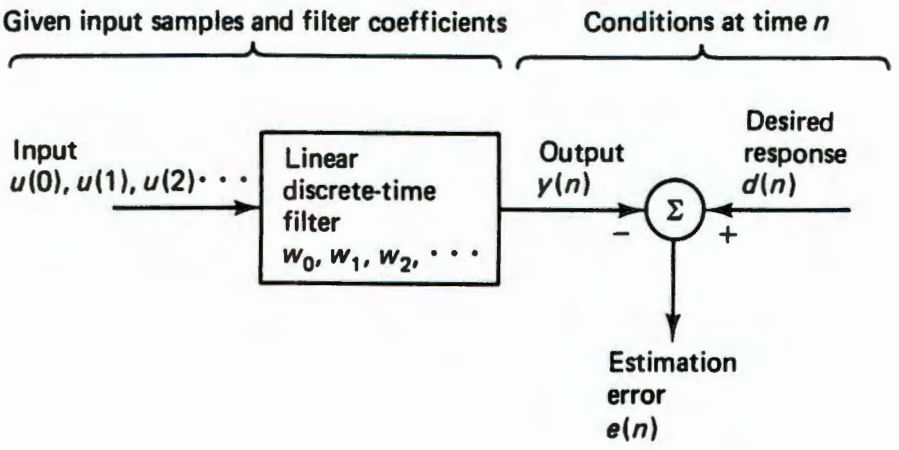

Figure 4.3: Block diagram of the statistical filtering problem [3, p.158]

Let the discrete-time filter be defined as in figure 4.4, which represents a complex-valued transversal filter consisting of M taps. w_0^* in the figure implies a complex multiplication of $u(n)$ with the complex conjugate of w_0. The filter output $y(n)$ in figure 4.4 is defined by the linear convolution sum:

$$y(n) = \sum_{k=0}^{M-1} w_k^*.u(n-k) \qquad n = 0, 1, 2, \ldots \qquad \textbf{(4.40)}$$

where the asterisk denotes complex conjugate.

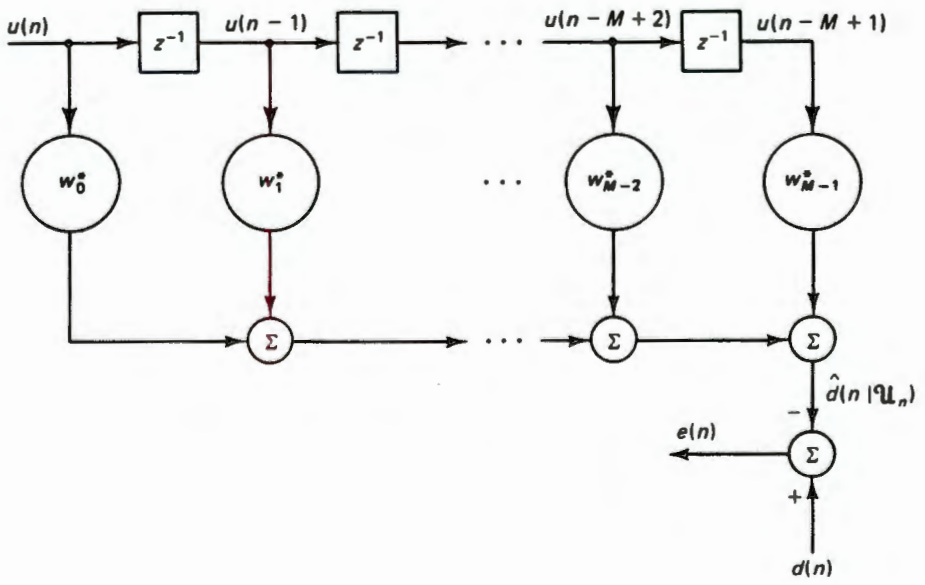

Figure 4.4: Transversal filter structure [3, p.166]

The estimation error is given by:

$$e(n) = d(n) - y(n) \tag{4.41}$$

The principle of orthogonality states that the necessary and sufficient condition for the mean-square error to attain its minimum value is that the corresponding value of the estimation error *e(n)* is orthogonal to each input sample that enters into the estimation of the desired response at time *n*. This is expressed mathematically as:

$$E\left[u(n-k).e^{*}(n) \right] = 0 \qquad k = 0, 1, 2, \ldots \tag{4.42}$$

Now substituting equation **(4.40)** and **(4.41)** into **(4.42)**, and rearranging the terms, one gets:

$$\sum_{i=0}^{\infty} w_{0i} \, E\left[u(n-k).u^{*}(n-i) \right] = E\left[u(n-k).d^{*}(n) \right] \qquad k = 0, 1, 2, \ldots \tag{4.43}$$

Now defining the autocorrelation function of the filter input for a lag of *i-k* as *r(i-k)*, we get:

$$r(i-k) = E\left[u(n-k).u^{*}(n-i) \right] \tag{4.44}$$

Defining the cross-correlation between the filter input *u(n-k)* and the desired response *d(n)* for a lag of *-k* as *p(-k)*, we get:

$$p(-k) = E\left[u(n-k).d^{*}(n) \right] \tag{4.45}$$

Using equation **(4.44)** and **(4.45)** in **(4.43)**, we get:

$$\sum_{i=0}^{M-1} w_{0i} \, r(i-k) = p(-k) \qquad k = 0, 1, 2, \ldots, M-1 \tag{4.46}$$

The system of M simultaneous equations given by **(4.46)**, are known as the *Wiener-Hopf equations*.

The Wiener-Hopf equations can be more conveniently written in matrix form as:

$$\boldsymbol{R}\boldsymbol{w}_0 = \boldsymbol{p} \tag{4.47}$$

where:

$$\boldsymbol{R} = E\left[\, \boldsymbol{u}(n)\, \boldsymbol{u}^{H}(n) \,\right] = \begin{bmatrix} r(0) & r(1) & \dots & r(M-1) \\ r^{*}(1) & r(0) & \dots & r(M-2) \\ \vdots & \vdots & \vdots & \vdots \\ r^{*}(M-1) & r^{*}(M-2) & \dots & r(0) \end{bmatrix} \tag{4.48}$$

$$\boldsymbol{w}_o = \left[\, w_{o0},\ w_{o1},\ \dots,\ w_{o(M-1)} \,\right]^{T} \tag{4.49}$$

$$\boldsymbol{u}(n) = \left[\, u(n),\ u(n-1),\ \dots,\ u(n-M+1) \,\right]^{T} \tag{4.50}$$

$$\boldsymbol{p} = E\left[\, \boldsymbol{u}(n)\, d^{*}(n) \,\right] = \left[\, p(0),\ p(-1),\ \dots,\ p(1-M) \,\right]^{T} \tag{4.51}$$

To solve equation **(4.47)** for $\boldsymbol{w}_o$, we assume that the correlation matrix $\boldsymbol{R}$ is nonsingular and then premultiply both sides of **(4.47)** by the inverse $\boldsymbol{R}^{-1}$, to obtain:

$$\boldsymbol{w}_o = \boldsymbol{R}^{-1}\boldsymbol{p} \tag{4.52}$$

where $\boldsymbol{w}_0$ is the vector of tap weights which minimises the mean-square error value.

Expressions are now presented which specify the mean-square error as a function of the tap weights $\boldsymbol{w}$, and for the special case when the taps are optimal, that is when $\boldsymbol{w} = \boldsymbol{w}_o$.

The mean-squared error can be written as:

$$\begin{aligned} J &= E\left[\, e(n)\; e^{*}(n) \,\right] \\ &= E\left[\, |e(n)|^2 \,\right] \end{aligned} \tag{4.53}$$

Substituting equation **(4.40)** and **(4.41)** into **(4.49)** and writing in matrix form, we get:

$$J = \sigma_d^2 - \boldsymbol{w}^{H}\boldsymbol{p} - \boldsymbol{p}^{H}\boldsymbol{w} + \boldsymbol{w}^{H}\boldsymbol{R}\boldsymbol{w} \tag{4.54}$$

where:

$$\sigma_d^2 = E\left[\, |d(n)|^2 \,\right] \tag{4.55}$$

is the variance of the desired response, assumed to be zero mean.
$\boldsymbol{w}^{H}$ is the Hermitian transpose of $\boldsymbol{w}$.

If the optimal taps $\boldsymbol{w}_0$ as given by **(4.48)**, are substituted into **(4.50)**, we obtain the minimum mean-squared error:

$$\begin{aligned} J_{\min} &= \sigma_d^2 - \boldsymbol{p}^{H}\boldsymbol{w}_o \\ &= \sigma_d^2 - \boldsymbol{p}^{H}\boldsymbol{R}^{-1}\boldsymbol{p} \end{aligned} \tag{4.56}$$

Applying the above theory, it is possible to calculate the optimal tap weights for a specific equalizer structure and predict the minimum mean-squared error value. If non-optimal taps, such as those restrained to be powers of two, are used, the resulting mean-squared error can be calculated and hence the system degradation assessed.

Now it is necessary to solve the Wiener-Hopf equations for the system as modeled on SystemView. If one simplifies the expressions for the elements of the correlation matrix and the cross-correlation vector, it turns out that $\boldsymbol{R}$ and $\boldsymbol{p}$ can be expressed in terms of the sampled impulse response of the system. The following section shows how this is achieved.

4.2.2. Solving the Wiener-Hopf equation

Consider that the impulse responses of the pulse shaping filter, the Three Path model and the receive filter can be convolved together to produce a combined impulse response *h(t)*. As the impulse response of a FIR filter is the same as the FIR filter's tap weights, one can approximate the combined impulse response *h(k)* with a complex FIR filter of adequate length. The taps are set equal to the sampled impulse response, where the sample rate is equal to the symbol rate. Thus:

$$u(n) = \sum_{k=-N}^{N} h(k).a(n-k) + v(n) \qquad \textbf{(4.57)}$$

where N is large enough to make $h(N)$ negligible.

Applying this expression in:

$$r(\alpha) = E\left[\, u(n).u^{*}(n-\alpha) \,\right] \qquad \textbf{(4.58)}$$

and setting $\alpha = 0$ we get an expression for $r(0)$:

$$r(0) = E\left[\left(\sum_{k=-N}^{N} h(k).a(n-k)+v(n) \right) \left(\sum_{l=-N}^{N} h^{*}(k).a^{*}(n-k)+v^{*}(n) \right) \right] \qquad \textbf{(4.59)}$$

If the above equation is multiplied out and the expectation taken, remembering that the noise is uncorrelated to the data, we get:

$$r(0) = E\left[\sum_{k=-N}^{N} h(k).a(n-k) \sum_{l=-N}^{N} h^{*}(l).a^{*}(n-l) \right] + E\left[\, v(n).v^{*}(n) \,\right] \qquad \textbf{(4.60)}$$

The last term of this equation is defined to be the variance of the white noise process:

$$E\left[\, v(n).v^{*}(n) \,\right] = \sigma_v^2 \qquad \textbf{(4.61)}$$

To simplify the first term, multiply out the summations on a term by term basis. As the data is random $E[a(n).a^{*}(n+\alpha)] = 0$. However $E\left[\, a(n).a^{*}(n) \,\right] = E\left[\, |a(n)|^2 \,\right] = 2$.
As the magnitude is arbitrary, it will be assumed to be 1 from now on.

Therefore, **(4.60)** becomes:

$$r(0) = \sum_{k=-N}^{N} h(k).h^{*}(k) + \sigma_v^2 \qquad \textbf{(4.62)}$$

Now solving for $r(1)$ in a similar manner, we get:

$$r(1) = \sum_{k=-N+1}^{N} h(k).h^{*}(k-1) \qquad \textbf{(4.63)}$$

For $r(2)$ we get:

$$r(2) = \sum_{k=-N+2}^{N} h(k).h^{*}(k-2) \qquad \textbf{(4.64)}$$

In general the elements of a new matrix $\boldsymbol{S}$ can be obtained from the following expression:

$$s(\alpha) = \sum_{k=-N+\alpha}^{N} h(k).h^{*}(k-\alpha) \qquad \textbf{(4.65)}$$

where $\alpha = 0$ to $2N$. This formula agrees with the one presented, without derivation, in [4].

Finally we can write:

$$\boldsymbol{R} = \boldsymbol{S} + \sigma_v^2 \boldsymbol{I} \qquad \textbf{(4.66)}$$

where $\boldsymbol{I}$ is the N by N identity matrix.

Now we need to develop an expression for the cross-correlation vector ***p***.

Remember:

$$p(-\alpha) = E\left[u(n-\alpha).d^{*}(n) \right] \tag{4.67}$$

and the expression for *u(n)* is:

$$u(n) = \sum_{k=-N}^{N} h(k).a(n-k) + v(n) \tag{4.68}$$

The desired response *d(n)* is identical to the original data *a(n)* except for the delay through the impulse approximating filter (N) and the delay to the reference tap of the equalizer ((M-1)/2). Thus *d(n)* can be written as follows:

$$d^{*}(n) = a^{*}(n-z) \tag{4.69}$$

where:

$$z = N + \frac{M-1}{2} \tag{4.70}$$

After substituting the above expressions and setting the uncorrelated expectations to zero, we get:

$$p(-\alpha) = E\left[\sum_{k=-N}^{N} h(k).a(n-\alpha-k).a^{*}(n-z) \right] \tag{4.71}$$

which simplifies to:

$$p(-\alpha) = h(z-\alpha) \tag{4.72}$$

where $\alpha = 0$ to M-1.

We are now in a position to solve **(4.47)** for the optimal taps. The impulse response of the system can be obtained directly from SystemView's analysis window. A Mathcad sheet was developed to solve the above equations and can be found in appendix III.

4.3. Chapter references

1. Gitlin, R.D., J.F. Hayes and S.B. Weinstein, **Data Communications Principles.** Plenum Press, New York, 1992.

2 . Stremler, F.G., **Introduction to communication systems.** Second Edition, Addison-Wiley, U.S.A., 1982, p.244-247.

3. Haykin, S., **Adaptive Filter Theory.** Second Edition, Prentice Hall, Englewood cliffs, NJ, 1991.

4. Bingham, J.A.C., **The theory and practice of modem design.** Wiley Interscience, New York.

CHAPTER 5

Development of the simulation model

The computer simulation model as implemented on SystemView is developed in this chapter. Before the model can be developed, it is important to present some background information. As was mentioned in chapter 2, an M-curve is a very useful concept when doing outage calculations. In order to produce an M-curve it is necessary to perform BER measurements, which are time consuming and require some effort to set-up in the simulation model. As absolute BER measurements are not required for this dissertation, it was decided to use the Eye Aperture (EA) as a more convenient means of system evaluation.

In order to further simplify the investigation, it was decided that noise would be ignored. The theory relating to noise has been included in the dissertation for completeness' sake, but will not be taken into account during the generation of the simulation results. This enables a further simplification in that a band-limiting filter does not need to be included at the receiver.

A further point to bear in mind is that if a symbol spaced equalizer is implemented, only one sample value is available per symbol. The result is a square "eye" diagram. Although this is unconventional, the aperture of this "eye" will still enable comparative evaluations to be performed.

A simple QPSK structure is implemented in the next section as a basic starting point, with BER measurements being performed to check its functionality and to demonstrate the procedure.

5.1. Basic QPSK structure

Figure 5.1. shows the model of a basic QPSK structure, implemented at baseband in accordance with the theory presented in the previous chapter. The serial data stream is converted to parallel format which forms the in-phase (I) and quadrature (Q) channels. This is $\tilde{m}(t)$ in figure 4.2 of the previous chapter. Note that $\tilde{h}_B(t)$ and $\tilde{c}_B(t)$ are equal to 1 here, and the gain of 0.5 can be

ignored because $\tilde{h}_B(t)$ is real in this situation. After the addition of noise, the received signal is fed to an integrate-and-dump circuit, sampled at the correct time, and combined into a serial output stream. No receiver filter is necessary here as the integrate-and-dump has a low-pass transfer function. The integrate-and-dump is the perfect matched filter for the transmitted square wave, which means that this system should yield performance equivalent to that of theoretical QPSK.

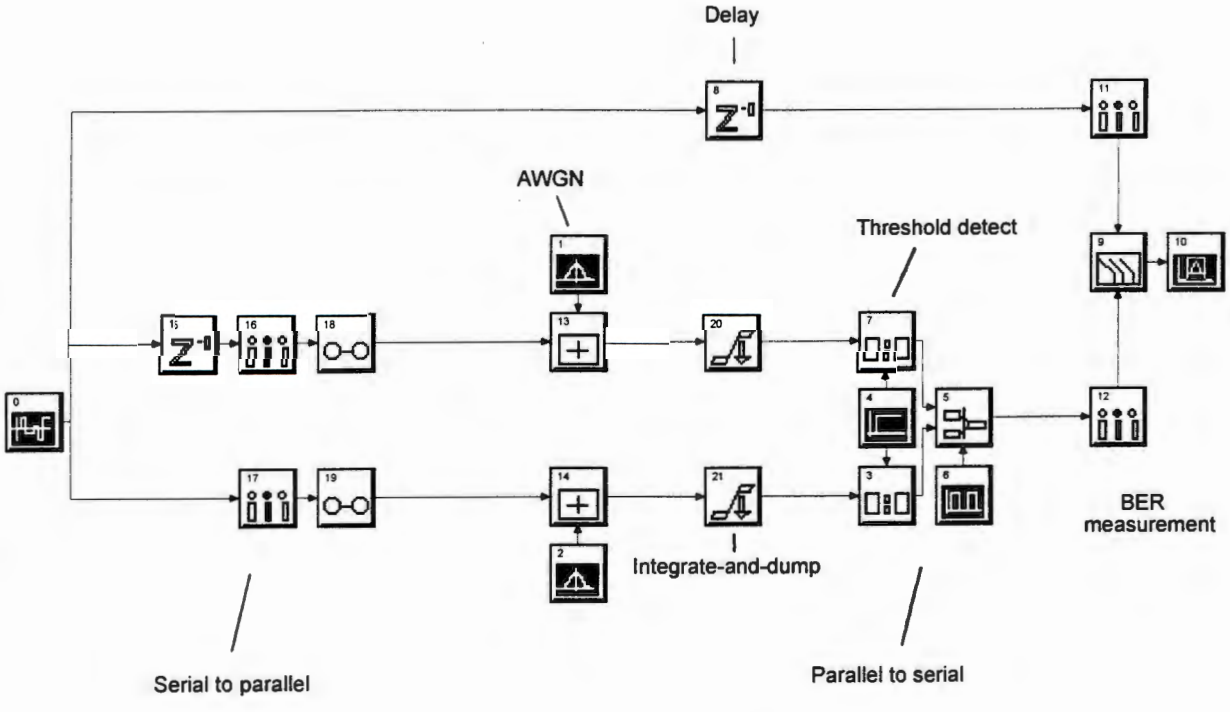

Figure 5.1: Basic QPSK structure

The BER is measured by comparing the transmitted data and the received data. A delay is necessary to compensate for the delay in the transmission path and can be calculated by cross-correlating the transmitted and received data in the SystemView analysis window. Using similar techniques, the optimal integrate-and-dump sampling time is also calculated.

Now it is necessary to determine what noise power should be added to get a certain E_b/N_0 ratio. The noise is assumed to be Additive White Gaussian Noise (AWGN), with double-sided power spectral density $N_0/2$. The energy contained in one bit is given by:

$$E_b = A^2.T_b \tag{5.1}$$

where: A is the amplitude of the NRZ data in Volts,

T_b is the symbol period in seconds.

Now define:

$$R = 10 \log \frac{E_b}{N_0} \tag{5.2}$$

and after rearranging we obtain the expression for the single-sided power spectral density N_0 needed to ensure a certain E_b/N_0 ratio R (in dB):

$$N_0 = \frac{A^2.T_b}{10^{R/10}} \tag{5.3}$$

Formulae exist to calculate the theoretical probability of error in a QPSK system [1]. It turns out that if Gray coding of the symbols is used, then the probability of error P_E for the whole system is the same as the probability of error for one channel. The model implementation has an inherent Gray encoding as no symbol-to-bit mapping is performed. Hence the following formula can be applied:

$$P_E = Q\left(\sqrt{\frac{E_b}{N_0}}\right) \tag{5.4}$$

See p.160 and p.689 of [1] for the definition of the Q-function, as well as tables and an approximation formula.

To check this basic QPSK model implementation, BER measurements were carried out on a data stream of 20 000 bits and the results are presented in table 5.2. It can be seen that, for high BER, the theory and measurements agree very well. However as the errors become less frequent, longer simulation times are required to capture enough events to generate accurate statistics. These long

simulation times are impractical and so it was decided to rather use the Eye Aperture (EA) as the means of evaluating system performance.

$10\log(E_b/N_0)$	N_0 (W/Hz)	Theory: $\log(P_E)$	Measured: $\log(P_E)$
0	$250*10^{-9}$	-1.10	-1.10
4	$100*10^{-9}$	-1.90	-1.90
8	$39.6*10^{-9}$	-3.69	-3.60
10.5	$22.2*10^{-9}$	-6.0	- infinity

Table 5.2: Comparison of theory and simulation results.

5.2. QPSK with pulse shaping

In a real microwave system one cannot transmit square pulses as there is a limit on the spectral bandwidth which a system may occupy. A possible solution is to filter the modulated signal before being transmitted. However, as it is impossible to make perfect analogue filters, this filtering will introduce some ISI. A better technique is to shape the baseband data such that a desired spectrum is obtained. The shaping technique must not introduce any ISI. A commonly used filter which satisfies these conditions is known as a raised-cosine filter. The raised-cosine characteristic as expressed in [2], can be written as:

$$X(w) = \begin{cases} T & 0 \le |w| \le (1-\alpha)W \\ \frac{T}{2}\left\{1-\sin\left[\frac{\pi}{2\alpha W}(|w|-W)\right]\right\} & (1-\alpha)W \le |w| (1+\alpha)W \\ 0 & |w| > (1+\alpha)W \end{cases} \qquad (5.5)$$

where $W = \frac{\pi}{T}$ and α, known as the roll-off factor, is the excess bandwidth used divided by the minimum Nyquist bandwidth. The corresponding impulse response is:

$$x(t) = \left(\frac{\sin Wt}{Wt}\right).\left(\frac{\cos \alpha Wt}{1-(2\alpha Wt/\pi)^2}\right) \qquad (5.6)$$

Plots of *x(t)* and *X(w)* are shown below in figure 5.3.

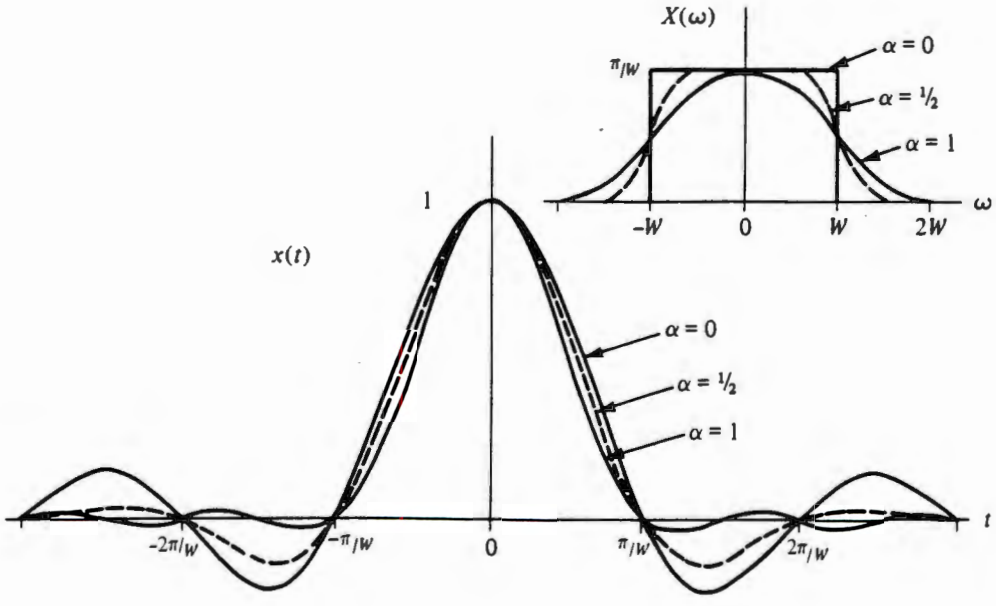

Figure 5.3: Raised-cosine pulse shaping characteristics [2, p.369]

The bandwidth occupied for a raised-cosine-type transmission characteristic can be expressed by the following formula:

$$B = \frac{(1+\alpha)}{2T} \tag{5.7}$$

In the simulation, this shaping is performed by means of a transversal filter. This is achieved by setting the coefficients, which multiply the taps of the filter, to sampled values of the raised-cosine impulse response.

The SystemView model to implement this is shown in figure 5.4. To simulate a realizable system, four samples were used to create each symbol shape. The hold circuit (zero-order) simulates a digital-to-analogue converter and the output filter removes the alias inherent in a sampled system. Figure 5.5 shows the eye diagram produced when α equals 0.5.
Figure 5.6 shows the spectrums for unshaped data (top) and shaped data (below).

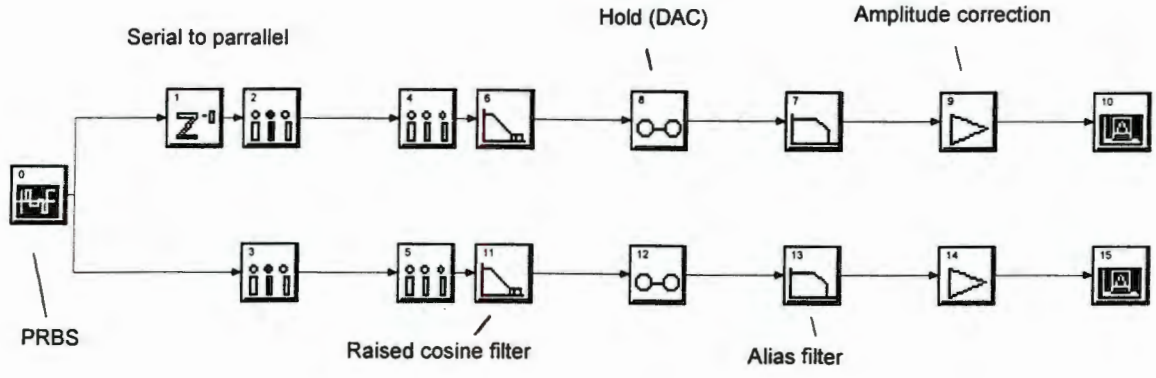

Figure 5.4: Raised-cosine SystemView model

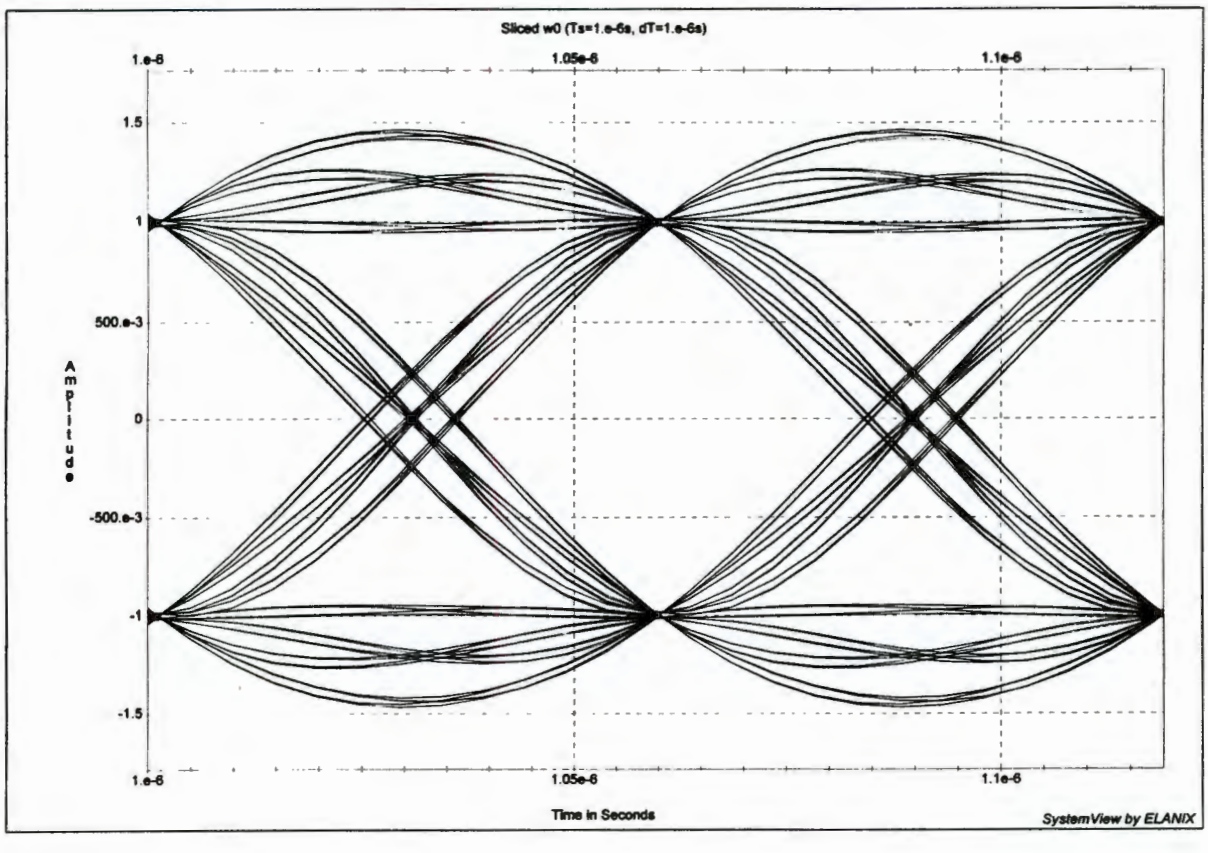

Figure 5.5: Eye diagram for raised-cosine shaping

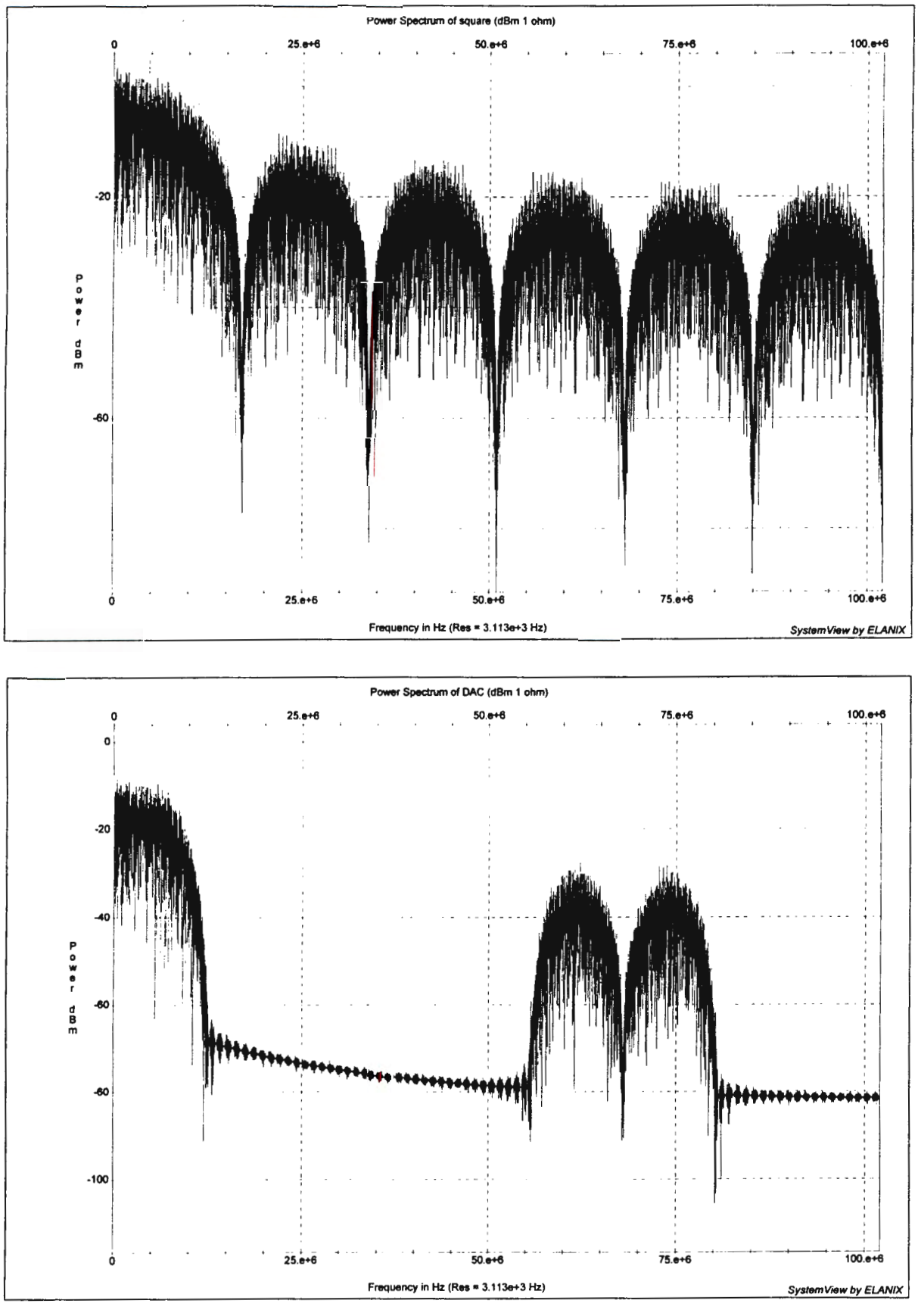

Figure 5.6: Spectrums for unshaped (top) and shaped (bottom) data

There is a subtle issue related to generating waveforms by digital techniques. The digital-to-analog convertion process introduces a sin(w)/w distortion in the spectrum, with the first null at the sampling frequency. This spectral distortion produces an effect in the time domain which looks like ISI on the eye diagram. Fortunately the effect is very small and it will be ignored here as the equalizer is capable of compensating for this distortion. Appendix IV presents a method for correcting this distortion.

The shaping of the data changes the energy contained within one bit interval, so it is no longer possible to apply **(5.1)** when calculating N_0 for a specific E_b/N_0 ratio. To calculate the energy in the new bit shape, we invoke Parseval's theorem:

$$E_b = \frac{1}{2\pi} \int_{-\infty}^{\infty} |X(w)|^2 \, dw \qquad \textbf{(5.8)}$$

Performing this integration with $\alpha = 0.5$, the following is obtained:

$$E_b = \frac{7}{8} A^2 T_b \qquad \textbf{(5.9)}$$

Thus our new formula for N_0 becomes:

$$N_0 = \frac{7}{8} \cdot \frac{A^2 T_b}{10^{R/10}} \qquad \textbf{(5.10)}$$

If there were a perfect matched filter at the receiver, the system BER performance would be the same as given by **(5.2)**. However, in practice it is not easy to implement a matched filter and so this is often approximated by a low-pass filter. See appendix V for a comparison of a real QPSK 8MBits/s system using this approximation and a simulation thereof.

5.3. The baseband Three Path Model.

In this section a model is developed which implements the equations as given in **(4.39)**. The model is shown in figure 5.7. In order to observe the operation of the fading model, consider the baseband equivalent spectrum. This can be obtained by doing a complex Fourier

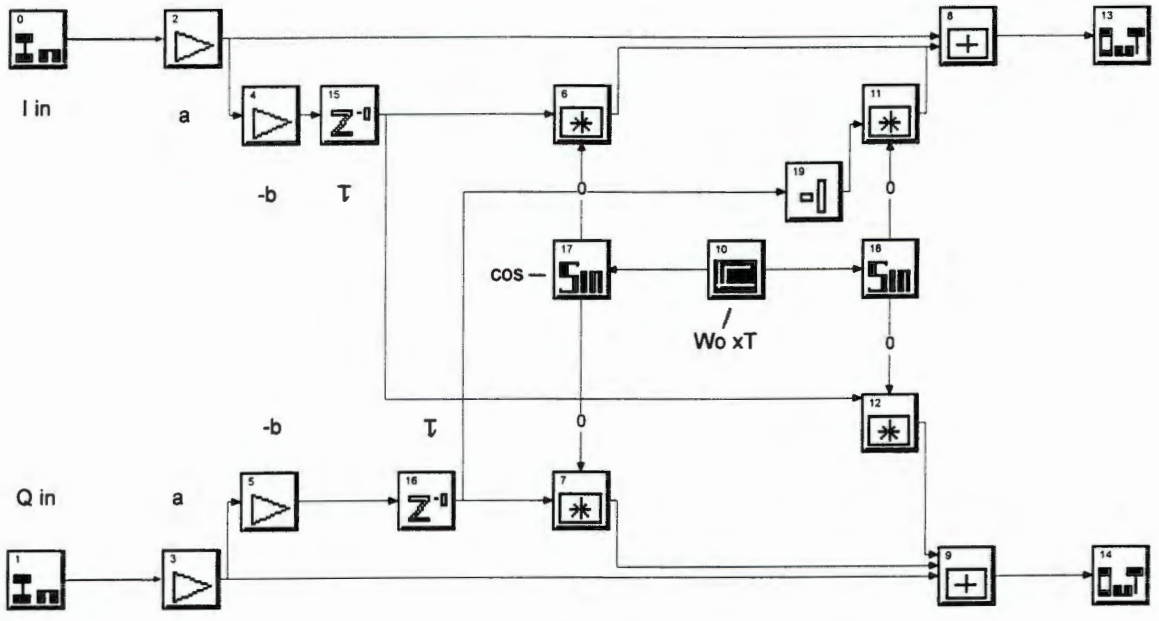

Figure 5.7: SystemView model for Rummler's fading model

Transform using the I channel for the real part and the Q channel for the imaginary part of the transform input sequence. The result of a 26dB deep notch ($b = 0.95$) for Rummler's model with $\tau = 24.5$ns, $a = 1$ and a notch frequency of 5MHz, is shown in figure 5.8. These values have been exaggerated so that the notch can be seen in the spectrum. Figure 5.9 shows the original spectrum for comparison purposes. As can be seen, the simulation yields the expected results.

Figure 5.10 shows the eye after being distorted by a channel with the following mild parameters: $\tau = 4.9$ns, $w_0 = 5$MHz, $a = 1$, $b = 0.6$. This eye must be interpreted as the projection of a phase shifted signal onto the reference phase, which is the transmitted carrier phase. To make this clearer, consider the constellation diagram as shown in figure 5.11. It can be seen that the constellation has rotated, and the amount of rotation is dependent on both notch depth and position. In figure 5.12, only the points sampled at the optimal symbol time have been shown to reduce the clutter caused by the ray paths. Observe that the constellation points have been spread out and rotated clockwise about their individual axes.

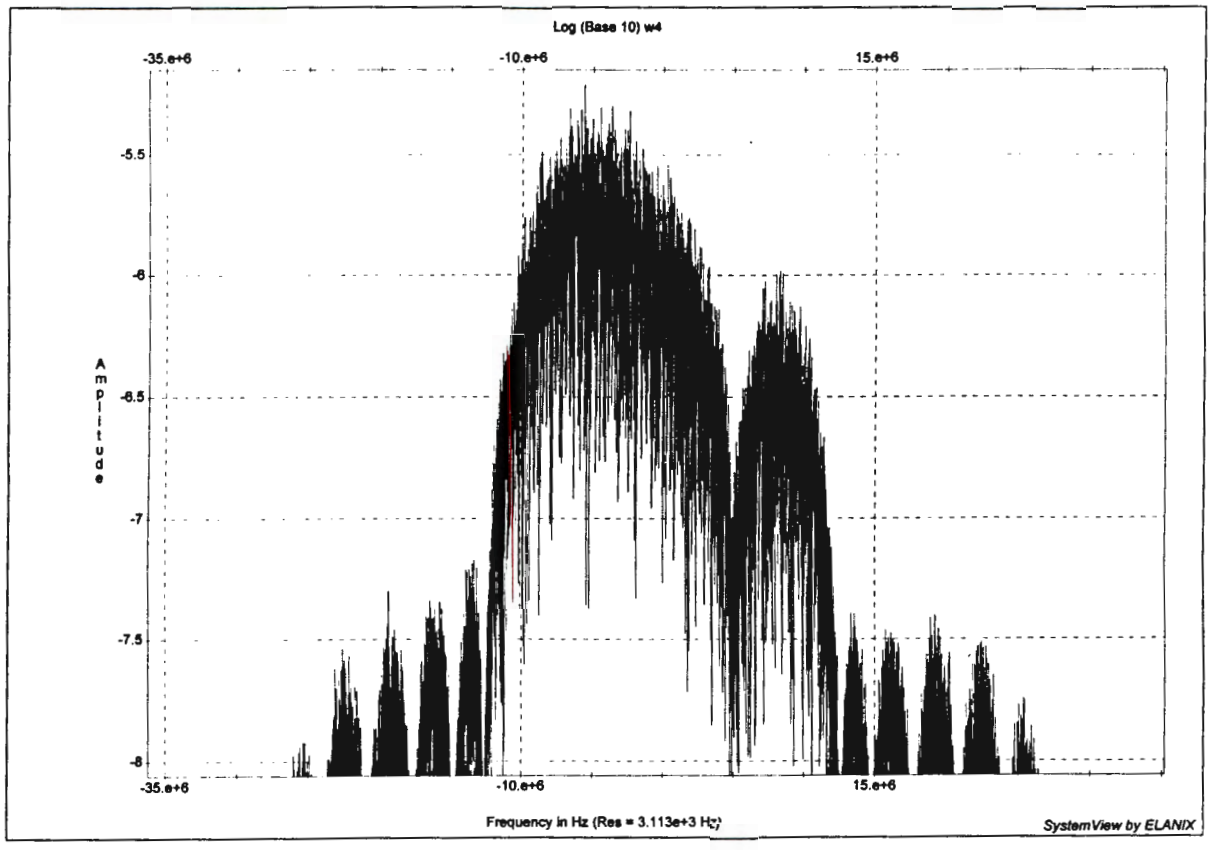

Figure 5.8: Spectrum containing notch

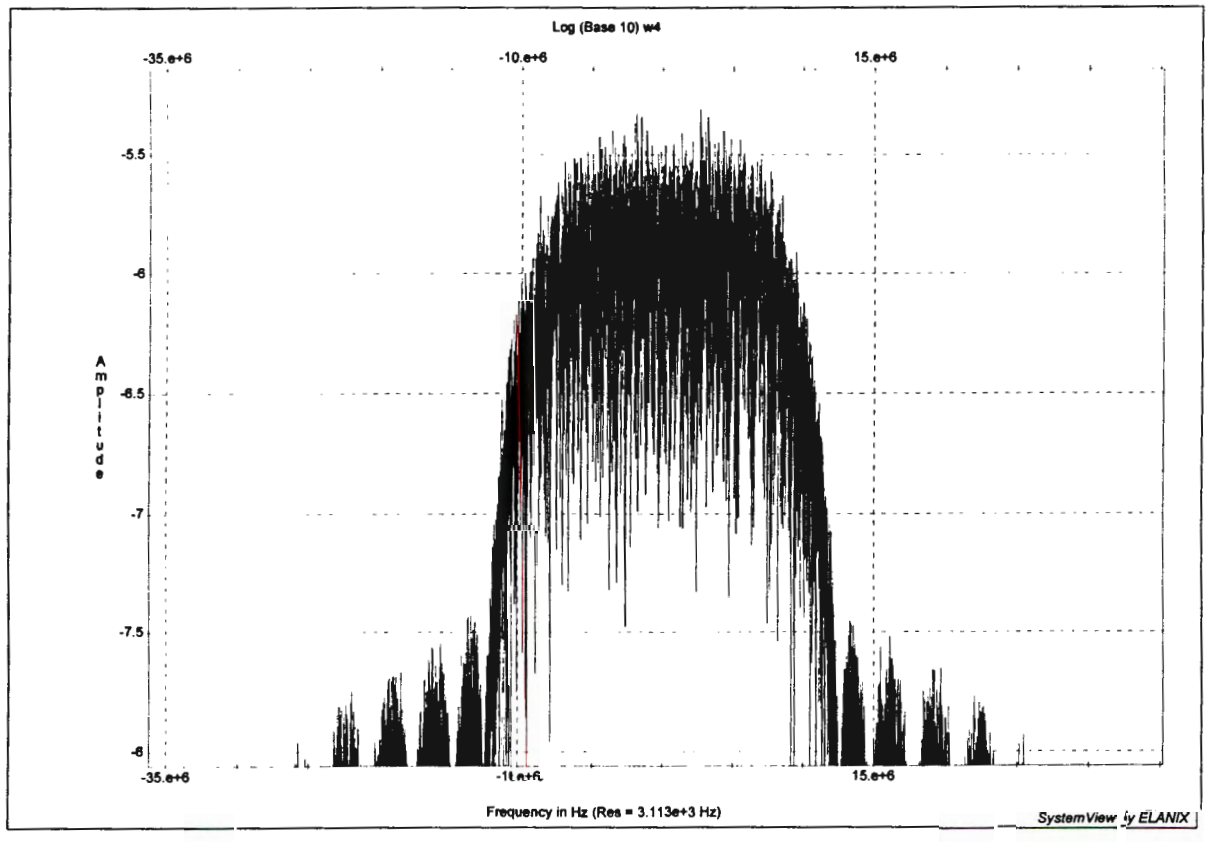

Figure 5.9: Undistorted spectrum

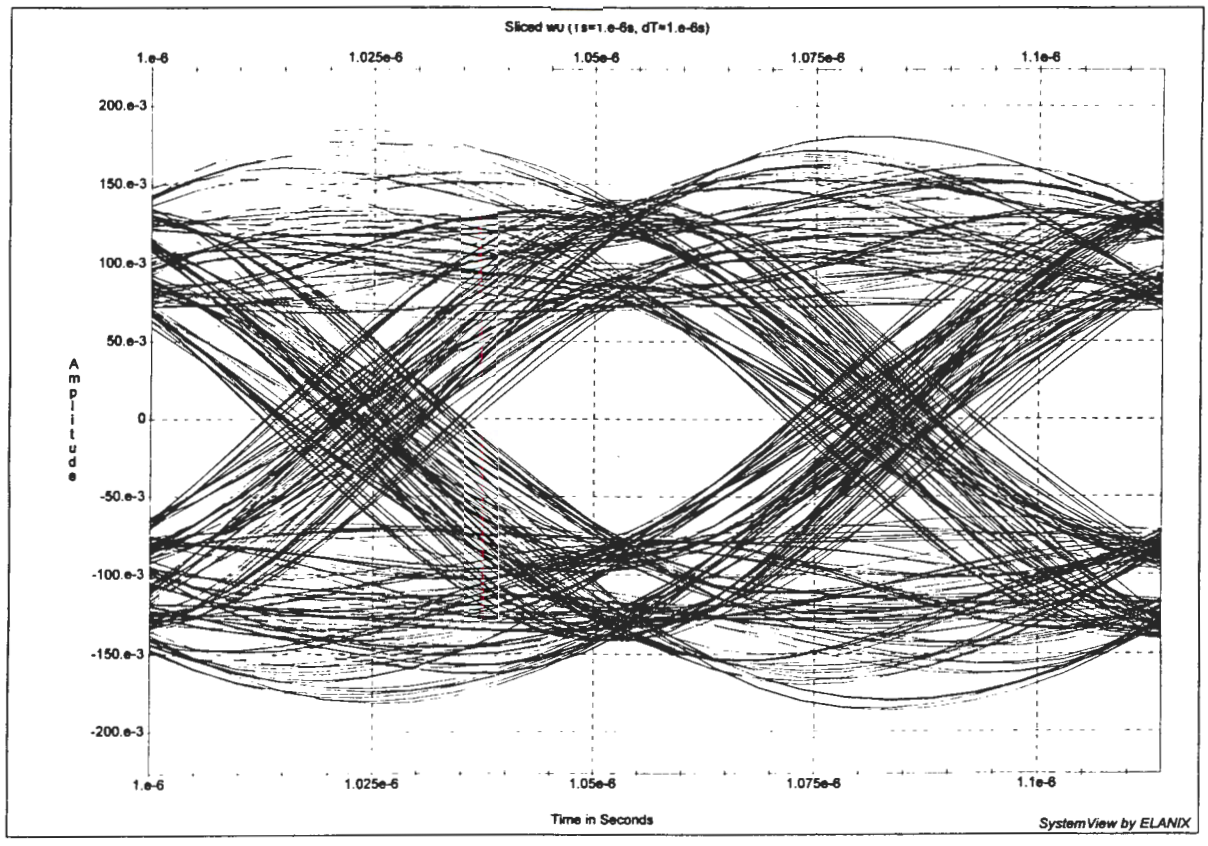

Figure 5.10: Distorted eye diagram

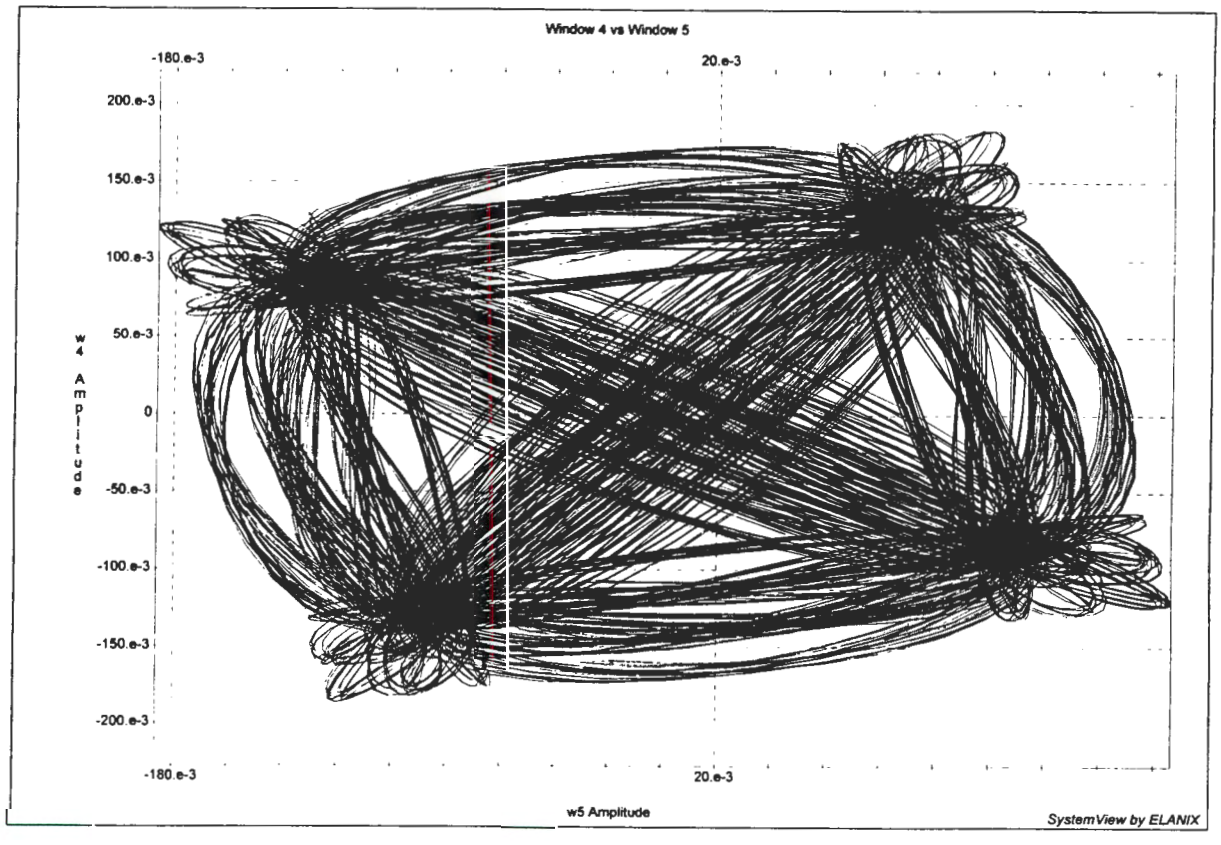

Figure 5.11: Rotated constellation diagram

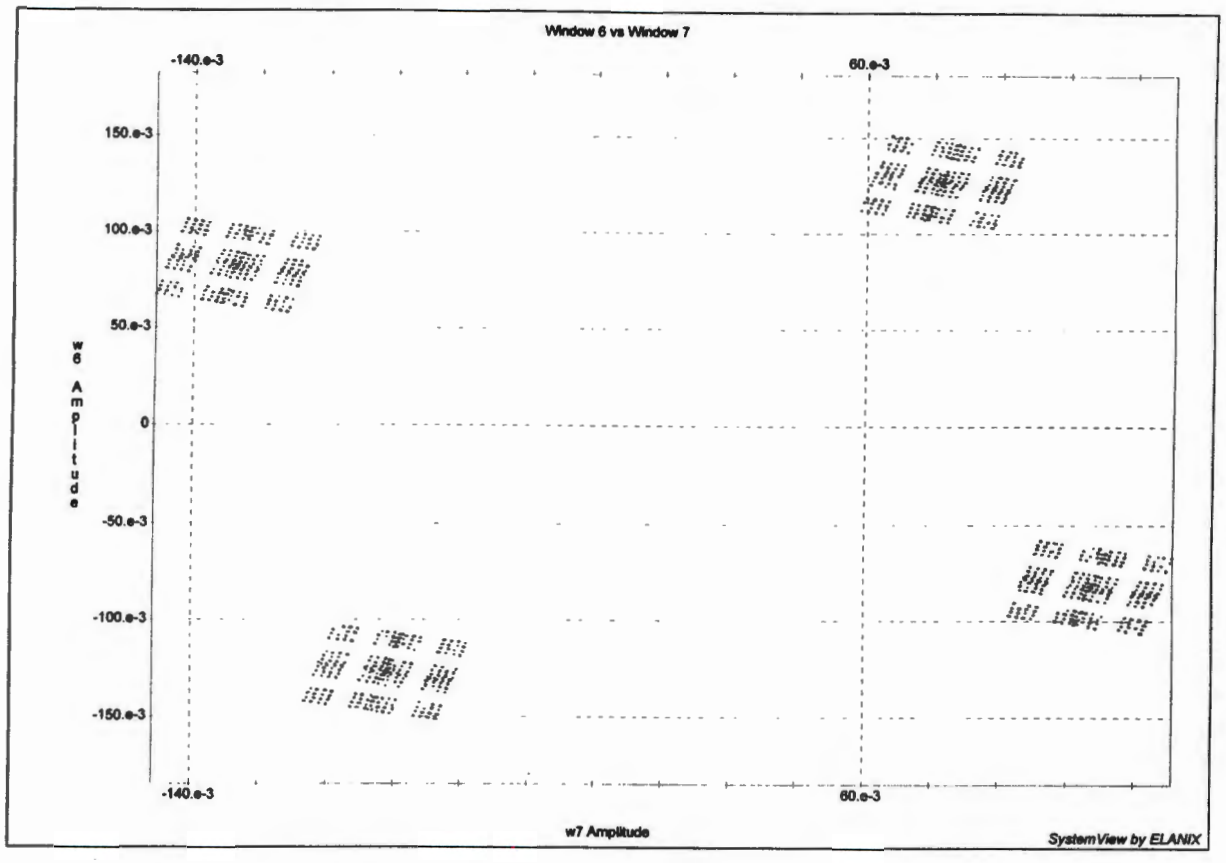

Figure 5.12: Optimally-sampled rotated constellation diagram

5.4. Costa's Loop simulation

In a practical system, a Costa's Loop is used to recover the carrier. In so doing, the Costa's Loop effectively rotates the constellation back to its original position, except for a tracking phase error. The behaviour of the Costa's loop is simulated as a rotation of the constellation diagram. Therefore, it is necessary to calculate the amount of rotation that the Three Path Model introduces and then to de-rotate the constellation by this amount, less the tracking error of the Costa's Loop.

Much insight can be gained by representing Rummler's model in terms of phasors, with a=1, given by:

$$y(t) = x(t) - be^{jw_0\tau}x(t-\tau) \qquad \textbf{(5.11)}$$

Now since $\tau << T$, it is assumed that :

$$x(t) \approx x(t-\tau) \tag{5.12}$$

so that **(5.11)** becomes:

$$y(t) = x(t).[\ 1 - be^{jw_0\tau}\ ] \tag{5.13}$$

Now consider the vector $\bar{x}$ as given by:

$$\bar{x} = 1 - be^{jw_0\tau} \tag{5.14}$$

which is represented in the phasor diagram of figure 5.13.

The magnitude of $\bar{x}$ yields the distance to the constellation points from the origin, while the angle of $\bar{x}$ indicates the amount of rotation that the constellation has undergone.

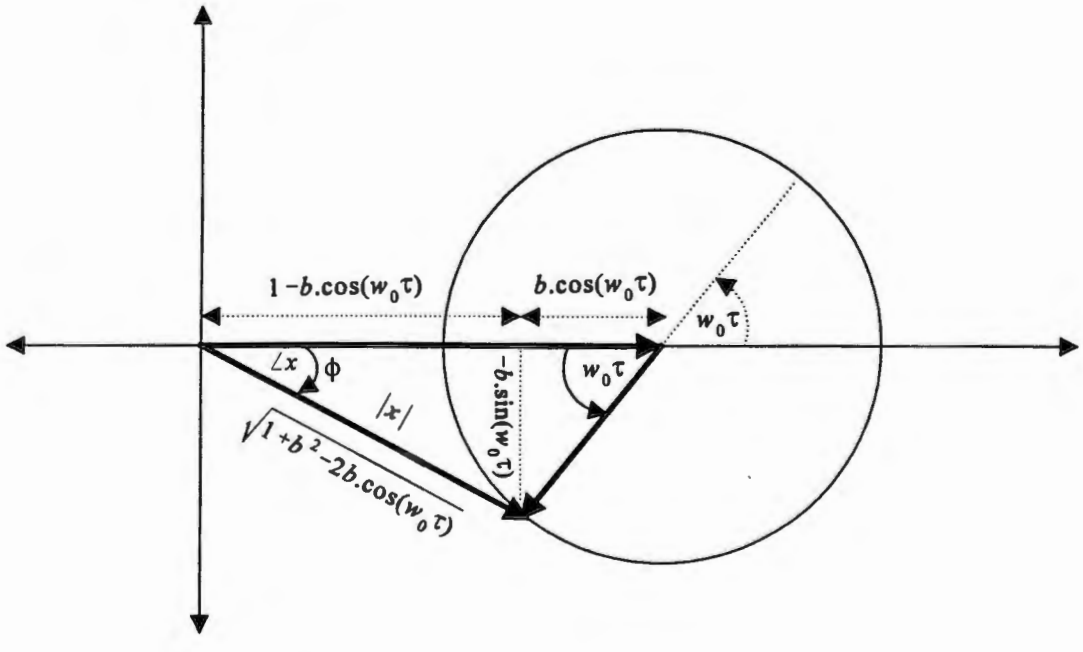

Figure 5.13: Phasor representation of the approximate 3PM phase shift

To include a phase de-rotation on the equivalent baseband system, a multiplication by $e^{-j\phi}$ is needed. Using Euler's formula and carrying out the complex multiplication with an arbitrary complex number, $z=a+jb$, results in:

$$\begin{aligned}(a+jb)e^{-j\phi} &= (a+jb).(\cos\phi - j\sin\phi) \\ &= (a.\cos\phi + b.\sin\phi) + j(b.\cos\phi - a.\sin\phi)\end{aligned} \tag{5.15}$$

This process can be implemented as shown in figure 5.14.

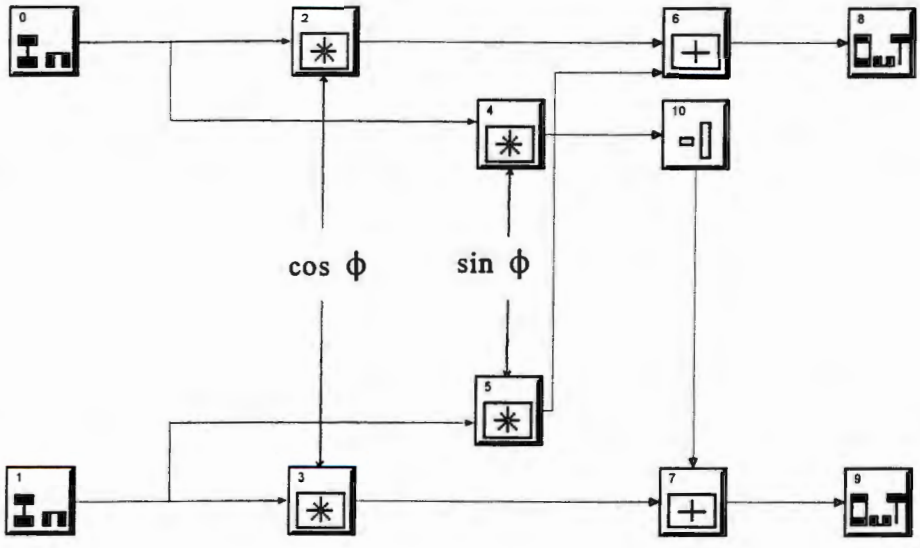

Figure 5.14: Complex baseband de-rotation process

Now it is necessary to calculate expressions for $\sin\phi$ and $\cos\phi$. From figure 5.13 it can be seen that:

$$\cos\phi = \frac{1 - b.\cos w_0\tau}{\sqrt{1 + b^2 - 2b.\cos w_0\tau}}$$
$$\sin\phi = \frac{-b.\sin w_0\tau}{\sqrt{1 + b^2 - 2b.\cos w_0\tau}} \qquad (5.16)$$

The model to implement this simulation of the behaviour of the Costa's Loop with a phase error, is shown in figure 5.15. It should be noted that the assumption **(5.12)** results in some phase error and it will be assumed that this error is an adequate representation of the behaviour of the Costa's Loop for simulation purposes. Therefore, the value for the phase-offset error module will be kept at zero when generating the results of the next chapter.

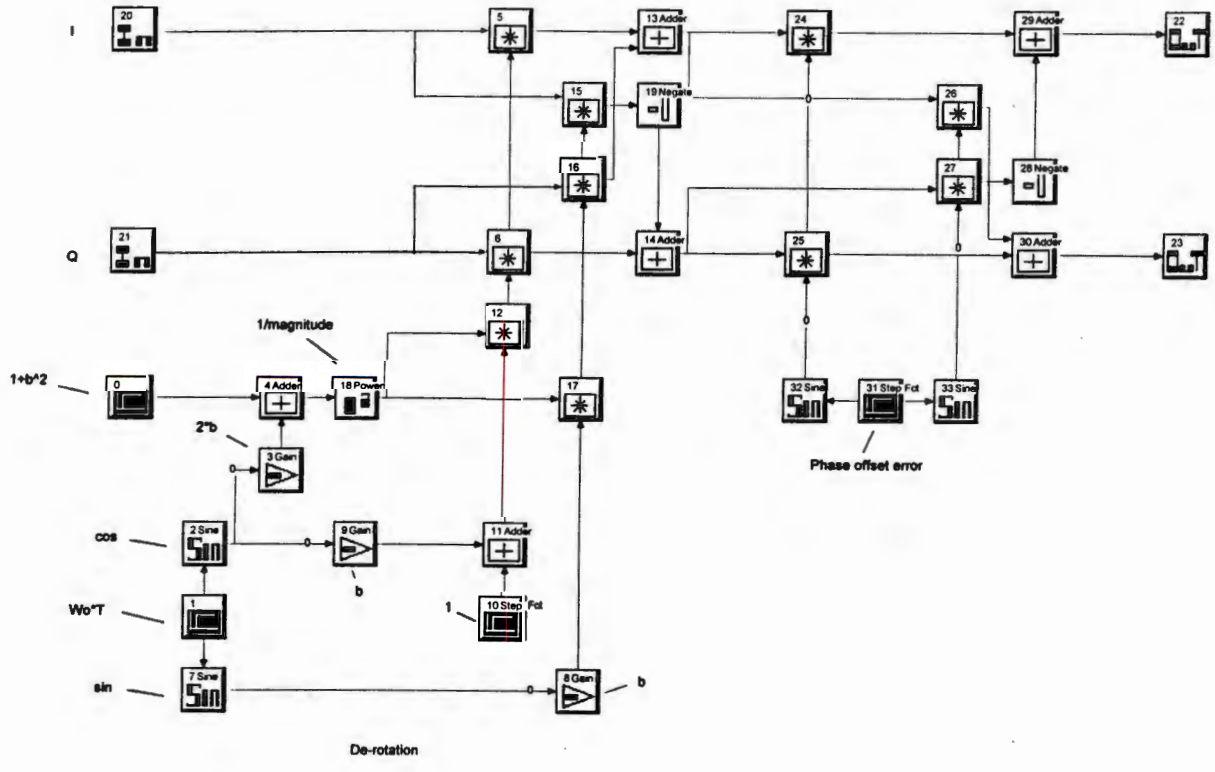

Figure 5.15: SystemView model of Costa's Loop.

5.5. Fixed complex equalizer implementation

The final simulation element needed is that of the equalizer. Using the same reasoning as in the last section, it can easily be seen that the complex baseband equivalent of the equalizer is as shown in figure 5.16. Each square marked with an * in the figure, is a transversal filter with optimal taps. Figure 5.17 shows the complete top-level simulation model.

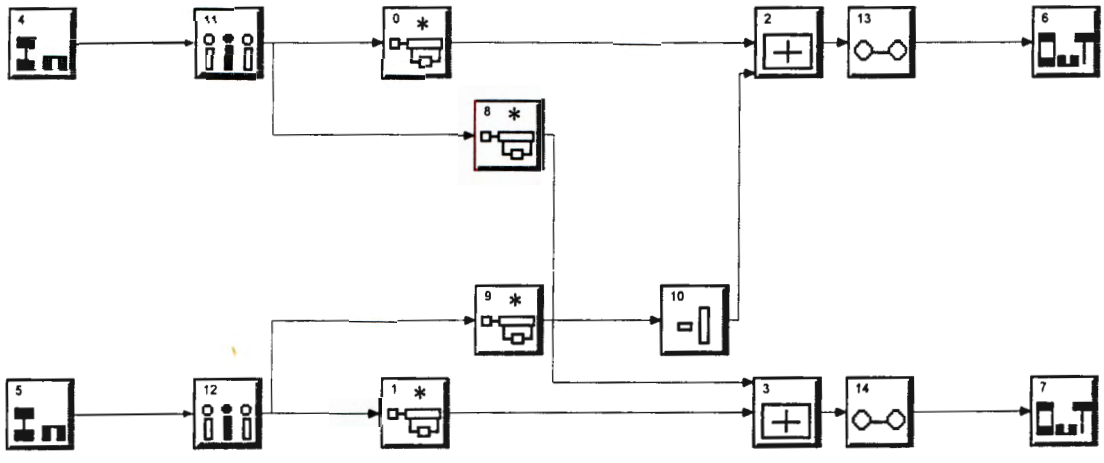

Figure 5.16: Complex equalizer model.

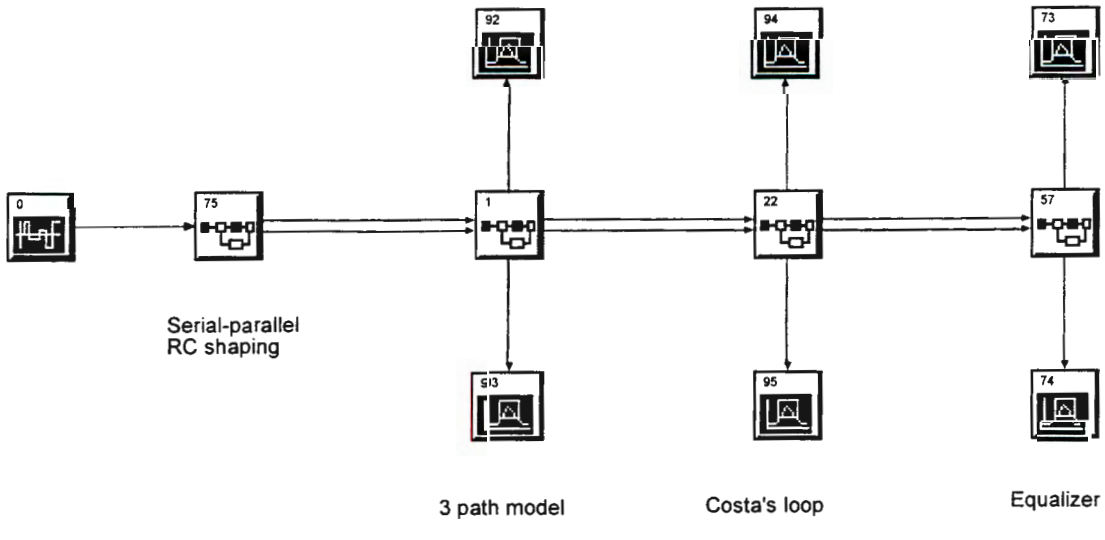

Figure 5.17: Complete simulation model.

5.6. Chapter references

1. Ziemer, R.E., and R.L. Peterson, **Introduction to digital communications.** Macmillan Publishing Company, 1992, p.202-225.

2. Stremler, F.G., **Introduction to communication systems.** 2ed, Addison-Wiley, U.S.A., 1982, p.244-247.

CHAPTER 6

Simulation results, discussion and conclusion

The simulation model as presented in chapter 5 will be used in this chapter to investigate the performance of QPSK for different fading model parameters. The amount of improvement due to equalization with optimal and PO2 coefficients, is then determined and conclusions drawn as to whether a PO2 equalizer is a viable pursuit.

6.1. Simulation assumptions and reductions

To limit the scope of the investigation, some simplifications are necessary, and will be discussed in this section.

As was mentioned in chapter 5, noise will be ignored in the generation of the simulation results. This was deemed justifiable in that the investigation is into the compromise of the PO2 coefficients and not into the equalizer's performance in a noisy environment. The necessary theory to enable an investigation into the noise performance has been presented in the dissertation, in case of future further investigations. By ignoring noise, the performance of the least mean-square equalizer is identical to that of a zero-forcing equalizer. A least mean-square equalizer is known to be superior to a zero-forcing equalizer in a noisy environment.

The Inverse Eye Aperture (IEA) is used, in preference to BER measurements, as the means of system performance evaluation as this reduces the simulation run-time and complexity. There are various definitions for EA, but the one used for these investigations, is simply:

$$Inverse\ Eye\ Aperture\ (IEA) = 20 \log\left[\frac{maximum\ eye\ opening}{minimum\ eye\ opening}\right] \qquad (6.1)$$

This choice was made because it yields a graph resembling an M-curve when the graph of IEA versus notch position is plotted.

To gain an intuitive feel for the IEA as defined above, consider figure 6.1 which represents some examples of IEA values related to physical eye diagrams. The eye diagrams were generated using the simulation model as used in the rest of this chapter. The notch frequency was set to 3MHz in order to introduce cross-talk between the in-phase and quadrature channels. The notch depth was varied to produce the desired distortion. If the eye is completely open, the IEA equals 0, but if the eye is completely closed then the IEA is infinite. Note from figure 6.1 how a relatively shallow notch of 12dB can cause severe distortion of the eye diagram. It must also be remembered that noise has been neglected here. If noise were also taken into account, the eye aperture would be even smaller.

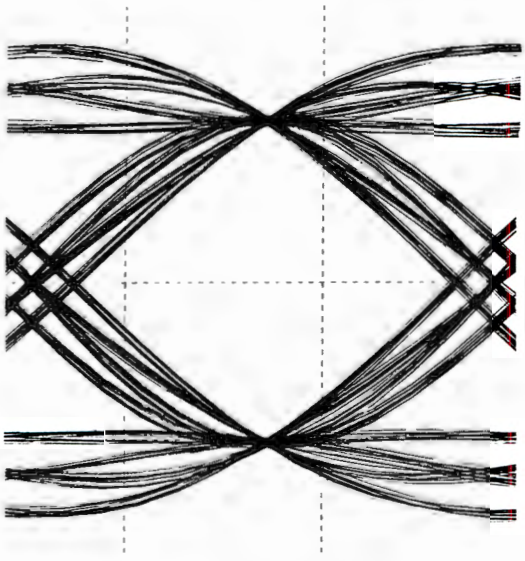

Notch depth = 2dB, IEA = 0.6dB

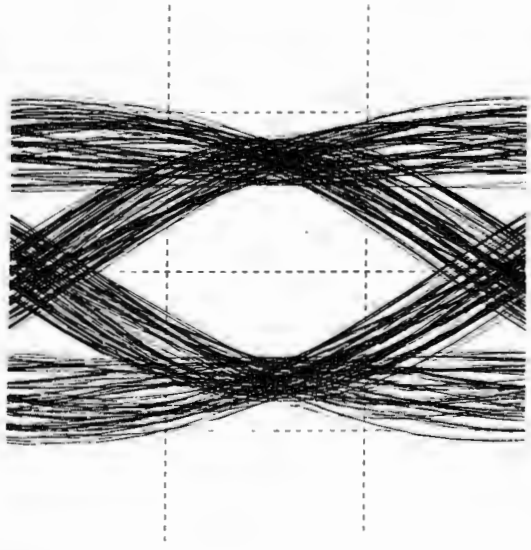

Notch depth = 6dB, IEA = 4.0dB

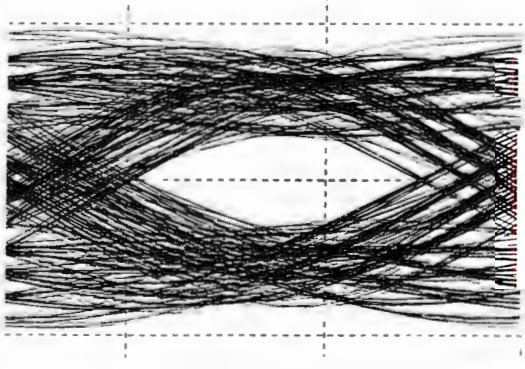

Notch depth = 9dB, IEA = 9.4dB

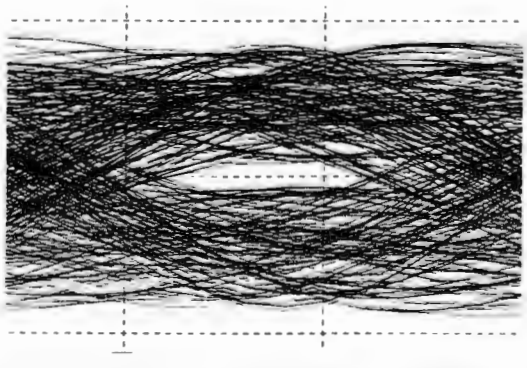

Notch depth = 12dB, IEA = 20.7dB

Figure 6.1: Examples of IEA values associated with eye diagrams

6.2. Simulation method

The method used to generate the simulation results is briefly described in this section. The combined impulse response of the QPSK modulator, the distortion channel and the receiver, was obtained directly from SystemView by using the impulse function in place of the 34MBit/s source. The channel parameters were entered, the simulation run, the impulse sampled at the correct instances and the output sent to a file.

This file was then read by a Mathcad sheet (see appendix III), the optimal and rounded coefficients calculated, and the values output to files. These files then had to be converted to SystemView format, after which they were used by SystemView to set the taps of the equalizer structure. The simulation was then run and the IEA measured. This process was repeated for each notch frequency and for each set of equalizer coefficients.

The above procedure could be done completely, and more efficiently, in SystemView by making use of the USER CODE module and writing C programs to perform the necessary operations. Time did not permit this refinement of the simulation model to be implemented.

6.3. Performance of unequalized QPSK

The first scenario investigated was that of the performance of QPSK in a fading environment without the assistance of an equalizer. The channel distortion was modelled with a constant τ of 9.8ns as this was convenient for simulation purposes. The system sampling frequency was 204MHz (6 samples for each data bit) which has a sample interval of 4.9ns. Thus τ is equal to two sample intervals.

The parameter *b* was set equal to 0.9, which is equivalent to a 20dB deep notch. The parameter *a* was set to 1 as it is not affected by frequency-selective fading. Further justification for this is that the purpose of *a* is to account for flat fades, but this effect is minimized by the operation of the Automatic Gain Control (AGC) circuitry in a real system.

As mentioned in the previous chapter, the offset-phase error was set to 0. This does not mean that there is no phase-error in the simulation, because the Costa's Loop module has a small amount

of varying residual phase error. As this varying phase characteristic will be the same for each of the scenarios investigated, performance comparisons can still be performed.

The number of taps in the complex equalizer was fixed at 7. This is an adequate number to capture most of the system's essential impulse response information and makes hardware implementation achievable.

From (5.7), the baseband spectrum can be calculated to be contained within the frequency range 0 to 12.75MHz for raised-cosine shaped data having a roll-off factor of 0.5. Thus the notch positions investigated, lay in this region.

The results of the simulated IEA for a QPSK system without equalization, are represented in figure 6.2 as the top trace.

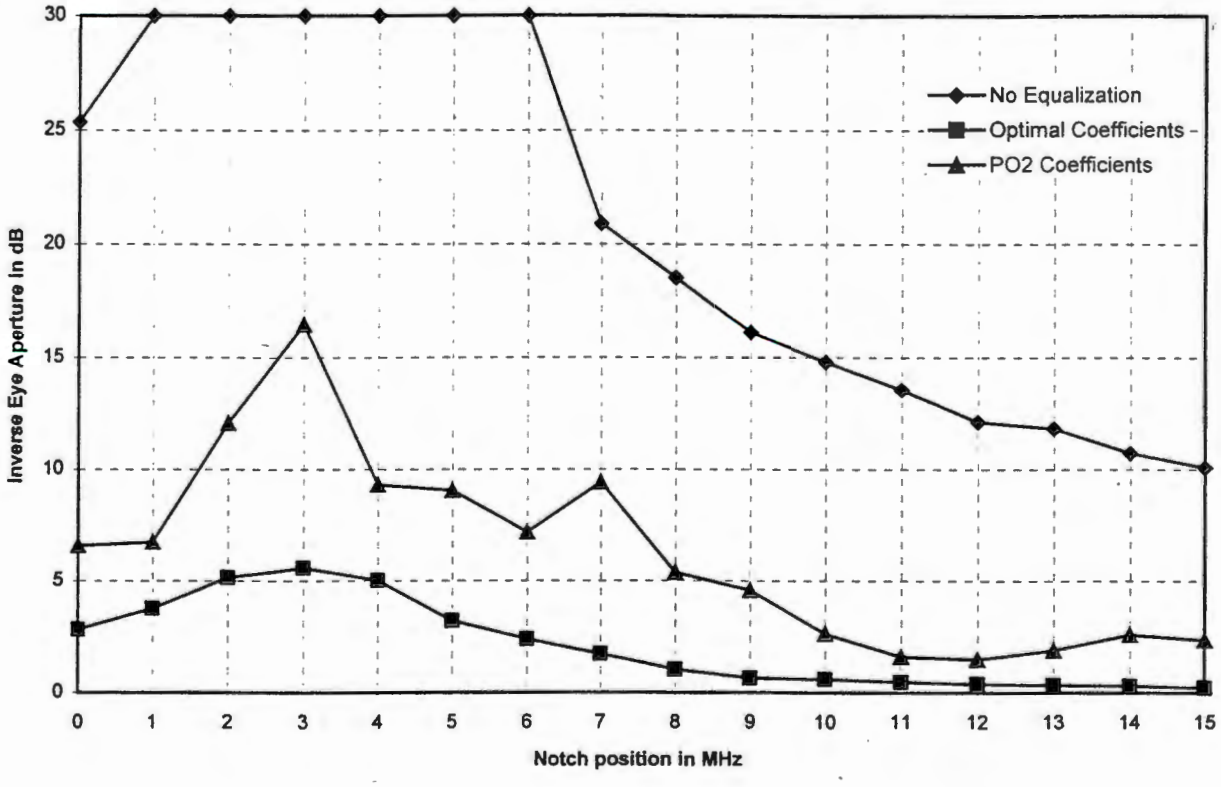

Figure 6.2: Graph of inverse eye aperture versus notch position

Note that for notch frequencies between 2 and 7 MHZ, no eye was visible and so could not be measured. The results presented in figure 6.2 follow a similar trend to those presented in chapter 3. When comparing figure 6.2 to an M-curve, it must be remembered that an M-curve is a contour of BER and so ends abruptly near the edge of the transmission bandwidth. Figure 6.2 does not display this abrupt characteristic because the IEA value changes more gradually. A BER curve has more of a threshold effect associated with it.

6.4. Performance with equalization

Having established the performance of QPSK without equalization, an equalizer was introduced into the simulation. The optimal coefficients were calculated for the different notch positions under consideration. These optimal values were then converted to ten bit binary numbers. The values were further processed to produce PO2 coefficients. This was achieved by comparing the optimal tap weight to the value half way between the two adjacent PO2 values. If the tap weight was larger than the half way value, it was set to the larger PO2 value, otherwise it was set to the smaller PO2 value.

The results of the simulation incorporating an equalizer having the tap weights just described, can be seen in figure 6.2. The bottom trace is for the optimal coefficients with infinite precision, and the middle trace represents the results for the 10 bit PO2 coefficients. Results were also generated for the 10 bit binary representation of the optimal coefficients, but these turned out to be so close to the infinite precision values, that there was no reason to record them. Table 6.3 records the numerical results.

The lower trace of figure 6.2 represents the best performance achievable with a 7-tap equalizer. The upper trace shows the worst performance. Both traces have shapes which are not unexpected, that is half of an M-type shape. Note also the smooth transition between notch positions.

w_0	No equalizer	Optimal equalizer	PO2 equalizer
0	25.36	2.82	6.58
1	inf	3.77	6.74
2	inf	5.14	12.07
3	inf	5.58	16.47
4	inf	5.03	9.31
5	inf	3.21	9.04
6	inf	2.38	7.17
7	20.91	1.72	9.41
8	18.53	1.04	5.37
9	16.09	0.65	4.58
10	14.80	0.59	2.62
11	13.55	0.48	1.61
12	12.12	0.39	1.49
13	11.82	0.34	1.89
14	10.72	0.30	2.59
15	10.09	0.23	2.35

Table 6.3: Results of IEA(dB) for various notch positions(MHZ)

The middle curve represents a graphical summary of the PO2 compromise. It too has approximately a half M-type shape, but more apparent is the jaggedness of the trace, which can be ascribed to the rounding process and the large jumps between values.

This rounded PO2 performance curve represents the worst case situation for a PO2 equalizer, as the PO2 adaption algorithm would ensure convergence to the set of optimal PO2 coefficients which minimises the IEA. These optimal values could be calculated using the branch-and-bound technique as mentioned in chapter 3 and the performance simulated. However, the upper bound as represented in figure 6.2, is considered to be adequate for practical purposes.

6.5. System performance in the absence of fading

Due to the fact that the receiver is not matched to the raised-cosine characteristic, there is an inherent performance degradation in the simulation model. The DAC distortion mentioned in chapter 5 further degrades the ideal system performance.

This degradation was assessed by measuring the IEA which was found to be 0.76. The inclusion of an equalizer with 10 bit precision reduced this figure to 0.09, while the PO2 equalizer reduced it to 0.21.

These figures are interesting in that they present the limit to which a faded system could be improved. Note that the ideal system without an equalizer is worse than an optimally equalized system experiencing a 20dB notch at an offset frequency of 9MHz or more.

6.6. Conclusion

From the investigation contained in this dissertation, it can be concluded that a 20dB notch just off the channel centre frequency is capable of severely degrading the performance of a QPSK system. The likelihood of such a notch occurring was discussed in chapter 2.

It was demonstrated that a 7-tap symbol spaced equalizer having 10 bit precision coefficients could greatly enhance the system's performance during frequency-selective fading activity. The PO2 equalizer performance was worse than the optimal equalizer's performance, but it would still significantly enhance the system's performance. At the worst notch offset frequency (3MHz), the PO2 equalizer's performance was 11dB worse than the optimal equalizer. However, the PO2 equalizer results in at least 13dB of improvement compared to the unequalized situation.

It was also demonstrated that even in the absence of frequency-selective fading, a PO2 equalizer can significantly improve a system's ideal performance. The improvement gained by the inclusion of the PO2 equalizer amounted to approximately 0.5dB.

In terms of hardware savings, the multiplication circuitry for each tap is reduced to a

simple shift register. The circuitry required to implement the shift register is approximately 5% of that required for a multiplier. Consideration of the fact that 28 multipliers are needed, the attractiveness of the PO2 simplification immediately becomes apparent.

The factor which will ultimately determine the usefulness of a PO2 equalizer, is the amount of hardware it will take to implement the adaption algorithm. If the PO2 algorithm has a comparable hardware requirement to that of the LMS adaption circuitry, the PO2 equalizer will be very attractive. The true LMS algorithm implementation requires 28 multipliers, but variations of the algorithm have reduced this requirement. Further investigation will be required to determine the performance and complexity of the PO2 adaptive equalizer which can then be compared with the known performance and complexity of the LMS equalizer, or one of its many derivatives.

The results of this investigation indicate that the PO2 equalizer is certainly a viable consideration for the equalization of QPSK. However, the practical implementation will depend on a suitable adaption algorithm being developed. With the emergence of Genetic Algorithm techniques, new opportunities have been created for the development of the PO2 adaption algorithm.

CHAPTER 7

Summary and recommendations for future investigation

The aim of this dissertation was to establish the usefulness of a PO2 equalizer in relation to a QPSK digital radio system experiencing frequency-selective fading. As there is some confusion as to how multipath and its associated fading effects, are defined, it was decided to commence the dissertation with a summary of the multipath phenomenon. This summary included the physics responsible for multipath and the likelihood of its occurrence, thereby putting the dissertation in context.

The obvious progression was to present a means of modelling the multipath effect and it was established that Rummler's three-path model is commonly used for this purpose. By using this model, a dispersion signature or M-curve can be calculated or simulated. It can also be used to evaluate the enhancement in performance of digital radio systems employing diversity as a means of multipath counter-measure.

The pertinent papers from an extensive literature survey were summarised in chapter 3. This chapter was also used to establish an introductory knowledge to the field of equalization. It was found that similar work to that which was being investigated had already been carried-out by other researchers, but none of the papers yielded the specific results being investigated in this dissertation. It was interesting to find that the concept of PO2 equalizers had already been considered, but the apparent lack of interest in the literature was surprising.

Having spent much time formulating the concepts of baseband equivalence theory, a more coherent version was found in the book by Gitlin et al. A summary of this version was presented in chapter 4. The essential feature of baseband equivalence theory is that a passband system can be simulated more easily at baseband. It enables one to ignore the modulation and associated filter implementation problems. This theory has the Hilbert Transform as its foundation and a brief summary of this fascinating transform was presented.

A summary of Wiener filter theory and its application to a transversal filter structure, in the form of the Wiener-Hopf equations, was then presented. The Wiener-Hopf equations were solved for the simulation model after the essential observation was made and that was, that the whole simulation model could be treated as a transversal filter. The impulse response of the transversal approximation was simply the sampled impulse response of the simulation model.

Having established a theoretical basis for the investigations, the SystemView model was developed. It consisted of a QPSK modulator with raised-cosine shaping of the data, a baseband version of Rummler's three-path model, a model simulating the behaviour of the Costa's Loop and a complex baseband equalizer. SystemView was found to be a most suitable and user friendly simulation package.

Having devoted much effort to defining the foundations of the investigation, results were finally generated. The simulation procedure was not optimal, thereby preventing the extension of investigation into additional scenarios, but the results obtained confirmed the validity of the approach. The results indicated that a 10 bit PO2 equalizer is capable of significantly enhancing a system's performance during frequency-selective fading conditions. It can also significantly improve a system's performance which has been degraded by a less than optimal hardware implementation.

It is unfortunate that this subject could not be investigated further, but here are some recommendations to assist if this were to happen. An essential item to consider in simulating system performance is the simulation time. The theory of baseband equivalence was developed to assist in this regard but the actual simulation procedure was time consuming and labourious. It would be worth spending time streamlining the procedure such that different scenarios could easily be evaluated, such as number of taps and different coefficient quantization.

Thereafter, it would be interesting to know how the PO2 equalizer performed in the presence of noise. Related to this, a literature search for methods of calculating BER's from the eye apertures should be conducted. This could be combined with noise theory, to yield an efficient means of simulating M-curves. This was one of the unachieved initial goals of this thesis. An M-curve is

very useful for doing outage calculations, besides which, it is the standard, most illustrative means of describing a system's performance during fading events.

The results could be extended to show the performance with calculated optimal PO2 coefficients. These optimal coefficients could be calculated easily with modern optimization techniques. The genetic algorithm seems like a good candidate and could be an investigation on its own. Somewhat related to this, the procedure for rounding the coefficients to yield the PO2 coefficients could be refined. The fact that the significance of the taps seems to decrease from the central tap outward, could be used to weight the rounding process. Favourable simulation results could suggest algorithms for PO2 adaption along these lines.

Finally, and most excitingly, the work could be extended by developing a practical PO2 adaption algorithm with special emphasis being placed on an FPGA implementation. As mentioned in chapter 3, algorithms do exist (and have been patented) for adapting PO2 equalizers, but these did not appear suitable for an FPGA implementation.

Bibliography

Papers:

1. Allen, E.W., **The multipath phenomenon in line-of-sight digital transmission systems.** Microwave Journal, May 1984, p.215-225.

2. Amitay, N. and L.J. Greenstein, **Multipath outage performance of radio receivers using finite-tap adaptive equalizers.** IEEE Transactions on Communications, Vol. COM-32 No. 5, May 1984, p.597-608.

3. Balaban, P., **Statistical Model for amplitude and delay of selective fading.** AT&T technical journal, Vol. 64, No. 10, December 1985, p.2525-2549.

4. Barnett, W.T., **Multipath Propagation at 4, 6, and 11 GHz.** Bell System Technical Journal, Vol. 51, No. 2, February 1971, p.321-361.

5. Beare, C.T., **The choice of the desired impulse response in combined Linear-Viterbi algorithm equalizers.** IEEE transactions on communications, Vol. COM-26 No. 8, August 1978, p.1301-1307.

6. Bello, P.A., **Characterization of randomly time-invariant linear channels.** IEEE transactions on communications systems, Vol. CS-11, December 1963, p.360-393.

7. Benveniste, A. and M. Goursat, **Blind equalizers.** IEEE transactions on communications, Vol. COM-32, No. 8, August 1984, p.871-883.

8. Bullington, K., **Phase and amplitude variations in multipath fading of microwave signals.** Bell System Technical Journal, Vol. 50, No. 6, July 1971, p.2039-2053.

9. Campbell, J.C., and R.P. Coutts, **Outage prediction of digital radio systems.** Microwave digital radio, IEEE press, 1988, p.78-79.

10. Cantoni, A. and P. Butler. **Properties of the Eigenvectors of Persymmetric Matrices with applications to communications theory.** IEEE transactions on communications, Vol. COM-24, No. 8, August 1976, p.804-809.

11. Cantoni, A. and K. Kwong, **Further results on the Viterbi Algorithm equalizer.** IEEE transactions on information theory, November 1974, p.764-767.

12. Caraiscos, C. and B. Liu, **A roundoff error analysis of the LMS adaptive algorithm.** IEEE transactions on acoustics, speech and signal processing, Vol. ASSP-32, No. 1, February 1984, p.34-41.

13. Chamberlain, J.K., F.M. Clayton, H. Sari and P. Vandamme, **Receiver techniques for microwave digital radio.** Microwave digital radio, IEEE press, 1988, p.131-141.

14. Chang, R.W., **A new equalizer structure for fast start-up digital communications.** Bell system technical journal, Vol. 50, No. 6, July 1971, p.1969-2014.

15. Chen, J. and R. Priemer, **An inequality by which to adjust the LMS algorithm step-size.** IEEE transactions on communications, Vol. COM-43, No. 2/3/4, Feb/March/April 1995, p.1477-1483.

16. Chen, S., B. Mulgrew and S. McLaughlin, **Adaptive Bayesian equalizer with decision feedback.** IEEE transactions on signal processing, Vol. 41, No. 9, September 1993, p.2918-2927.

17. Chen, S., S. McLaughlin, P.M. Grant and B. Mulgrew, **Multi-stage blind clustering equalizer.** IEEE transactions on communications, Vol. 43, No. 2/3/4, Feb/March/April 1994, p.701-705.

18. Chen, S., G.J. Gibson and C.F.N. Cowan, **Adaptive channel equalization using a polynomial-perceptron structure.** IEE proceedings-I, Vol. 137, No. 5, October 1990, p.257-264.

19. Daido, Y., E. Fukuda, Y. Takeda and H. Nakamura, **Theoretical evaluation of signatures and CNR penalties caused by modem impairments in multilevel QAM digital radio modems.** IEEE transactions on communications, Vol. COM-34, No. 7, July 1986, p.654-661.

20. Elanix Incorporated, **SystemView: A guide to the communications library.** 1995, p.58-67.

21. Emshwiller, M., **Characterization of the performance of PSK digital radio transmission in the presence of multipath fading.** Microwave digital radio, IEEE press, 1988, p.209-214.

22. Ernst, D., **LMS adaptive algorithms for joint forward and decision feedback equalization.** IEE proceedings-F, Vol. 138, No. 5, October 1991, p.520-524.

23. Falconer, D.D., **Jointly adaptive equalization and carrier recovery in two dimensional communication systems.** Bell System Technical Journal, Vol. 55, March 1976, p.317-334.

24. Fenderson, G.L., J.W. Parker, P.D. Quigley, S.R. Shepard, C.A. Siller, **Adaptive transversal equalization of multipath propagation for 16-QAM, 90-Mb/s digital radio.** Bell system journal, Vol. 63, No. 8, October 1984, p.1447-1463.

25. Forney, G.D., **Maximum-likelihood sequence estimation of digital sequences in the presence of intersymbol interference.** IEEE transactions on information theory, Vol. IT-18, No. 3, May 1972, p.363-378.

26. Foschini, G.J., **Equalizing without altering or detecting data.** Bell system journal, Vol. 64, no. 8, October 1985, p.1885

27. Foschini, G.J., and J. Salz, **Digital communications over fading radio channels.** Bell system technical journal, Vol. 62, No. 2, February 1983, p.429-455.

28. Gardner, W.A., **Nonstationary learning characteristics of the LMS algorithm.** IEEE transactions on circuits and systems, Vol. CAS-34, No. 10, October 1987, p.1199-1207.

29. Gatherer, A. and T. Meng, **A robust adaptive parallel DFE using extended LMS.** IEEE transactions on signal processing, Vol. 41, No. 2, February 1993, p.1000-1005.

30. George, D.A., R.R. Bowen and J.R. Storey, **An adaptive decision feedback equalizer.** IEEE transactions on communications, Vol. COM-19, No. 3, June 1971, p.281-293.

31. Giger, A.J. and W.T. Barnett, **Effects of multipath propagation on digital radio.** IEEE transactions on communications, Vol. COM-29, No. 9, September 1981, p.1345-1352.

32. Gitlin, R.D., and S.B. Weinstein, **On the required tap-weight precision for digitally implemented, adaptive, mean-squared equalizers.** Bell System Technical Journal, Vol. 58, No. 2, February 1979.

33. Gitlin, R.D., H.C. Meadors and S.B. Weinstein, **The tap-leakage algorithm: An algorithm for the stable operation of a digitally implemented, fractionally spaced adaptive equalizer.** Bell System Journal, Vol. 61, October 1982, p.1817-1839.

34. Gitlin, R.D., J.E. Mazo and M.G. Taylor, **On the design of gradient algorithms for digitally implemented adaptive filters.** IEEE transactions on circuit theory, Vol. CT-20, No. 2, March 1973, p.125-136.

35. Godard, D.N., **Self-recovering equalization and carrier tracking in two-dimensional data communications systems.** IEEE transactions on communications, Vol. COM-28, Nov 1980, p.1867-1875.

36. Greenstein, L.J. and V.K. Prabhu, **Analysis of multipath outage with application to 90-Mbits/s PSK systems a 6 and 11 GHz.** IEEE transactions on communications, Vol. COM-27 No. 1, January 1979, p.68-75.

37. Greenstein, L.J. and B.A. Czekaj-Augun, **Performance comparisons among digital radio techniques subjected to multipath fading.** IEEE transactions on communications, vol. COM-30, No. 5, May 1982, p.1184-1197.

38. Greenstein, L.J. and M. Shafi, **Outage calculation methods for microwave digital radio.** Microwave digital radio, IEEE press, 1988, p.179-187.

39. Gustafsson, F. and B. Wahlberg, **Blind equalization by direct examination of the input sequences.** IEEE transactions on communications, Vol. 43, No. 7, July 1995, p.2213-2222.

40. Hawksford, M.J. and N. Rezaee, **Adaptive mean-square-error transversal equalizer.** IEE proceedings-F, Vol. 128, No. 5, October 1981, p.296-304.

41. Hewlett Packard Application Note 379-1, **Measuring digital microwave radio M-curves/signatures.**

42. Hinedi, S. and W.C. Lindsey, **Intersymbol interference effects on BPSK and QPSK carrier tracking loops,** IEEE transactions on communication, Vol. 38, No. 10, October 1990, p.1670-1676.

43. Iltis, R.A., J.J. Shynk and K. Giridhar, **Bayesian algorithms for blind equalization using parallel adaptive filtering.** IEEE transactions on communications, Vol. 42, No. 2/3/4, Feb/March/April 1994, p.1017-1032.

44. Jakes, W.C., **An approximate method to estimate an upper bound on the effect of multipath delay distortion on digital transmission.** IEEE transaction on communications, Vol. COM-27 No. 1, January 1979, p.76-81.

45. Johnson, C.R., **On the interaction of adaptive filtering, identification, and control.** IEEE signal processing magazine, March 1995, p.22-37.

46. Kabal, P. **The stability of adaptive minimum mean square error equalizers using delayed adjustment.** IEEE transactions on communications, Vol. COM-31, No. 3, March 1983, p.430-432.

47. Li, Y. and Z. Ding, **A simplified approach to optimum diversity combining and equalization in digital data transmission.** IEEE transactions on communications, Vol. 43, No. 8, August 1995, p.2285-2288.

48. Liu, G.S. and C.H. Wei, **Multipath fading effects on carrier recovery of BPSK signal in digital radio.** IEE proceedings-I, Vol. 140, No. 5, October 1993, p.381-388.

49. Long, G., F. Ling and J.G. Proakis, **The LMS algorithm with delayed coefficient adaption.** IEEE transactions on acoustics, speech and signal processing, Vol. 37, No. 9, September 1989, p.1397-1405.

50. Long, G., F. Ling and J.G. Proakis, **Corrections to "The LMS algorithm with delayed coefficient adaption".** IEEE transactions on signal processing, Vol. 40, No. 1, January 1992, p.230-232.

51. Lu, F., and H. Samueli, **A 60-MBd, 480-Mb/s, 256-QAM decision-feedback equalizer in 1.2μm CMOS.** IEEE journal of solid state circuits, Vol. 28, No. 3, March 1993, p.330-338.

52. Lucky, R.W., **Automatic equalization for digital communication.** Bell System Journal, Vol. 44, April 1965, p.547-588.

53. Luk, E., A.D. Fagan and J.O. Scanlan, **Application of neural network-based equalizers in tracking time-varying non-linear multipath microwave radio channels.** 6th International Conference on Signal Processing Applications & Technology, 1995, p.79-83.

54. Lundgren, C.W., and W.D. Rummler, **Digital radio outage due to selective fading - Observation vs prediction from laboratory simulation.** Bell system journal, Vol. 58, No. 5, May 1979, p.1073-1100.

55. Lyon, R.F., **Two's complement pipelined multipliers.** IEEE transactions on communications, April 1976, p.418-424.

56. Max, J., **Quantization for minimum distortion.** IRE Transactions on Information Theory, Vol. IT-6, 1960, p.7-12.

57. Mazo, J.E., **Analysis of decision-directed equalizer convergence.** Bell System Technical Journal, Vol. 59, December 1980, p.1857-1876.

58. Metzger, K. and R. Valentin, **An analysis of the sensitivity of digital modulation techniques to frequency-selective fading.** IEEE transactions on communications, Vol. COM-33, No. 9, September 1985, p.986-992.

59. Meyer, M. and G. Pfeiffer, **Multilayer perceptron based decision feedback equalizers for channels with intersymbol interference.** IEE proceedings-I, Vol. 140, No. 6, December 1993, p.420-424.

60. Meyer, M.D. and D.P. Agrawal, **A high sampling rate delayed LMS filter architecture.** IEEE transactions on circuits and systems-II, Vol. 40, No. 11, November 1993, p.727-729.

61. Mikhael, W.B. and F.H. Wu, **Fast algorithms for block FIR adaptive digital filtering.** IEEE transactions on circuits and systems, Vol. CAS-34, No. 10, October 1987, p.1152-1160.

62. Monsen, P., **Fading channel communications.**, IEEE Communications Magazine, Jan 1980, 18, p.27-36.

63. Morais, D.H., A. Sewerinson and K. Feher. **The effects of the amplitude and delay slope components of frequency selective fading on QPSK, Offset QPSK and 8 PSK systems.** IEEE transactions on communications, Vol. COM-27 No. 12, December 1979, p.1849-1853.

64. Moridi, S. and H. Sari, **Analysis of four decision-feedback carrier recovery loops in the presence of intersymbol interference.** IEEE transactions on communications, Vol. COM-33, No. 6, June 1985, p.543-550.

65. Mulgrew, B., **Applying Radial Basis Functions.** IEEE Signal Processing, March 1996, p.50-65.

66. Treichler, J.R., I. Fijalkow and C.R. Johnson, **Fractionally spaced equalizers: How long should they really be?** IEEE Signal Processing, May 1996, p.65-81.

67. Nowlan, S.J. and G.E. Hinton, **A soft decision-directed LMS algorithm for blind equalization.** IEEE transactions on communications, Vol. 41, No. 2, February 1993, p.275-279.

68. Ott, R.H., M.C. Thompson, E.J. Violette and K.C. Allen, **Experimental and theoretical assessment of multipath effects on QPSK.** IEEE transactions on communications, Vol. COM-26 No. 10, October 1978, p.1475-1477.

69. Parhi, K.K. and D.G. Messerschmitt, **Concurrent cellular VLSI adaptive filter architectures.** IEEE transactions on circuits and systems, Vol. CAS-34, No. 10, October 1987, p.1141-1151.

70. Patra, J.C. and R.N. Pal, **Functional link artificial neural network model for channel equalization.** Int. conf. on Signal Processing Appl. and Techn., October 1994, p.1251-1256.

71. Pirani, G. and V. Zingarelli, **Adaptive multiplication-free transversal equalizers with application to digital radio systems.** IEEE Trans. Comm, Vol. COM-32 no. 9, September 1984, p.1025-1033.

72. Qureshi, S., **Adjustment of the position of the reference tap of an adaptive equalizer.** IEEE transactions on communications, Vol. COM-21, September 1973, p.1046-1052.

73. Qureshi, S., **Adaptive equalization.** IEEE communications magazine, March 1982, p.9-16.

74. Rafie, M.S., and W. Newman, **A new complex neural network-based decision-feedback equalizer: Application to bandlimited nonlinear satellite links.** Int. conf. on Signal Processing Appl. and Techn., October 1994, p.1257-1261.

75. Raghavan, S.H.R. and R.E. Ziemer, **Improving QPSK transmission in band-limited channels with interchannel interference through equalization.** IEEE transactions on communication, Vol. COM-25, No. 10, October 1977, p.1222-1226.

76. Raghunath, K.J. and K.K. Parhi, **Parallel adaptive decision feedback equalizers.** IEEE transactions on signal processing, Vol. 41, No. 5, May 1993, p.1956-1961.

77. Ramadan, M., **Availability Prediction of 8 PSK digital microwave system during multipath propagation.** IEEE transactions on communications, Vol. COM-27 No. 12, December 1979, p.1862-1869.

78. Recommendation ITU-R PN.453-4, 1994, **The radio refractive index: its formula and refractivity data.** p.206-213.

79. Recommendation ITU-R F.1101, 1994, **Characteristics of digital radio-relay systems below about 17GHz.** p.231-249.

105. Yan, T.-Y. and K. Yao, **A multiplication-free solution for the linear minimum mean-square estimation and equalization using the branch-and-bound principle.** IEEE transactions on information theory, Vol. IT-26, No. 3, May 1980, p.316-326.

106. Yoshida, S., F. Ikegami and T. Takeuchi, **Causes of burst errors in multipath fading channel.** IEEE transaction on communications Vol. COM-36, No. 1, January 1988, p.107-113.

107. Young, M.C.S. and Grant, P.M., **Reduction of multipath propagation effects in microwave digital radio communication systems.**, Electronics and Communication Engineering Journal, Feb 1990, p.4-10.

108. Ziemer, R.E. and C.R. Ryan, **Equalization of QPSK data transmission in specular multipath.** IEEE transactions on aerospace and electronic systems, Vol. AES-10, No. 5, September 1974, p.588-594.

Books:

1. Baccetti, B. and G. Tartara, **Equalization and quality predictions in digital radio systems.** GTE Telecomunicazioni S.p.A, 1983.

2. Bingham, J.A.C., **The theory and practice of modem design.** Wiley Interscience, New York.

3. Clarkson, P.M., **Optimal and adaptive signal processing.** CRC Press.

4. Feher, K., **Telecommunications measurements, analysis, and instrumentation.** Prentice-Hall Books, New Jersey, 1987.

5. Feher, K., **Advanced digital communications**, Prentice-Hall Books, Chapter 12.

6. Gitlin, R.D., J.F. Hayes and S.B. Weinstein, **Data Communications Principles.** Plenum Press, New York, 1992.

7. Haykin, S., Adaptive Filter Theory, Second Edition, Prentice Hall, Englewood cliffs, NJ, 1991.

8. Ivanek, F., **Terrestrial Digital Microwave Communications.** Artech House, 1989, CH4.

9. Jeruchim, M.C., P. Balaban and K.S. Shanmugan, **Simulation of communication systems.** Plenum Publishing Corporation, New York, 1994.

10. Lee, E.A. and D.G. Messerschmitt, **Digital Communication.** Kluwer Academic Publishers.

11. Oppenheim, A.V. and R.W. Schafer, **Discrete-time signal processing.** Prentice-Hall, Englewood Cliffs, 1989, p.123-127.

12. Stremler, F.G., **Introduction to communication systems.** Second Edition, Addison-Wiley, U.S.A., 1982, p.244-247.

13. Townsend, A.A.R., **Analog line-of-sight radio links.** Prentice-Hall, UK, 1987.

14. Westall, F.A. and S.F.A. Ip, **Digital Signal Processing in Telecommunications.** Chapman and Hall, 1993, p.72-83.

15. Ziemer, R.E. and R.L. Peterson, **Introduction to digital communications.** Macmillan Publishing Company, 1992, p.202-225.

16. Ziemer, R.E. and R.L. Peterson, **Digital communications and spread spectrum systems**, p.146-183.

17. Ziemer and Tranter, **Principles of communications**, Third Edition, p.499-516.

Appendix I

Method for predicting fading occurrence as a function of pathlength and frequency

The following procedure describes a method for predicting the narrow-band fading distribution at variuos fade depths in any part of the world. It was based on the information contained in ITU-R PN.530-5. This method does not take the path profile into account but there are other methods which do.

$pl \equiv 10$ %

$D \equiv 200$ Distance in Km

$f \equiv 8$ Frequency in GHz

$Clat \equiv 0$

$Clon \equiv 0.3$

$K \equiv 10^{(6.5 - Clat - Clon)} \cdot pl^{1.5}$

$$pw(A,d) := K \cdot d^{3.6} \cdot f^{0.89} \cdot 10^{-\frac{A}{10}}$$

$$qac(A,temp) := \frac{-20 \cdot \log\left(\ln\left(\frac{100 - temp}{100}\right)\right)}{A}$$

$$qt1(A,temp) := \frac{qac(A,temp) - 2}{1 - 0.3 \cdot 10^{-\frac{A}{20}} \cdot 10^{-0.016 \cdot A}} - 4.3 \cdot 10^{-\frac{A}{20}} - \frac{A}{800}$$

$$qa(A,AA,temp) := 2 - \left(1 - 0.3 \cdot 10^{-\frac{A}{20}} \cdot 10^{0.016 \cdot A}\right) \cdot qt1(AA,temp) - 4.3 \cdot 10^{-\frac{A}{20}} - \frac{A}{800}$$

$$pwc(A,AA,temp) := 100 \cdot \left(1 - \exp\left(-10^{-\frac{qa(A,AA,temp) \cdot A}{20}}\right)\right)$$

```
perc := | for d ∈ 1..D
        |   A ← 35
        |   temp ← pw(A,d)
        |   qtf ← qt1(A,temp)
        |   if qtf > 0
        |     A ← 25
        |     temp ← pw(A,d)
        |   for a ∈ 1..50
        |     P_{a,d} ← (pw(a,d))  if a > A
        |               (pwc(a,A,temp))  otherwise
        | P
```

Appendix II

Intuitive development of a baseband Three-Path Model

This appendix presents the initial development of the baseband three-path model. It was derived on intuition and so it is valuable for providing more insight into the base-band 3PM.

As the simulations are being carried out at baseband, it is necessary to transform the Three Path model. Consider a quadrature modulation process which incorporates the Three-Path model, as depicted in figure 1.

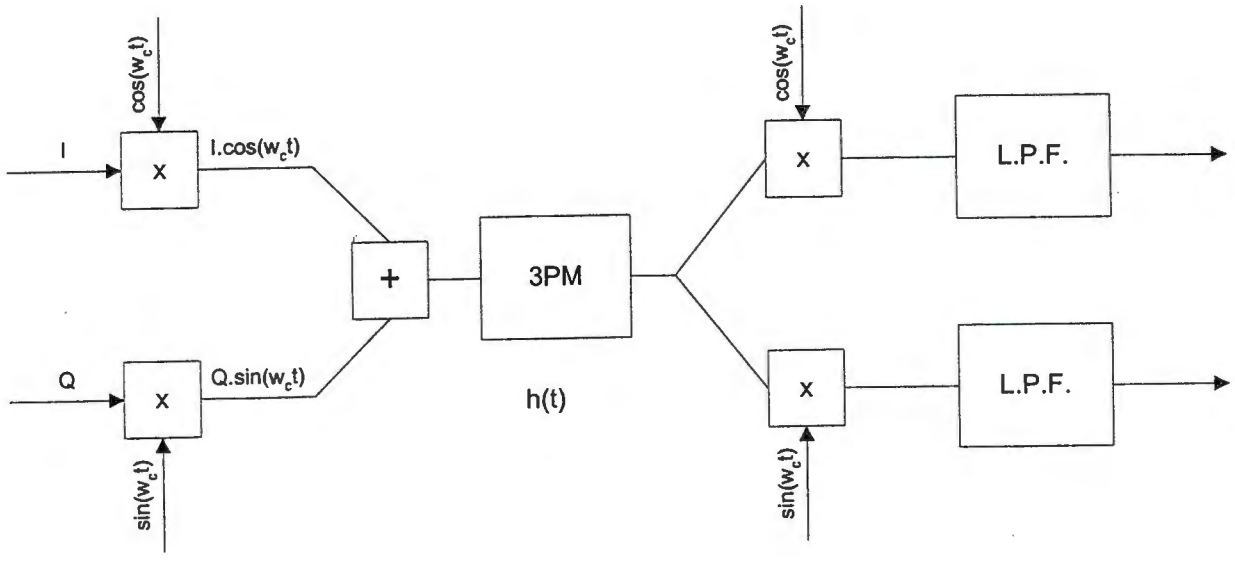

Figure 1: Modulator structure with Three-Path model

The baseband data comes in as the in-phase channel, I(t), and as the quadrature channel, Q(t). These are physical signals and so are real valued. They are then quadrature modulated onto a carrier, combined, and the resulting signal is transmitted. The effect of multipath is included by multiplying the signal spectrum by the frequency transfer function of the Three Path model, which is given by:

$$H(w) = a.(1 - b.e^{-j(w - w_o)\pi})$$ (1)

Note that the notch can be placed at any frequency, w_o, in the above equation. The notch position is normally described relative to the carrier frequency, but can be shifted to IF or baseband.

The distorted waveform is then demodulated and low pass filtered to produce two real valued data streams. This demodulation process is equivalent to taking the real and imaginary parts of the received waveform.

If one considers the above process in terms of phasors, the situation can be represented as in figure 2. The process of multiplying by $\sin(w_c t)$ and $\cos(w_c t)$ is replaced by a multiplication by j and 1, respectively. The quadrature demodulator multiplies by -j to ensure sign preservation.

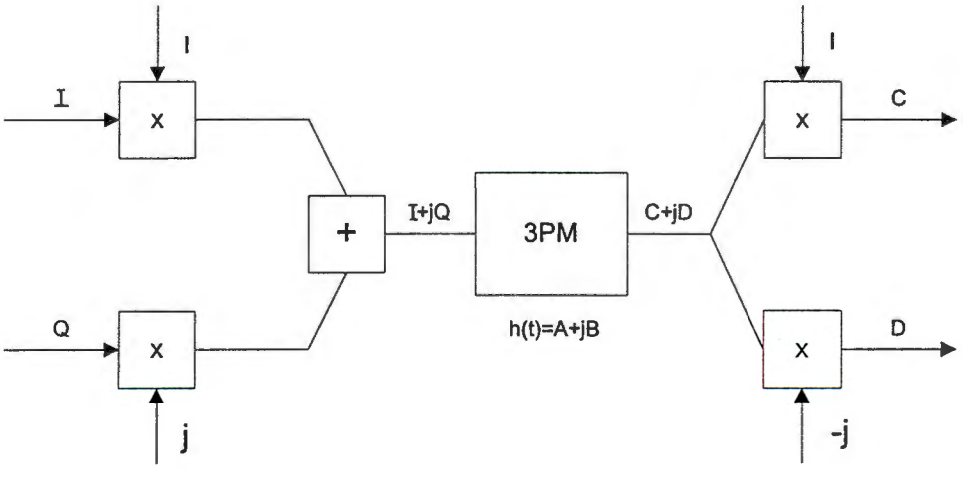

Figure 2: Phasor representation of figure 1.

Writing the complex impulse response of the Three-Path model as A(t)+jB(t), and convolving with the complex input sequence, we get:

$$Y(t) = \{I(t) + jQ(t)\} * \{A(t) + jB(t)\}$$ (2)

$$= \{I(t)*A(t) - Q(t)*B(t)\} * j\{Q(t)*A(t) + I(t)*B(t)\}$$

$$= C(t) + jD(t)$$

where * denotes convolution here.

Applying the complex signal Y(t) to the demodulation process, which extracts the real and imaginary components of Y(t), the real signals C(t) and D(t) appear at the in-phase and quadrature channel outputs. Therefore viewing this process as a black-box which has I(t) and Q(t) going into the box and C(t) and D(t) emerging, one can represent this process as in figure 3.

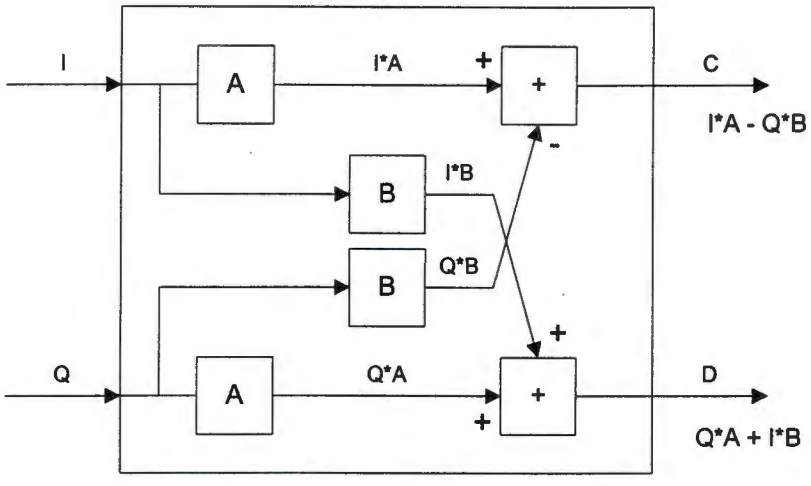

Figure 3: Baseband representation

To calculate A(t) and B(t), consider the impulse response of the Three-Path model, which is:

$$h(t) = a\delta(t) - ab.e^{jw\tau}\delta(t-\tau) \qquad (3)$$
$$= a\delta(t) - ab.\cos(w_o\tau)\delta(t-\tau) - jab.\sin(w_o\tau)\delta(t-\tau)$$
$$= A(t) + jB(t)$$

Therefore,

$$A(t) = a\delta(t) - ab.\cos(w_o\tau)\delta(t-\tau) \qquad (4)$$
$$B(t) = - ab.\sin(w_o\tau)\delta(t-\tau) \qquad (5)$$

To produce expressions for C(t) and D(t), the convolution process as given by equation (2), must be performed. This results in the following expressions:

$$C(t) = I(t)*A(t) - Q(t)*B(t) \qquad (6)$$
$$= aI(t) - ab.\cos(w_o\tau).I(t-\tau) + ab.\sin(w_o\tau).Q(t-\tau)$$

$$D(t) = Q(t)*A(t) + I(t)*B(t) \qquad (7)$$
$$= aQ(t) - ab.\cos(w_o\tau).Q(t-\tau) - ab.\sin(w_o\tau).I(t-\tau)$$

An inspection of the above equations gives one a good insight as to what actually happens during multipath fading as the notch moves through the transmission bandwidth. It can be seen that the model reduces to the simple two path model when the notch is in the centre of the band, that is when $w_o = 0$ for the baseband case. As the notch moves off frequency, a fraction of the delayed in-phase signal is combined into the quadrature channel and the same applies for the in-phase channel except for a sign change of the delayed quadrature signal. Thus an asymmetric transmission channel distortion produces cross-talk between the in-phase and quadrature data channels. The function of an equalizer is to minimise the distortion due to both the delay and the cross-talk.

Appendix III

Calculation of the optimal equalizer coefficients

Define the number of equalizer taps.

taps := 7

i := 0 .. taps - 1

Define the amount of noise in the system.

n := 0

Read the impulse response and convert to complex format.

I_i := READ $i9_{snk}$ Q_i := READ $q9_{snk}$

$h_i := I_i - (j \cdot Q)_i$

$$h = \begin{bmatrix} 39.707 + 80.121j \\ 1.776 \cdot 10^5 - 6.796 \cdot 10^5 j \\ -6.311 \cdot 10^5 + 3.986 \cdot 10^6 j \\ 2.663 \cdot 10^7 + 3.042 \cdot 10^6 j \\ 1.33 \cdot 10^6 - 7.863 \cdot 10^6 j \\ -2.945 \cdot 10^5 + 1.775 \cdot 10^6 j \\ -8.517 \cdot 10^4 + 4.145 \cdot 10^4 j \end{bmatrix}$$

Calculate the Wiener-Hopf equations.

$$s(a) := \sum_{k=a}^{6} h_k \cdot \overline{h_{k-a}}$$

$$S = \begin{bmatrix} s(0) & s(1) & s(2) & s(3) & s(4) & s(5) & s(6) \\ \overline{s(1)} & s(0) & s(1) & s(2) & s(3) & s(4) & s(5) \\ \overline{s(2)} & \overline{s(1)} & s(0) & s(1) & s(2) & s(3) & s(4) \\ \overline{s(3)} & \overline{s(2)} & \overline{s(1)} & s(0) & s(1) & s(2) & s(3) \\ \overline{s(4)} & \overline{s(3)} & \overline{s(2)} & \overline{s(1)} & s(0) & s(1) & s(2) \\ \overline{s(5)} & \overline{s(4)} & \overline{s(3)} & \overline{s(2)} & \overline{s(1)} & s(0) & s(1) \\ \overline{s(6)} & \overline{s(5)} & \overline{s(4)} & \overline{s(3)} & \overline{s(2)} & \overline{s(1)} & s(0) \end{bmatrix}$$

$N := identity(7) \cdot n$ Create noise matrix.

$R := S + N$

$z := 6$ Delay through system composed of 7 sample impulse approximation and 7 tap equalizer.

$p(a) := h_{z-a}$

$$P := \begin{matrix} p(0) \\ p(1) \\ p(2) \\ p(3) \\ p(4) \\ p(5) \\ p(6) \end{matrix}$$

The optimal coefficients are obtained from the following formula:

$W := R^{-1} \cdot P$

$$W = \begin{matrix} 3.483 \cdot 10^{-10} - 1.701 \cdot 10^{-10} j \\ -1.097 \cdot 10^{-9} - 1.296 \cdot 10^{-9} j \\ -1.067 \cdot 10^{-9} + 6.637 \cdot 10^{-9} j \\ 4.116 \cdot 10^{-8} + 4.329 \cdot 10^{-9} j \\ -3.044 \cdot 10^{-10} - 1.294 \cdot 10^{-8} j \\ -4.078 \cdot 10^{-9} + 3.289 \cdot 10^{-9} j \\ 1.755 \cdot 10^{-9} + 1.124 \cdot 10^{-9} j \end{matrix}$$

These optimal coefficients are now written to a file.

$WR := Re(W)$
$WI := Im(W)$

$WRITE(opt\_r\_9) := WR$
$WRITE(opt\_i\_9) := WI$

The following section computes the effect of binary quantization on the optimal coefficients.

$WRmax := max(WR)$ $WImax := max(WI)$

$WRmin := min(WR)$ $WImin := min(WI)$

$$Wm = \begin{matrix} WRmax & WRmin \\ WImax & WImin \end{matrix}$$

$$Wmax = \max(Wm)$$

Normalizing the tap weights, we get:

$$WRn = \frac{WR}{Wmax} \qquad WIn = \frac{WI}{Wmax}$$

The binary quantization of the coefficients is now defined, and the coefficients are converted to binary. The binary number is then converted back to a fraction and de-normalized. The quantized values are then sent to a file.

$bits = 10$

$BN = 2^{bits} - 1$

$WRb_i = \text{floor}(WRn_i \cdot BN)$ $\qquad WIb_i = \text{floor}(WIn_i \cdot BN)$

$$WRd = \frac{WRb \cdot Wmax}{BN} \qquad WId = \frac{WIb \cdot Wmax}{BN}$$

$WRITE(b\_rI\_10) = WRd$ $\qquad WRITE(b\_rI\_I0) = WId$

The rounded power-of-two coefficients are now calculated, converted back to a fraction, denormalized and sent to a file.

$$WRrb = \left|\begin{array}{l} \text{for } i \in 0..taps-1 \\ \quad \left|\begin{array}{l} mag \leftarrow WRb_i \\ n \leftarrow 0 \\ \text{while } mag > 2^n \\ \quad n \leftarrow n-1 \\ temp1 \leftarrow \left|\begin{array}{ll} 2^{n-1} & \text{if } mag < 2^{n-1} - \frac{2^{n-1}}{2} \\ 2^n & \text{otherwise} \end{array}\right. \\ temp \leftarrow \left|\begin{array}{ll} 0 & \text{if } temp1 = 0.5 \\ temp1 & \text{otherwise} \end{array}\right. \\ final_i \leftarrow \left|\begin{array}{ll} temp & \text{if } WRb_i \geq 0 \\ (-temp) & \text{otherwise} \end{array}\right. \end{array}\right. \\ final \end{array}\right.$$

$$WIrb = \left|\begin{array}{l} \text{for } i \in 0..taps-1 \\ \quad \left|\begin{array}{l} mag \leftarrow WIb_i \\ n \leftarrow 0 \\ \text{while } mag > 2^n \\ \quad n \leftarrow n-1 \\ temp1 \leftarrow \left|\begin{array}{ll} 2^{n-1} & \text{if } mag < 2^{n-1} - \frac{2^{n-1}}{2} \\ 2^n & \text{otherwise} \end{array}\right. \\ temp \leftarrow \left|\begin{array}{ll} 0 & \text{if } temp1 = 0.5 \\ temp1 & \text{otherwise} \end{array}\right. \\ final_i \leftarrow \left|\begin{array}{ll} temp & \text{if } WIb_i \geq 0 \\ (-temp) & \text{otherwise} \end{array}\right. \end{array}\right. \\ final \end{array}\right.$$

$$WRrd := \frac{WRrb \cdot Wmax}{BN} \qquad WIrd := \frac{WIrb \cdot Wmax}{BN}$$

WRITE(rb_rl_9) := WRrd WRITE(rb_im_9) := WIrd

The values below demonstrate the effect of the various rounding operations.

$$WR = \begin{pmatrix} 3.483 \cdot 10^{-10} \\ -1.097 \cdot 10^{-9} \\ -1.067 \cdot 10^{-9} \\ 4.116 \cdot 10^{-8} \\ -3.044 \cdot 10^{-10} \\ -4.078 \cdot 10^{-9} \\ 1.755 \cdot 10^{-9} \end{pmatrix} \qquad WI = \begin{pmatrix} -1.701 \cdot 10^{-10} \\ -1.296 \cdot 10^{-9} \\ 6.637 \cdot 10^{-9} \\ 4.329 \cdot 10^{-9} \\ -1.294 \cdot 10^{-8} \\ 3.289 \cdot 10^{-9} \\ 1.124 \cdot 10^{-9} \end{pmatrix}$$

$$WRd = \begin{pmatrix} 3.219 \cdot 10^{-10} \\ -1.127 \cdot 10^{-9} \\ -1.086 \cdot 10^{-9} \\ 4.116 \cdot 10^{-8} \\ -3.219 \cdot 10^{-10} \\ -4.104 \cdot 10^{-9} \\ 1.73 \cdot 10^{-9} \end{pmatrix} \qquad WId = \begin{pmatrix} -2.012 \cdot 10^{-10} \\ -1.328 \cdot 10^{-9} \\ 6.599 \cdot 10^{-9} \\ 4.306 \cdot 10^{-9} \\ -1.296 \cdot 10^{-8} \\ 3.259 \cdot 10^{-9} \\ 1.086 \cdot 10^{-9} \end{pmatrix}$$

$$WRrd = \begin{pmatrix} 3.219 \cdot 10^{-10} \\ 1.288 \cdot 10^{-9} \\ -1.288 \cdot 10^{-9} \\ 4.12 \cdot 10^{-8} \\ 3.219 \cdot 10^{-10} \\ -5.151 \cdot 10^{-9} \\ 1.288 \cdot 10^{-9} \end{pmatrix} \qquad WIrd = \begin{pmatrix} -1.61 \cdot 10^{-10} \\ -1.288 \cdot 10^{-9} \\ 5.151 \cdot 10^{-9} \\ 5.151 \cdot 10^{-9} \\ -1.03 \cdot 10^{-8} \\ 2.575 \cdot 10^{-9} \\ 1.288 \cdot 10^{-9} \end{pmatrix}$$

----oOo----

Appendix IV

DAC distortion compensation

1. Effect of a DAC on the signal spectrum

The DAC introduces a sin(x)/x distortion in the spectrum of a sequence of samples on which the DAC has operated. In the time domain, this distortion manifests as ISI, which means that the eye cross-over point is slightly enlarged.

To see how this effect comes about, consider figure 1 as presented in *Digital Signal Processing* by R.A. Roberts and C.T. Mullis, p.122. A DAC can be modelled as a zero-order hold filter. If the input sample sequence is convolved with the zero-order hold, the discrete Fourier Transform of the sampled sequence is multiplied by the sin(x)/x function, which has its zeros at multiples of the sampling rate. This results in the spectral characteristics shown below.

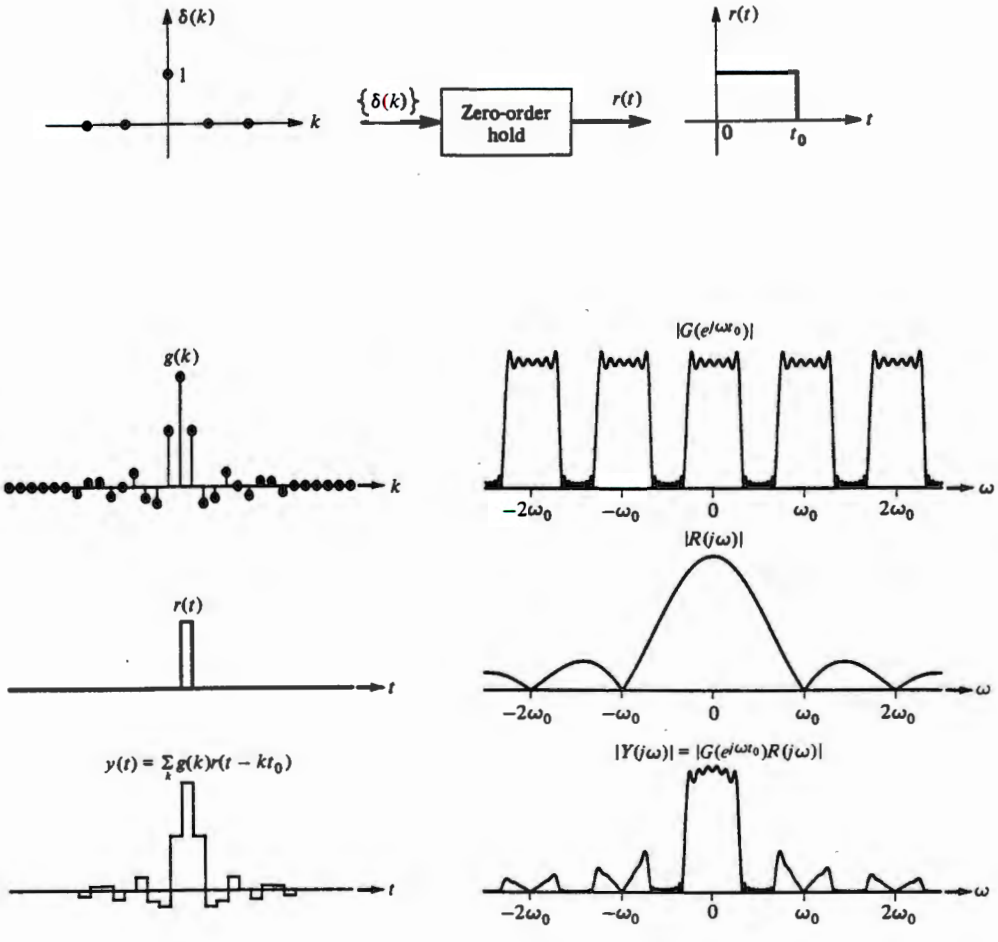

Figure 1: Reconstrunction of an analog signal y(t) from samples g(k) using the zero-order hold r(t).

To compensate for this effect, two strategies are proposed. The first is to modify the raised-cosine filter in such a way as to produce a raised-cosine spectral shape multiplied by the x/sin(x) function. The Parks-Mc Clellan algorithm can be used to achieve this and it is described on p.485 of *Discrete-Time Signal Processing* by Oppenheim and Schaffer.

In the second method, which was the one used to generate the results which follow, the inverse Fourier Transform of the x/sin(x) function, truncated at half the sampling frequency, is convolved with the raised-cosine FIR filter output. Alternatively, it can be convolved with the impulse response of the raised-cosine filter to obtain an equalized raised-cosine FIR filter. It proved extremely difficult to perform the inverse Fourier Transform of the x/sin(x) function, so it was necessary to take the inverse Fourier Transform of an approximation to the x/sin(x) function.

2. Approximating the x/sin(x) function and inverse transforming

Considering the parabola-type shape of the x/sin(x) function, it was decided to approximate this function by fitting a second order polynomial. As the important information is contained in the lower part of the spectrum, the fitting points were chosen to be $\pm$ pi/8. This yielded:

$$y = 0.1697x^2 + 1 \qquad \textbf{(1)}$$

Figure 2 shows a comparison of the ideal and approximated functions. A 17MBaud raised-cosine shaped spectrum with alpha equal to 0.5, has a one-sided bandwidth of 12.75MHz. Using a sample rate of 68MHz implies that all the spectral information will be contained within the region -0.589 to +0.589 in figure 2. As can be seen there is an excellent match in this region.

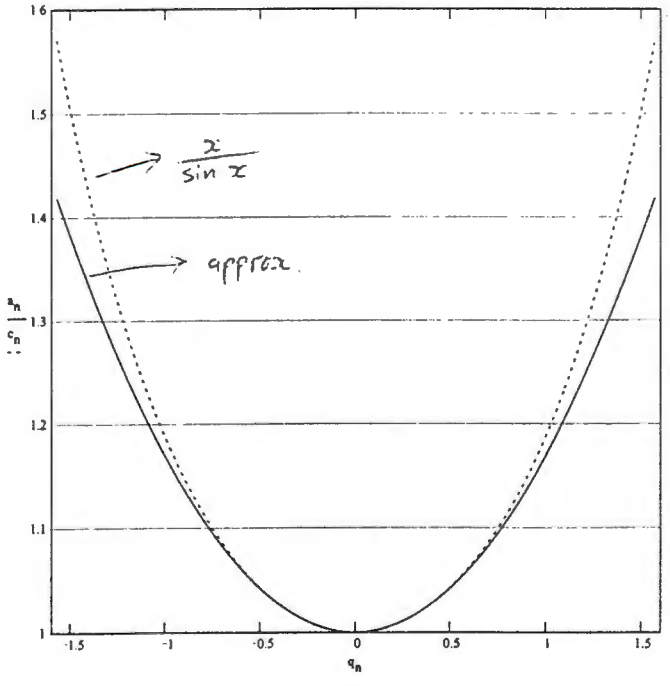

Figure 2: Approximation of the x/sin(x) function

Scaling **(1)** to accomodate a sampling frequency of 68MHz, the following is obtained:

$$y(w) = Kw^2 + 1$$
$$K = \frac{0.1697}{(136e6)^2} \qquad (2)$$

To obtain the inverse Fourier Transform, f(t), the following integral needs to be evaluated, where A is equal to half the sampling frequency:

$$f(t) = \frac{K}{2\pi} \int_{-A}^{A} \left(w^2 + \frac{1}{K} \right) e^{jtw} \, dw \qquad (3)$$

This integral can be written as the sum of two separate integrals. The left-hand one is solved with two applications of *integration by parts*, while the right-hand one is straight forward. After some simplification, the inverse transform can be written as:

$$f(t) = \frac{(KA^2t^2 - 2K + t^2) \sin At}{\pi t^3} + \frac{2KA \cos At}{\pi t^2} \qquad (4)$$

This function has a singularity at $t=0$, but by applying L'Hopital's rule it can be seen that the function approaches the following value as t tends toward zero:

$$\lim_{t \to 0} f(t) = \frac{KA^3 + 3A}{3\pi} \qquad (5)$$

This impulse response can now be sampled at the appropriate intervals and the sampled values assigned as the coefficients of a FIR filter.

3. Compensated results

In order to demonstrate the validity of the above derivation, consider the eye diagram represented in figure 3. Note the slightly unfocused eye cross-over point. This diagram was produced by sending a 17MBaud data stream through a 128 tap raised-cosine FIR filter with infinite precision coefficients. Four samples per symbol were taken and the output of the DAC is filtered with an analog low pass 5-pole Chebychev filter with cut-off at 25MHz. This diagram represents the limit which can be achieved with 4 samples per symbol. If a higher sample rate is used, the distortion effect can be reduced, but the digital circuit implementation then becomes impractical.

Figure 4 shows the eye diagram produced by the same raised-cosine filter cascaded with a seven tap compensation filter.
The eye cross-over area has been greatly reduced, thereby justifying the approach taken. Figure 5 shows the spectrum achieved under these conditions.

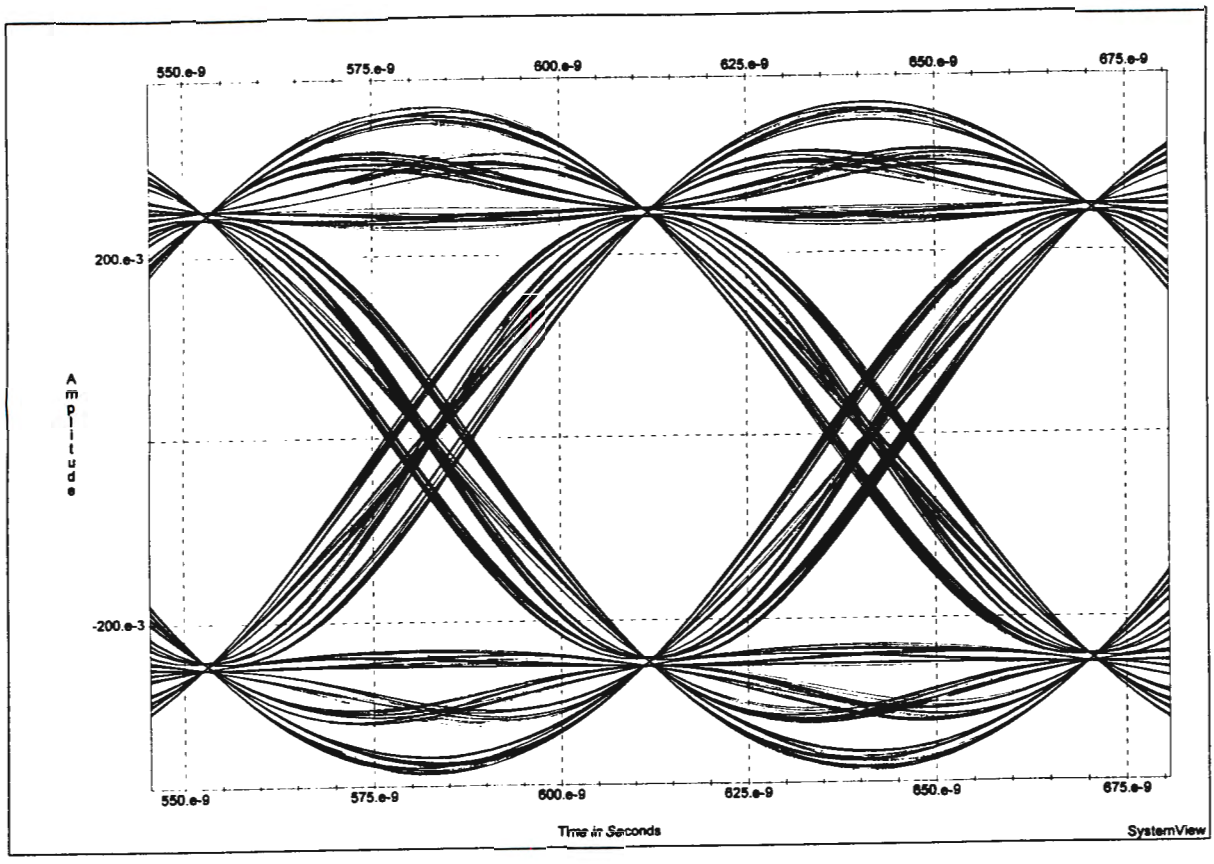

Figure 3: Uncompensated eye diagram

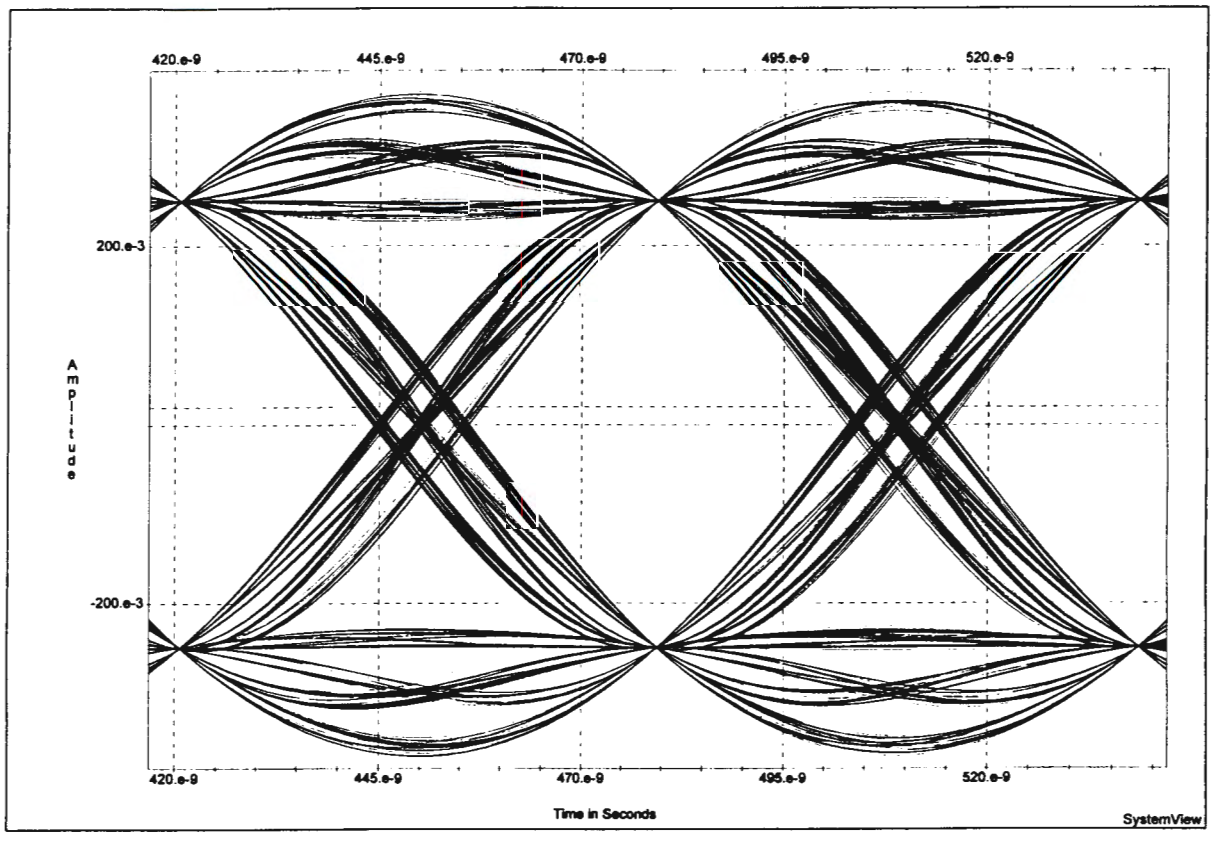

Figure 4: Compensated eye diagram

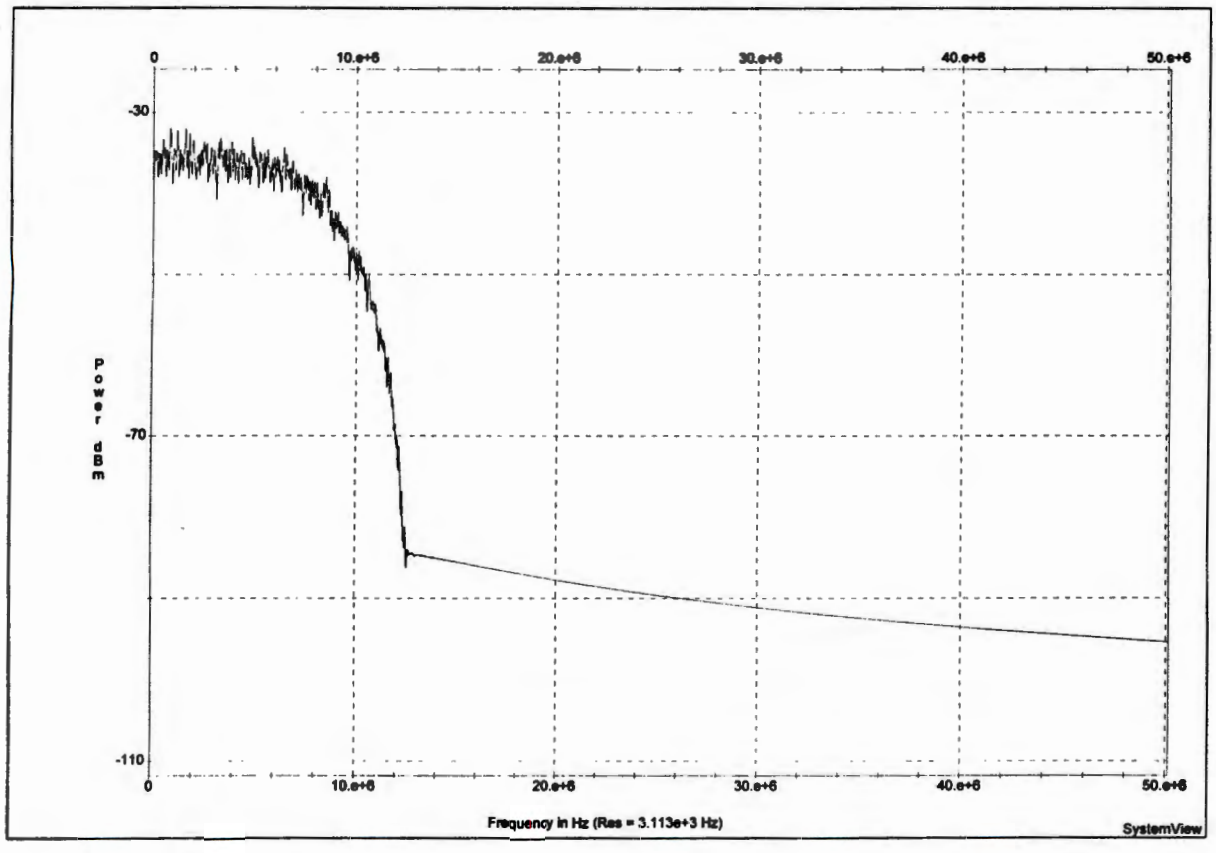

Figure 5: Compensated raised-cosine spectrum

It can be concluded from this investigation that a seven tap compensation filter designed in the manner described in this section, is adequate for pulse shaping applications.

Appendix V

Comparison of real and simulated 8MBit/s QPSK modem

This appendix is included to demonstrate that the simulation model and formulae as presented in chapter 5, do yield plausible results. An interesting approach is adopted to simulate the real QPSK modem and that is to produce an eye which looks identical to the eye measured on an oscilloscope. This was achieved by adjusting the receive low-pass filter cut-off until the required eye was obtained. Apart from the receive filter, which comes before the integrate-and-dump circuit, the simulation model was identical to that shown in figure 5.1.

In the filter simulation, the phase was kept constant so that the group delay was zero. This enabled the filter to be placed directly in the I and Q channel, without worrying about cross-talk. The appropriate amount of noise, as given by **(5.10)**, was injected into the simulation and the BER measured for various E_b/N_0 values. A million bits were used to ensure accuracy.

A QPSK modem was set-up in loop back mode with an HP Noise Generator located in the system's 70MHz IF. Various values for E_b/N_0 were entered into the instrument and the errors were monitored on a Data Transmission Analyser. Table 1 shows the results.

E_b/N_0 in dB	Measured: log BER	Simulated: log BER
8	-2.63	-2.72
10.5	-3.79	-3.70
12.5	-4.87	-4.82

Table 1: Comparison of measured and simulated QPSK results

The results are surprisingly close to each other. As this is unlikely to be due to chance, it is proposed that the method is a useful technique. The results boost one's confidence in the simulation model and noise formula.